

DTIC FILE COPY

②

GL-TR-89-0114

SSS-TR-89-10395

**REGIONAL DISCRIMINATION OF  
QUARRY BLASTS, EARTHQUAKES  
AND UNDERGROUND  
NUCLEAR EXPLOSIONS**

**AD-A223 148**

**T. J. Bennett  
B. W. Barker  
K. L. McLaughlin  
J. R. Murphy**

**S-CUBED**

**A Division of Maxwell Laboratories, Inc.  
P. O. Box 1620  
La Jolla, California 92038-1620**

**7 April 1989**

**Final Report**

**23 March 1987-22 March 1989**

**Approved for Public Release,  
Distribution Unlimited.**

**GEOPHYSICS LABORATORY  
Air Force Systems Command  
Hanscom Air Force Base  
Massachusetts 01731-5000**

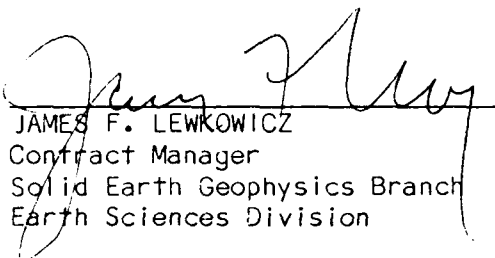
66 50 20 105

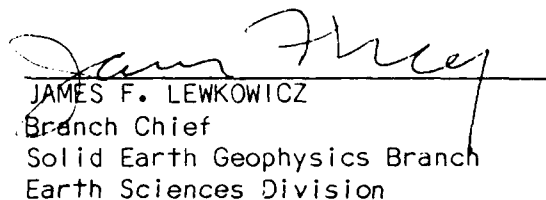
SPONSORED BY  
Defense Advanced Research Projects Agency  
Nuclear Monitoring Research Office  
ARPA ORDER NO. 5307

MONITORED BY  
Geophysics Laboratory  
Contract No. F19628-87-C-0093

The views and conclusions contained in this document are those of the authors and should not be interpreted as representing the official policies, either expressed or implied, of the Defense Advanced Research Projects Agency or the U.S. Government.

This technical report has been reviewed and is approved for publication.

  
JAMES F. LEWKOWICZ  
Contract Manager  
Solid Earth Geophysics Branch  
Earth Sciences Division

  
JAMES F. LEWKOWICZ  
Branch Chief  
Solid Earth Geophysics Branch  
Earth Sciences Division

FOR THE COMMANDER

  
DONALD H. ECKHARDT, Director  
Earth Sciences Division

This report has been reviewed by the ESD Public Affairs Office (PA) and is releasable to the National Technical Information Service (NTIS).

Qualified requestors may obtain additional copies from the Defense Technical Information Center. All others should apply to the National Technical Information Service.

If your address has changed, or if you wish to be removed from the mailing list, or if the addressee is no longer employed by your organization, please notify AFGL/DAA, Hanscom AFB, MA 01731-5000. This will assist us in maintaining a current mailing list.

Do not return copies of this report unless contractual obligations or notices on a specific document requires that it be returned.

UNCLASSIFIED

SECURITY CLASSIFICATION OF THIS PAGE

## REPORT DOCUMENTATION PAGE

1a. REPORT SECURITY CLASSIFICATION Unclassified			1b. RESTRICTIVE MARKINGS		
2a. SECURITY CLASSIFICATION AUTHORITY			3. DISTRIBUTION/AVAILABILITY OF REPORT Approved for public release; distribution unlimited.		
2b. DECLASSIFICATION/DOWNGRADING SCHEDULE					
4. PERFORMING ORGANIZATION REPORT NUMBER(S)			5. MONITORING ORGANIZATION REPORT NUMBER(S)  GL-TR-89-0114		
6a. NAME OF PERFORMING ORGANIZATION S-Cubed, Division of Maxwell Laboratories, Inc.		6b. OFFICE SYMBOL (If applicable)	7a. NAME OF MONITORING ORGANIZATION Geophysics Laboratory		
6c. ADDRESS (City, State, and ZIP Code) P.O. Box 1620 La Jolla, CA 92038-1620			7b. ADDRESS (City, State, and ZIP Code) Hanscom Air Force Base Massachusetts 01731-5000		
8a. NAME OF FUNDING/SPONSORING ORGANIZATION Defense Advanced Research Projects Agency		8b. OFFICE SYMBOL (If applicable)	9. PROCUREMENT INSTRUMENT IDENTIFICATION NUMBER  F19628-87-C-0093		
8c. ADDRESS (City, State, and ZIP Code) 1400 Wilson Boulevard Arlington, VA 22209-2308			10. SOURCE OF FUNDING NUMBERS		
			PROGRAM ELEMENT NO. 62714E	PROJECT NO. 7A10	TASK NO. DA
11. TITLE (Include Security Classification) REGIONAL DISCRIMINATION OF QUARRY BLASTS, EARTHQUAKES AND UNDERGROUND NUCLEAR EXPLOSIONS (U)					
12. PERSONAL AUTHOR(S) Bennett, T. J., Barker, B. W., McLaughlin, K. L., Murphy, J. R.					
13a. TYPE OF REPORT Final	13b. TIME COVERED FROM 870323 TO 890322		14. DATE OF REPORT (Year, Month, Day) 890407		15. PAGE COUNT 146
16. SUPPLEMENTARY NOTATION					
17. COSATI CODES			18. SUBJECT TERMS (Continue on reverse if necessary and identify by block number) Seismic NTS Explosions Mine/Quarry Blasts Discrimination East Kazakh Explosions Regional Phases		
FIELD	GROUP	SUB-GROUP			
19. ABSTRACT (Continue on reverse if necessary and identify by block number) The investigations conducted under this contract focused on analyses of the higher-frequency phases observed at regional distances from underground nuclear explosions, earthquakes, and commercial blasts. These analyses systematically compared the time-domain amplitude and spectral characteristics of the observed regional seismic signals in order to identify diagnostic differences which would be indicative of source type. The sources were located in three tectonic environments: (1) eastern North America, (2) southern Soviet Union, and (3) western United States. Each source environment provides a unique contribution to the regional discrimination problem. For these source regions digital data from several different high-quality seismic networks were analyzed. The data sources were the Regional Seismic Test Network (RSTN), the Eastern Canada Telemetered Network (ECTN), the Chinese Digital Seismic Network (CDSN), the Soviet/Natural Resources Defense Council (NRDC) network, and the Lawrence Livermore National Laboratory (LLNL) network.					
20. DISTRIBUTION/AVAILABILITY OF ABSTRACT <input checked="" type="checkbox"/> UNCLASSIFIED/UNLIMITED <input type="checkbox"/> SAME AS RPT. <input type="checkbox"/> DTIC USERS			21. ABSTRACT SECURITY CLASSIFICATION UNCLASSIFIED		
22a. NAME OF RESPONSIBLE INDIVIDUAL James Lewkowicz			22b. TELEPHONE (Include Area Code) 617/377-3028		22c. OFFICE SYMBOL LWH

9. ABSTRACT (Continued)

The eastern North America database included small commercial blasts and earthquakes recorded at RSTN station RSCP and stations in the ECTN. At RSCP the blasts frequently produced strong  $R_g$  signals not seen in the earthquakes.  $L_g$  and  $P_g$  spectra for the blasts appeared to decay more rapidly at high frequencies than corresponding earthquake spectra.  $L_g/P$  amplitude ratios were observed to be larger for earthquakes, but these results were intermingled. The study of ECTN data focused on cepstral analysis of regional P-waves to distinguish source multiplicity. The results showed evidence of deterministic modulation in the P-wave spectra for both quarry blasts and earthquakes, but this observation does not appear to be caused by multiple sources.

For the southern Soviet Union we compared regional phases recorded at CDSN station BMQ from East Kazakh nuclear explosions and regional earthquakes with similar magnitudes and ranges. Broadband  $L_g/P$  amplitude ratios were observed to be larger for earthquakes than comparable explosions, and the differences were found to be concentrated at higher frequencies based on bandpass filter analyses. The Soviet/NRDC network around the East Kazakh test site was found to record a large number of presumed mine blasts.  $R_g$  was strong for many of these events, and in some cases there was evidence of spectral scalloping in the recorded  $L_g$  signals which could be related to time-delayed blasting.

For the western U.S. the primary analysis was performed on a sample of NTS explosions and nearby earthquakes recorded by the LLNL stations at ranges from 160 to 485 km. Spectral analyses of the  $P_g$  and  $L_g$  signals for these events indicated that the earthquake signals appeared relatively richer in high frequencies in agreement with prior observations. The differences may be enhanced at higher frequencies and appear to show some dependence on explosion depth. For NTS explosions and California earthquakes recorded at larger ranges at RSTN station RSSD, spectral analysis of the regional  $L_g$  signals also showed a tendency for the explosion spectra to be more sharply peaked; but path differences may again be affecting the observation.



Accession For	
NTIS GRA&I	<input checked="" type="checkbox"/>
DTIC TAB	<input checked="" type="checkbox"/>
Unannounced	<input type="checkbox"/>
Justification	
By	
Distribution/	
Avail. and/or Codes	
/or	
Dist. and/or	
A-1	

## Table of Contents

List of Illustrations .....	iv
List of Tables .....	ix
SECTION I: INTRODUCTION .....	1
SECTION II: EASTERN NORTH AMERICAN QUARRY BLASTS AND EARTH- QUAKES .....	5
2.1 Eastern North America Data Sources .....	5
2.2 Analysis of RSTN Data .....	5
2.3 Analysis of ECTN Data .....	24
2.3.1 A Review of Cepstral Theory .....	30
2.3.2 Cepstral Analysis of ECTN Data .....	38
SECTION III: IDENTIFICATION OF SEISMIC SOURCES IN THE SOUTHERN SOVIET UNION .....	46
3.1 Regional Observations from Soviet Events .....	46
3.2 Analysis of Regional Signals from the CDSN .....	47
3.3 Identification of Events from the Vicinity of the East Kazakh Test Site Recorded by the Soviet/NRDC Network .....	69
SECTION IV. NTS UNDERGROUND NUCLEAR EXPLOSIONS AND COMPARABLE EARTHQUAKES .....	85
4.1 Empirical Derivation of Techniques for Regional Discrimination of Nuclear Explosions .....	85
4.2 Analysis of LLNL Data .....	86
4.3 NTS Explosions and Earthquakes at RSSD .....	103
SECTION V. CONCLUSIONS AND RECOMMENDATIONS .....	112
REFERENCES .....	118

## List of Illustrations

FIGURE 1. Locations of regional events recorded at RSCP. Earthquakes (●), presumed blasts (x), and mine collapse (M). .....	10
FIGURE 2. Vertical-component records at RSCP from typical regional events. ....	12
FIGURE 3. Peak amplitude ratio ( $S_{max}/P_{max}$ ) observed at RSCP as a function of magnitude (top) and epicentral distance (bottom). ....	13
FIGURE 4. Application of band-pass filter at RSCP to enhance $R_g$ signals. ....	15
FIGURE 5. Vertical-component records for four events recorded at RSCP. ....	16
FIGURE 6. $L_g$ spectra (solid line) and noise (dashed line) for the four events in Figure 5. ....	18
FIGURE 7. $P_g$ spectra (solid line) and noise (dashed line) for the four events from Figure 5. ....	19
FIGURE 8. Vertical-component records for four other events recorded at RSCP. ....	21
FIGURE 9. $L_g$ spectra (solid line) and noise (dashed line) for the four events from Figure 8. ....	22
FIGURE 10. $P_g$ spectra (solid line) and noise (dashed line) for the four events from Figure 8. ....	23
FIGURE 11. Instrument responses for the MARK-I, MARK-II and GAC systems at ECTN. ....	26
FIGURE 12. Map of ECTN stations and events. Stations indicated with triangles, events with crosses, and probable quarry blasts with circled crosses. ....	29
FIGURE 13. A flow chart describing the estimation of cepstra using a low-pass smoother $\gamma(f)$ to derive a baseline log-power spectrum to prewhiten the log-power spectra prior to estimation of cepstra. ....	35

FIGURE 14. A synthetic rectangular source array of 10 by 10 shots with delays of 50 msec in both orthogonal directions (left) and delays of 50 msec and 30 msec in the two orthogonal directions (right) with 5 msec standard deviation assumed for the blasting caps. The ideal source is shown at the bottom and the theoretical cepstra at the top. ....	37
FIGURE 15. Network-averaged P-wave spectra for events of 11/01/83 (a), 12/28/83 (b), 12/21/83 (c), and 09/25/84 (d). Spectra were normalized in 4-7 Hz passband prior to averaging. Dashed lines indicate $\pm$ one sigma bounds. ....	39
FIGURE 16. Detrended average P-wave spectra for events from Figure 15. ....	40
FIGURE 17. Individual cepstra for 8 different stations for the 12/21/83 event (bottom). Geometric mean of the 8 cepstra (solid line) and a "scaled" version of the product of the individual cepstra (dashed line) (top). ....	41
FIGURE 18. Comparison of the stacked cepstra from Figure 17 (dashed line) with the cepstra derived from the stacked log-power spectra (solid line). ....	43
FIGURE 19. Cepstra from the detrended stacked log-power spectra of Figure 16 for events of 11/01/83 (a), 12/28/83 (b), 12/21/83 (c) and 09/25/84 (d). ....	44
FIGURE 20. Locations of East Kazakh nuclear explosions (x) and regional earthquakes (•) in WMQ database. ....	48
FIGURE 21. Vertical-component records at WMQ from four nuclear explosions (top) and four regional earthquakes (bottom). ....	52
FIGURE 22. Peak amplitude ratios for $S_{\max}/P_{\max}$ (top) and for $L_g/P_g$ (bottom) measured from broad-band recordings at WMQ. ....	54
FIGURE 23. $L_g/P_{\max}$ ratios as a function of frequency for explosions and earthquakes recorded at WMQ. ....	55
FIGURE 24. Average $L_g/P_{\max}$ ratios as a function of frequency for explosions and earthquakes recorded at WMQ. ....	56
FIGURE 25. Comparison of $S_{\max}/P_{\max}$ ratios at WMQ for 3-6 Hz passband (top) and 0-1 Hz passband (bottom). ....	58
FIGURE 26. Comparison of $L_g/P_n$ ratios at WMQ for 3-6 Hz passband (top) and 0-1 Hz passband (bottom). ....	59
FIGURE 27. Comparison of $L_g/P_g$ ratios at WMQ for 3-6 Hz passband (top) and 0-1 Hz passband (bottom). ....	60

FIGURE 28. Dependence of $S_{\max}/P_{\max}$ ratios at WMQ on epicentral distance for 3-6 Hz passband (top) and 0-1 passband (bottom). .....	62
FIGURE 29. $L_g$ spectra for seven East Kazakh underground nuclear explosions measured at WMQ. ....	64
FIGURE 30. Comparison of schematic $L_g$ spectra observed at WMQ for seven East Kazakh explosions and seven regional earthquakes. ....	65
FIGURE 31. Comparison of $L_g$ spectra at WMQ after Q correction for magnitude 5.9 $m_b$ explosion and earthquake. ....	67
FIGURE 32. Comparison of $L_g$ spectra at WMQ after Q corrections for magnitude 5.3 $m_b$ explosion and earthquake. ....	68
FIGURE 33. Locations of presumed mine blasts in East Kazakh recorded by the Soviet/NRDC network. ....	70
FIGURE 34. Vertical-component records at station BA from eight presumed mine blasts near Ekibastuz ( $R \approx 100$ km). ....	72
FIGURE 35. Vertical-component records at station KK from same eight presumed mine blasts near Ekibastuz ( $R \approx 270$ km). ....	73
FIGURE 36. Vertical-component records at station KK from six presumed mine blasts from vicinity of $47.0^\circ\text{N}$ , $76.5^\circ\text{E}$ . ....	74
FIGURE 37. Vertical-component records at station BA from same six presumed mine blasts from vicinity of $47.0^\circ\text{N}$ , $76.5^\circ\text{E}$ . ....	75
FIGURE 38. Three-component records at station KK for three presumed mine blasts located 25-30 km to the east. ....	77
FIGURE 39. Three-component records at station BA for two presumed mine blasts located near Ekibastuz ( $R \approx 100$ km). ....	78
FIGURE 40. Vertical-component displacement at station KK from presumed mine blast near East Kazakh (top). Comparison of observed $R_g$ (solid line) and Airy phase approximation (dots) for an explosion source (bottom). ....	81
FIGURE 41. Evidence of notches in $L_g$ spectra from presumed mine blast near Ekibastuz. ....	84
FIGURE 42. LLNL station locations and event sample from vicinity of NTS. ....	87



FIGURE 43. Typical vertical-component records at LLNL stations from NTS explosions (left) and regional earthquakes (right). .....	90
FIGURE 44. Comparison of average $L_g$ spectral shapes for NTS explosions and nearby earthquakes recorded by LLNL stations. ....	92
FIGURE 45. Comparison of one-sigma bounds on average $L_g$ spectral shapes from Figure 44. ....	93
FIGURE 46. Comparison of average $P_g$ spectral shapes for NTS explosions and nearby earthquakes recorded by LLNL stations. ....	94
FIGURE 47. Bandpass filter analysis applied to explosion (left) and nearby earthquake (right) recorded at LLNL station KANAB. ....	96
FIGURE 48. Bandpass filter analysis applied to different explosion (left) and earthquake (right) recorded at LLNL station KANAB. ....	97
FIGURE 49. Comparison of $L_g$ spectral shapes for NTS explosions above and below the water table recorded by LLNL stations. ....	99
FIGURE 50. Comparison of $P_g$ spectral shapes for NTS explosions above and below the water table recorded by LLNL stations. ....	100
FIGURE 51. Comparison of $L_g$ spectral shapes for average explosions below the water table and average earthquakes recorded by LLNL stations. ....	101
FIGURE 52. Comparison of $P_g$ spectral shapes for average explosions below the water table and average earthquakes recorded by LLNL stations. ....	102
FIGURE 53. Vertical-component records at station RSSD from five Yucca Flat explosions. ....	105
FIGURE 54. Vertical-component records at station RSSD from two Pahute Mesa explosions and three California earthquakes. ....	106
FIGURE 55. Comparison of regional phase spectra at RSSD for Yucca Flat explosion CAPROCK, $m_b = 5.8$ , (left) and the Round Valley, California earthquake, $m_b = 5.6$ , (right). ....	107
FIGURE 56. Bandpass filter analyses of vertical component records at station RSSD for explosion KINIBITO, $m_b = 5.7$ , (left) and Round Valley, California earthquake, $m_b = 5.6$ , (right). ....	109

FIGURE 57. Bandpass filter analyses of vertical component records at station RSSD for explosion SALUT, $m_b = 5.5$ , (left) and Morgan Hill, California earthquake, $m_b =$ 5.7, (right). .....	110
---	-----

## **List of Tables**

TABLE 1. Presumed Mine Blasts Recorded at RSCP .....	8
TABLE 2. Regional Earthquakes and Mine Collapse Recorded at RSCP .....	9
TABLE 3. Origins for Available ECTN Data .....	25
TABLE 4. ECTN Station Locations .....	27
TABLE 5. East Kazakh Underground Nuclear Explosions .....	50
TABLE 6. Regional Earthquakes Recorded at WMQ .....	51
TABLE 7. LLNL Data Sample .....	88

## I. INTRODUCTION

Although the majority of large seismic events can be identified as earthquakes or explosions on the basis of teleseismic measurements, regional signal properties are expected to play an important part in identifying smaller events. Since the early days of interest in seismic discrimination, numerous methods have been proposed for using regional signal measurements to achieve identification (cf. Blandford, 1981; Pomeroy *et al.*, 1982). However, the discovery of suitable regional discriminant measures has proven to be elusive. Determination of reliable regional discrimination techniques requires testing of signal measurements on well-controlled samples of explosions and nearby earthquakes so as to minimize differences which are not related to the source type. Ideally, the methods should be tested in the areas where they are intended to be used. If regional discriminants cannot be suitably tested in such areas, methods must be developed to extrapolate the experience from other areas. The latter requires development of understanding of why a regional discriminant works including knowledge of the signal behavior to permit separation of source and propagation effects. The research described here was designed to improve regional discrimination capability by analyzing the regional seismic signal characteristics from a variety of sources observed in different tectonic environments.

The investigations conducted under this contract have focused on analyses of the higher-frequency phases observed at regional distances from three different types of sources: (1) underground nuclear explosions, (2) earthquakes, and (3) mine or quarry blasts. In our analyses we systematically compared the time-domain amplitude and spectral characteristics of the observed regional seismic signals while seeking to identify diagnostic differences which would be indicative of the source. Tectonic environments which were investigated in this study included (1) eastern North America, (2) the southern Soviet Union and (3) the western United States. Each of these environments provides a unique contribution to the regional discrimination problem. Stable continental areas of central and eastern North America are thought to be analogous in many ways to platform regions of the Soviet Union with regard to regional seismic wave generation and transmission. Past studies of regional

phases from Soviet underground nuclear explosions were frequently forced to rely on measurements at far-regional stations where the signals were extremely weak (cf. Nuttli, 1981; 1986). Recent installation of new stations have made available regional data from the southern Soviet Union enabling relevant testing of regional discrimination methods for this area where the capability is most needed. Finally, the western U.S. sample of underground nuclear explosions and nearby earthquakes provides the controlled source sample which permits closer analyses of how regional signal generation is influenced by various source factors.

The analyses were performed on the high-quality digital seismic data which were available from each of these tectonic environments. For eastern North America we used data from the Regional Seismic Test Network (RSTN) and the Eastern Canada Telemetered Network (ECTN). For the southern Soviet Union the data sources were the Chinese Digital Seismic Network (CDSN) and the Soviet/Natural Resources Defense Council (NRDC) seismic network surrounding the East Kazakh test site. For the western U.S. we relied on data from the Lawrence Livermore National Laboratory Network (LLNL) and some RSTN stations. Although the useful frequency range of these different seismic systems varies, in general the data permit analysis of higher frequency signals than those used in most previous investigations of regional discrimination. Furthermore, because of the potential interest in extending discrimination capability to lower thresholds, added focus in these investigations was given to consideration of commercial blasts which appear to be frequent contributors to the regional event samples in areas of interest for nuclear monitoring.

For eastern North America we compared the characteristics of the regional signals from mine blasts and earthquakes recorded by the RSTN and ECTN systems. The RSTN analysis included data from 22 presumed mine blasts, 14 earthquakes and a mine collapse recorded at station RSCP. The records showed good P and  $L_g$  phases. The  $L_g/P_{max}$  amplitude ratios were generally larger for the earthquakes than the blasts, but observations showed considerable scatter and intermingling which made the distinction unreliable. Many blasts and the mine collapse produced strong, short-period Rayleigh waves,  $R_g$ , but this was not the case for all blasts.  $L_g$  and  $P_g$  spectra indicated more rapid spectral decay above the corner frequency for blasts than for earthquakes.

The North America database at ECTN consisted of 36 events with magnitudes between 1.0 and 5.1 including seven presumed quarry blasts. These were recorded at multiple stations in the network to a fairly high digitizing rate (viz 60 samples per second). Our analyses of these data focused on an attempt to identify potential evidence of multiplicity in the source which is expected from the delay shooting typical of commercial blasting practice. Using the multiple station data, cepstral analyses were performed on the P-wave spectra from selected events. These analyses revealed evidence of deterministic modulation in the spectra from both quarry blasts and earthquakes with fairly large quefrequencies. It is suspected that this observation may correspond to a propagation effect rather than a source effect.

For the southern Soviet Union we analyzed observed regional phases from East Kazakh explosions and comparable earthquakes recorded at the CDSN station WMQ and from presumed mine blasts recorded at the Soviet/NRDC network stations. The WMQ database included 12 East Kazakh explosions and 20 earthquakes with magnitudes from 4.5 to 6.1  $m_b$ . Because of the lack of natural seismicity near East Kazakh, the comparable earthquakes were selected from throughout the region surrounding WMQ. The records showed strong P and  $L_g$  phases from both earthquakes and explosions. Broadband  $L_g/P$  amplitude ratios tended to be larger for earthquakes than for explosions, and the differences were concentrated at high frequencies. This result suggests a promising discriminant, but it must be strongly noted that the effects of attenuation differences in the crustal paths for the explosions and earthquakes have not been completely taken into account.

The analysis of the Soviet/NRDC network data focused on the characteristics of the regional phases from a large number of presumed mine blasts in the East Kazakh region which were recorded during the operation of the network. These events produced strong  $P_g$  and  $L_g$  signals to ranges of at least 400 km.  $R_g$  was also strong for many but not all events, and some evidence was found of spectral scalloping which might have been associated with shot delays in the presumed blasts.

For the western U.S. we used the LLNL database to continue our analysis (cf. Bennett *et al.*, 1987a,b) of the  $L_g$  and  $P_g$  spectral characteristics of 10 NTS explosions and eight nearby earthquakes. The observations were

generally in agreement with previous findings (cf. Murphy and Bennett, 1982; Bennett and Murphy, 1986) that the earthquake  $L_g$  signals appear to be relatively richer in high frequencies than comparable explosions. We also found evidence that burial of the explosion below the water table at Yucca Flat may enhance high frequencies in the regional phase signals, but this effect may not be adequate to compromise the discriminant.

For the western U.S. we also compared amplitude and spectral characteristics of the regional signals recorded at RSTN station RSSD from several larger NTS explosions and comparable earthquakes in California. The observed  $L_g$  spectra seemed to be somewhat more sharply peaked for the explosions than the earthquakes. Bandpass filter analyses of the signals revealed some interesting dependencies of the  $L_g$ -to-P amplitude ratio on frequency; but significant source and path differences exist between the events compared, and the dependence on these factors needs further study.

This report is divided into five sections including this introduction. Section II describes the analysis of eastern North American quarry blasts and earthquakes using the RSTN and ECTN data. Section III presents the observations for the southern Soviet Union using the CDSN and Soviet/NRDC network data. Section IV describes the analysis of the LLNL and RSTN data from western U.S. nuclear explosions and earthquakes. Finally, in Section V we summarize the main conclusions from these studies and offer recommendations for further investigations of regional discrimination techniques.

## **II. EASTERN NORTH AMERICAN QUARRY BLASTS AND EARTHQUAKES**

### **2.1 Eastern North America Data Sources**

The stable continental areas of the central and eastern U.S. are thought to be analogous in many ways to the platform regions of the Soviet Union with regard to crustal properties and seismic wave transmission. Based on this analogy considerable research efforts (cf. Blandford, 1981; Pomeroy, 1977, 1979; Pomeroy *et al.*, 1982; Gupta *et al.*, 1984) over more than a decade have focused on understanding the propagation of regional phases in the eastern U.S. with the idea that this experience could be extended to the Soviet Union when regional seismic monitoring stations become available there. A particular problem in such monitoring environments is likely to be the identification of the frequent small explosions used in commercial development such as quarrying, mining and construction activities. The seismic discrimination problem could be greatly facilitated if simple procedures could be determined to distinguish these commercial blasts from small underground nuclear explosions. With this in mind a part of the current research effort was devoted to investigation of the regional phase seismic signals from small commercial blasts and nearby earthquakes in eastern North America. In these investigations we utilized data from two sources: the Regional Seismic Test Network (RSTN), in particular station RSCP, and the Eastern Canada Telemetered Network (ECTN). Each of these sources provided good quality digital seismic data with relatively high sampling rates permitting extraction and analysis of high frequency characteristics of the regional signals.

### **2.2 Analysis of RSTN Data**

The Regional Seismic Test Network was established in the early 1980's as a prototype of a high quality network of digital seismic stations providing real-time regional monitoring capability for North America. The network consisted of five stations located in New York (RSNY), Tennessee (RSCP), South Dakota (RSSD), Ontario, Canada (RSON) and Northwest Territories, Canada (RSNT) with digital data transmitted by satellite link to a central processing



facility.

It is well known from historical seismic monitoring in the eastern U.S. that the region frequently experiences small mine and quarry blasts which are detected on seismographs out to large regional distances. So it was not unexpected that the RSTN network stations would record numerous commercial blasts as well as regional earthquake activity; and a review of the recorded data revealed this to be true. In assembling a database of commercial blasts and regional earthquakes recorded at RSTN stations, we initially reviewed published reports and earthquake catalogs and bulletins appropriate to the regions surrounding the RSTN stations. Goncz *et al.* (1987) analyzed regional  $L_g$ ,  $P_n$  and  $S_n$  attenuation using recordings at the RSTN stations from earthquakes located throughout much of eastern North America during 1983 and 1984. The report provides a fairly extensive catalog of the larger eastern U.S. earthquakes during that time interval which were well recorded at the RSTN stations. To supplement that data set, we reviewed the NEIS catalogs, as well as regional catalogs published by St. Louis University, the Tennessee Earthquake Information Center (now Center for Earthquake Research Information), the Virginia Polytechnic Institute and State University and Boston College. Because of the extensive local seismic networks, the coverage is thought to be nearly complete for much of the eastern U.S. down to fairly low magnitudes ( $\approx 2 M_L$ ). However, for most of these bulletins an attempt has been made to exclude known or suspected quarry and mine blasts from the reported events. As a result only a few such explosions have been identified in the regional bulletins. Gupta *et al.*, (1984) identified six quarry blasts recorded at RSTN stations (5 at RSCP and 1 at RSNY) from a list of 20 such events provided by local university or state network operators. Smith (1987) looked for evidence of ripple firing in several northern Minnesota quarry blasts, but his primary data source was a temporary station near RSON although signals from some of these blasts were also recorded at RSON and RSSD. Personal communications with several operators of local seismic networks in the eastern U.S. suggested that formal catalogs of quarry and mine blasts detected by the networks do not exist. Most of the operators indicated that suspect events with strong short-period Rayleigh waves or with signals and locations close to those of known quarries in the region were eliminated from the earthquake catalogs on an ad hoc basis.

In the current investigation it was decided to focus on regional seismic signals recorded at station RSCP because it is well known from historical monitoring that the station records frequent mine blasts from the surrounding region which could be compared to similarly recorded earthquakes. Starting with the five blasts identified by Gupta *et al.* (1984), we found two additional presumed blasts identified in the Southeastern U.S. Seismic Network Bulletins. A few other presumed quarry blasts identified in the catalogs were not recorded at RSCP. To supplement the quarry blast database for RSCP, the detections recorded during a single day (viz June 19, 1985) were analyzed. Of the total detections on that date, about 40 events appear to have waveforms which look like real seismic signals (i.e., not typical ground or cultural noise). Sixteen of those 40 events which had the strongest signals were selected for further analysis. Only one of the 16 events selected was reported in the regional earthquake catalogs, and that was an apparent mine collapse in southwestern Virginia. None of the other 15 events were reported as earthquakes, and we therefore assume that they were mine or quarry blasts. The identification of these events as blasts appears to be corroborated by the observations of strong, short-period  $R_g$  phases in most cases suggesting a shallow focus and by the repetitive character of the waveforms for several of the events. The relative times of the P and  $L_g$  phases were used to estimate the epicentral distances and three-component analyses were performed on clear P-wave first motions to determine event azimuths. This location procedure was tested on the signals from the mine collapse, for which the location was known, and was found to give a nearly comparable result. So, although the locations determined by this single station procedure for these events would not be expected to have the precision of network locations, we believe them to be reasonable.

Table 1 provides the event locations and magnitudes (estimated from the  $L_g$  amplitudes) for 22 presumed mine blasts recorded at RSCP including the 15 newly identified events described in the preceding paragraph. The blasts had magnitudes from 2.2 to 3.5  $m_b(L_g)$  and epicentral distances in the range from 210 km to 369 km. Table 2 provides the locations and magnitudes of the 15 earthquakes and the mine collapse included in the database. The magnitudes were in the range 2.2 to 4.1  $m_b(L_g)$ ; and the epicentral distances were between 147 km and 490 km, except for one more distant earthquake at 942 km. The locations of all the events in the database relative to RSCP are shown in Figure 1. The events cover a wide range of azimuths surrounding RSCP; and, as

Table 1  
Presumed Mine Blasts Recorded at RSCP

Date	Origin Time	Lat. (°N)	Lon. (°W)	$\Delta$ (km)	$m_b(L_g)^\dagger$	h (km)
01-29-83	16:05:31.7	34.70	88.37	274	2.9	0
02-05-83	13:08:19.5	34.70	88.37	274	3.5	0
02-22-83	13:09:18.2	38.05	82.77	369	3.0	0
06-09-83	21:07:43.7	37.42	83.12	298	2.9	0
06-21-83	21:13:20.4	37.42	83.12	298	3.0	0
06-23-83	21:06:09.3	37.41	83.11	298	3.2	0
06-19-85	00:06:22*	37.0*	87.3*	220	3.1	0
06-19-85	01:37:58*	-	-	210	3.0	0
06-19-85	14:57:04*	37.3*	82.7*	310	2.5	0
06-19-85	15:59:58*	37.0*	87.3*	220	3.0	0
06-19-85	17:14:21*	33.2*	86.7*	280	3.3	0
06-19-85	18:20:29*	33.2*	86.7*	280	3.7	0
06-19-85	19:02:21*	37.3*	82.7*	310	2.9	0
06-19-85	19:22:26*	-	-	220	2.8	0
06-19-85	20:25:32*	33.2*	86.7*	280	3.2	0
06-19-85	20:55:34*	37.3*	82.7*	310	2.9	0
06-19-85	21:26:47*	-	-	210	3.1	0
06-19-85	22:10:26*	37.0*	87.3*	220	2.2	0
06-19-85	23:01:07*	37.0*	87.3*	220	2.4	0
06-19-85	23:11:22*	33.2*	86.7*	280	2.9	0
06-19-85	23:35:18*	-	-	200	2.6	0
11-07-85	08:17:13.0	33.77	84.07	245	2.3	1.1

\* Approximate origin times and locations estimated from relative times of P and  $L_g$  phases and three-component analysis of clear P-wave first motion.

† Magnitudes estimated from  $L_g$  amplitudes observed at RSCP using the magnitude formula for the Central U.S. -  $m_b(L_g) = 1.91 + 0.9 \log \Delta(\text{km}) + \log A(\mu\text{m})$ .

Table 2  
Regional Earthquakes and Mine Collapse Recorded at RSCP

Earthquakes

Date	Origin Time	Lat. (°N)	Lon. (°W)	Δ (km)	$m_b(L_g)$	h (km)
01-26-83	14:07:44.7	32.85	83.56	356	3.5	0
01-27-83	22:09:35.1	36.06	83.63	182	2.6*	12.8
03-25-83	02:47:11.1	35.33	82.46	283	3.2*	11.5
08-28-83	22:45:07.4	36.68	83.82	198	3.1*	18.1
02-14-84	22:56:20.4	37.21	89.00	356	3.6	2.0
04-17-84	04:44:44.9	38.41	88.48	405	3.2	14.3
04-23-84	01:36:00.1	39.92	76.36	942	4.1*	5.0
06-26-84	15:15:19.9	36.10	89.39	349	3.2	11.8
06-29-84	07:58:29.3	37.70	88.47	348	3.8	1.6
06-10-85	12:22:38.3	37.25	80.49	491	2.9 <sup>†</sup>	11.1
08-15-85	17:31:52.9	35.67	83.95	147	2.6 <sup>†</sup>	13.8
12-22-85	00:56:05.0	35.70	83.72	170	3.6 <sup>†</sup>	13.4
04-27-86	22:30:26.4	35.92	83.73	170	2.2 <sup>†</sup>	19.7
06-24-86	19:22:42.0	35.99	83.93	154	3.3 <sup>†</sup>	24.3

Mine Collapse

Date	Origin Time	Lat. (°N)	Lon. (°W)	Δ (km)	$m_b(L_g)$	h (km)
06-19-85	22:28:08.9	37.22	82.04	360	3.5	0

\* Magnitudes reported by Goncz et al., 1987.

† Magnitudes estimated from  $L_g$  amplitudes observed at RSCP using the magnitude formula for the Central U.S. -  $m_b(L_g) = 1.91 + 0.9 \log \Delta(\text{km}) + \log A(\mu\text{m})$ .

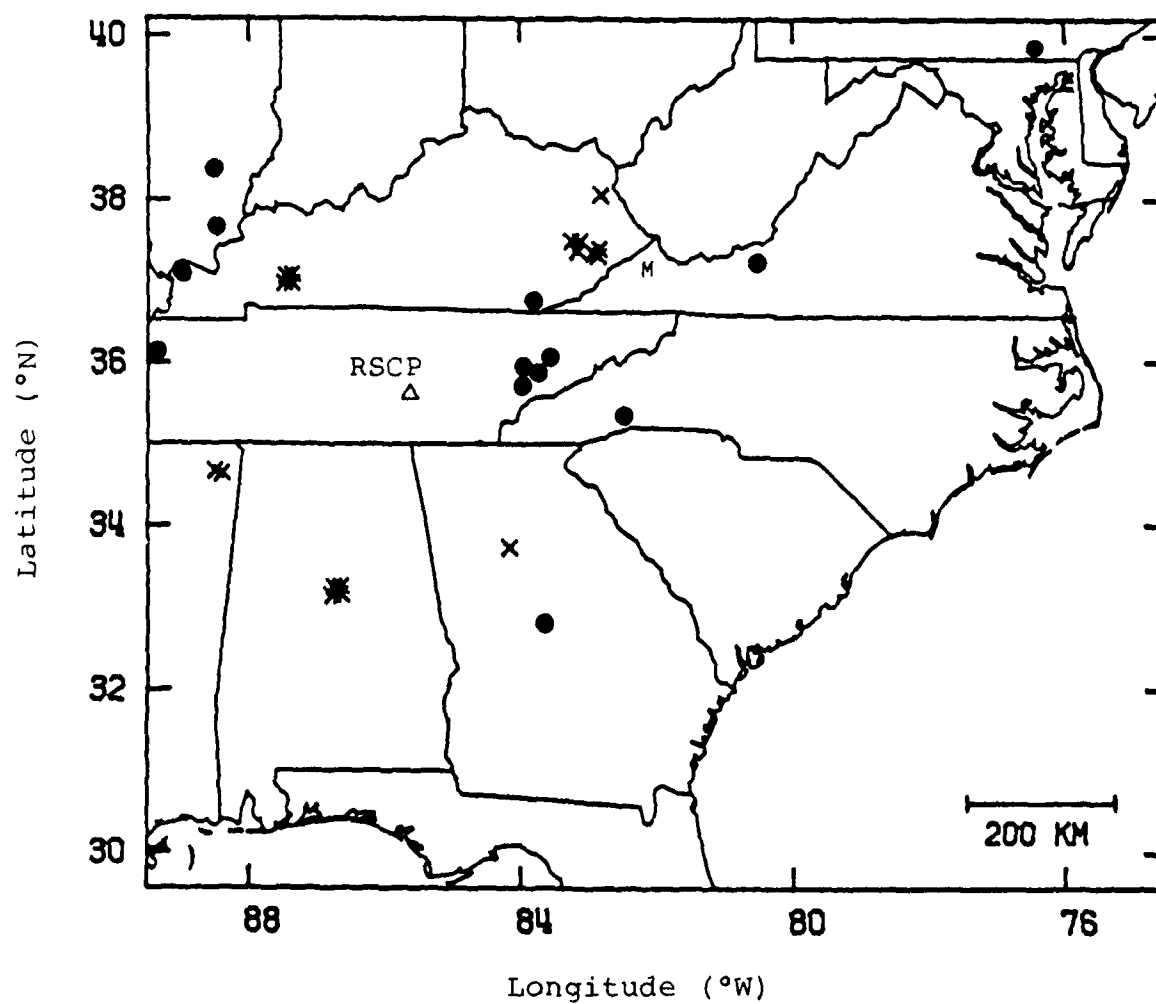


Figure 1. Locations of regional events recorded at RSCP. Earthquakes (●), presumed blasts (x), and mine collapse (M).

a result, there are some variations in propagation path. In general, events to the north and east were located in the Appalachian mountain chain while those to the west and south were located in stable continental platform areas as is the station.

Figure 2 shows typical vertical-component recordings of the seismic signals at RSCP from several source types at different ranges and azimuths. In all cases the records include clear P and  $L_g$  phases. These phases are typically quite complex in character apparently because of structure in the crust and upper mantle which controls propagation of these phases. The top three records illustrate the strong short-period dispersed Rayleigh-wave ( $R_g$ ) signals which are usually recorded from the mine and quarry blasts in the region. The observed  $R_g$  phase frequently has a predominant frequency near 1 Hz. Similar  $R_g$  signals have been reported for mine and quarry blasts throughout eastern North America (e.g., McEvilly, 1964; Herrmann, 1969; Kafka, 1988) and are believed to be associated with seismic excitation of shallow sedimentary layers in the crust by the near surface blast sources (cf. McEvilly, 1964; Kafka, 1987). The bottom four records in Figure 2 show the signals at RSCP from two additional mine blasts, an earthquake, and a mine collapse. In these records the  $R_g$  signals from the blasts are not nearly as obvious as for the top three examples. If the  $R_g$  signals are present, they are apparently buried in the coda of the  $L_g$  phase. There is little evidence of  $R_g$  in the earthquake, but the mine collapse produced a strong  $R_g$ .

First, considering the P and  $L_g$  phases, we compared the maximum P and  $L_g$  signal amplitudes for evidence of any source-dependent differences. The maximum amplitudes before and after the  $S_n$  arrival time (excluding the  $R_g$  signal), were measured from the broadband records for this purpose. In all cases the post- $S_n$  maximum corresponded to  $L_g$  while the pre- $S_n$  maximum sometimes corresponded to  $P_g$  but also was frequently the initial P( $P_n$ ) particularly for more distant events. For all 37 events in the RSCP database, the maximum P amplitude was smaller than the maximum S (viz  $L_g$ ) amplitude; this was true for the presumed blasts as well as the earthquakes and mine collapse. Figure 3 shows the amplitude ratio ( $L_g$  maximum/ P maximum) for all the events. The data overlap in magnitude (top) and epicentral distance range (bottom); and there appears to be little evidence of dependence of the amplitude ratio on either magnitude or distance. The results indicate that on

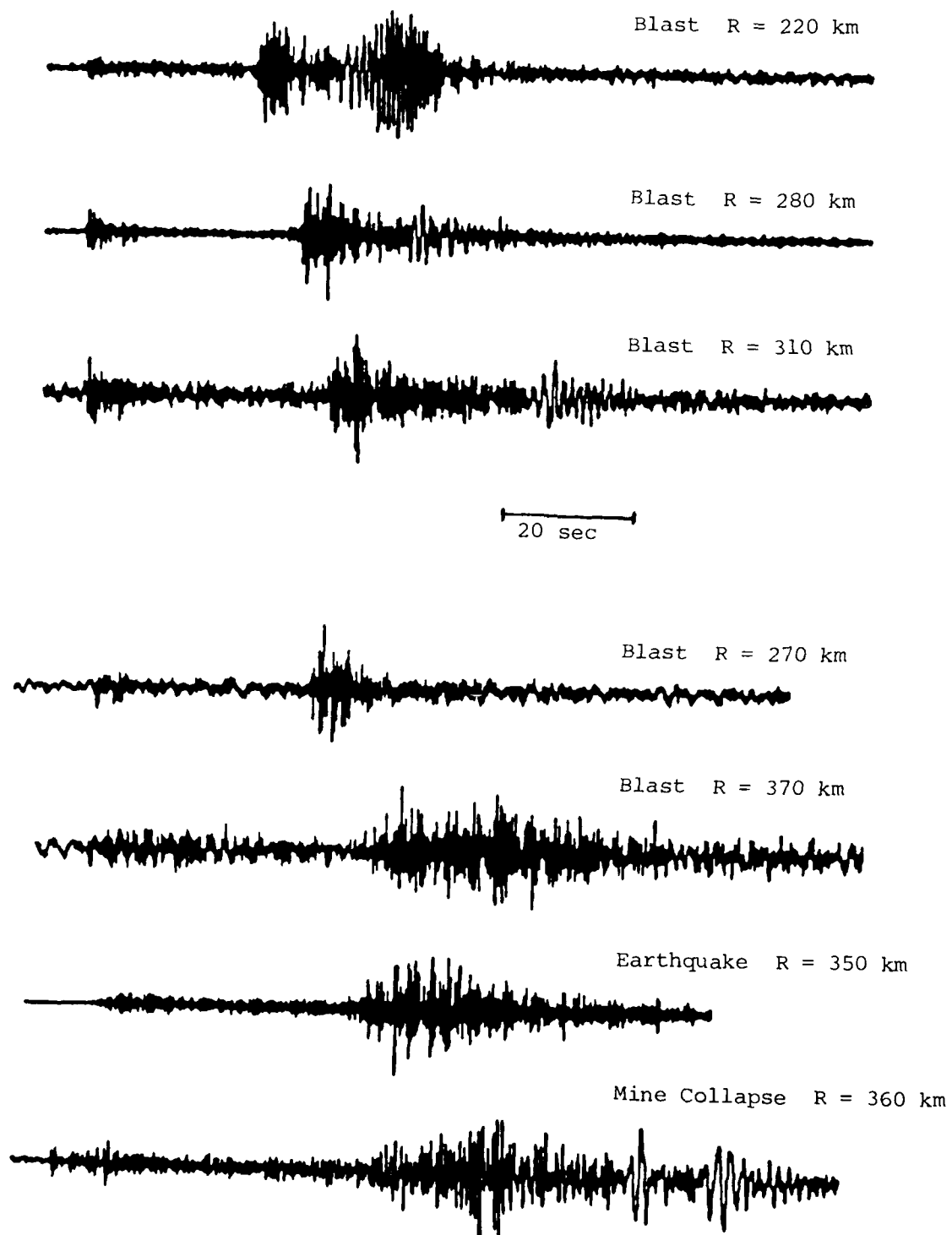


Figure 2. Vertical-component records at RSCP from typical regional events.

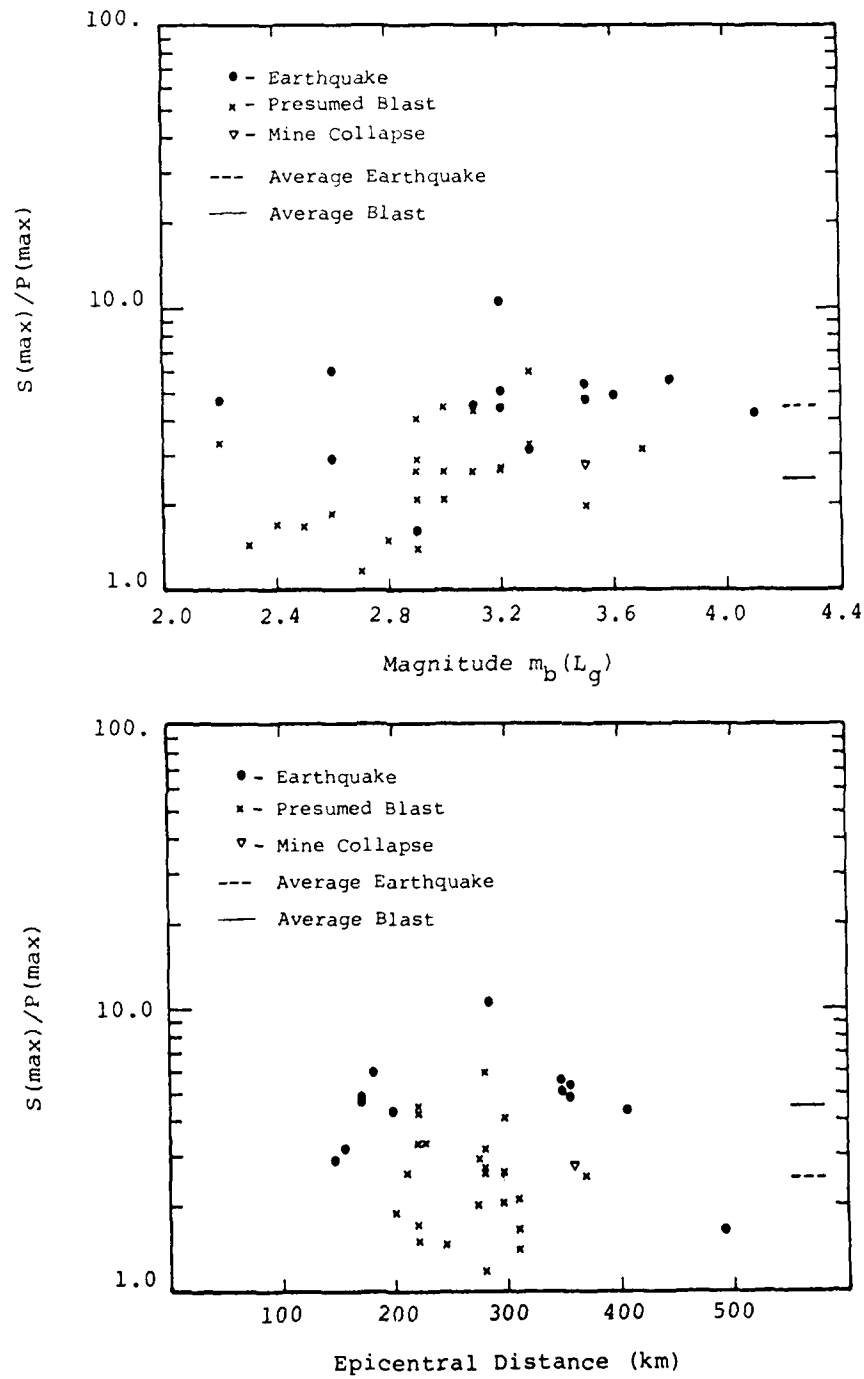


Figure 3. Peak amplitude ratio ( $S_{\max}/P_{\max}$ ) observed at RSCP as a function of magnitude (top) and epicentral distance (bottom).



average the earthquakes tend to have larger  $S(\max)/P(\max)$  ratios than the explosions in the sample, but there is considerable intermingling. So, simple peak-amplitude comparisons of the broadband  $P$  and  $L_g$  signals would not appear to provide reliable discrimination of the blast and earthquake sources.

In Figure 2 above we also found that the relative excitation of the  $R_g$  signal may not always provide a clear distinction between blasts and earthquakes. In an effort to enhance such differences, we band-pass filtered the records from several blasts, earthquakes and the mine collapse. These results are shown in Figure 4 where two alternate band-pass filters were applied to the vertical-component signals. The filter passbands were 0.5 to 1.5 Hz and 2.0 to 4.0 Hz; the unfiltered traces are also shown with each set for reference. For the first three blasts (cf. Figure 4, top), the 0.5 to 1.5 Hz filter sharply enhances the  $R_g$  signal relative to the  $P$  and  $L_g$  phases, which are concentrated in the higher frequency band. The 0.5 to 1.5 Hz filter in Figure 4, bottom, also enhances the  $R_g$  phase for the nearer blast and for the collapse, but the  $R_g$  phase does not stand-out in the filtered trace for the more distant blast. To some extent this is caused by relatively high ground noise in the filter passband for the latter event, but low excitation of the  $R_g$  phase may also be associated with some unusual blasting practice or depth for this event. We have no specific information on any of the blasts which have been analyzed, but normal shooting practice involves spatially-distributed and time-delayed charges which should enhance or nullify specific frequencies of the ground motion (cf. Willis, 1963; Frantti, 1963; Baumgardt and Ziegler, 1988). Finally, application of the filters to the earthquake record produces little evidence of any  $R_g$  signal. A slight trace of  $R_g$  appears in the second earthquake which was the shallowest of the three events with a focal depth of 2 km. In all cases the low-frequency  $R_g$  signal in the earthquakes is smaller relative to the higher-frequency  $P$  and  $L_g$  signals than in the explosions.

Spectral analyses were performed on the  $P$  and  $L_g$  signals from selected eastern U.S. earthquakes and quarry blasts to identify characteristics which could be distinctive. From the available data sample in Tables 1 and 2 above, we selected eight events which had relatively large signal-to-noise levels. An effort was made to pick events which correspond to different source types at somewhat comparable epicentral distance ranges. Figure 5 shows the vertical-component records for four events with ranges between about 170 km

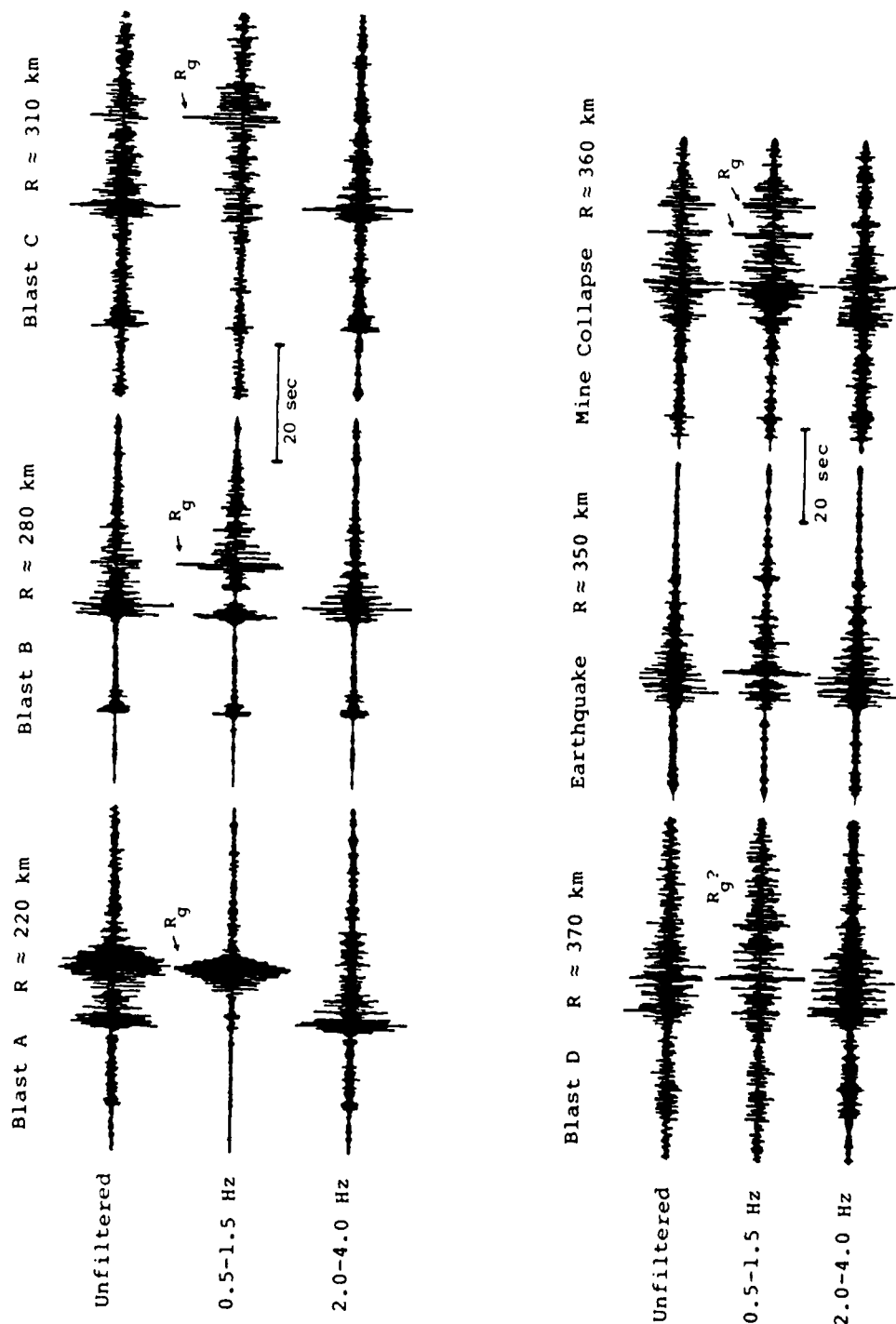


Figure 4. Application of band-pass filter at RSCP to enhance  $R_g$  signals.

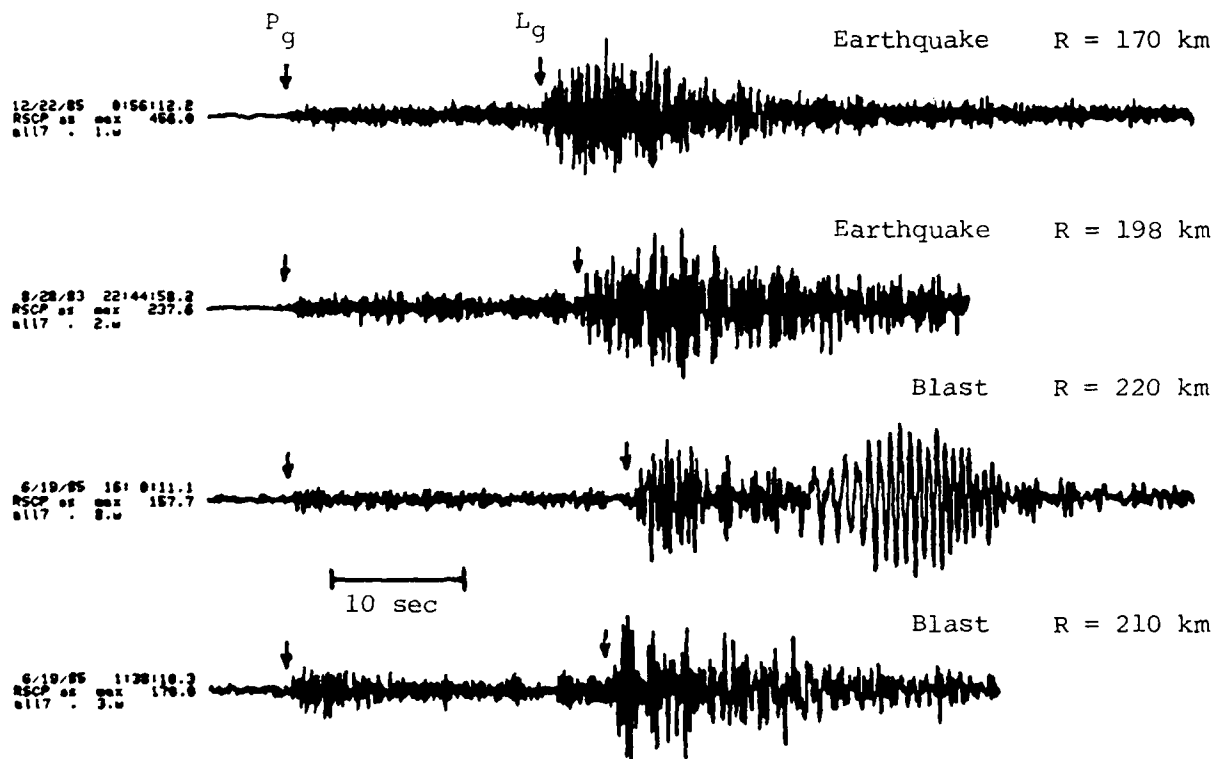


Figure 5. Vertical-component records for four events recorded at RSCP.

and 220 km from RSCP. The top two events are from the regional earthquake list (Table 2, above) and the bottom two are from the presumed regional blast list (Table 1, above). The events have roughly comparable magnitudes in the range 3.0 to 3.5  $m_b(L_g)$  with the earthquakes in the upper part and the blasts in the lower part of that range. We computed the spectra for windows surrounding the rather clear  $P_g$  and  $L_g$  signals whose starts are indicated by the arrows in Figure 5. The  $P_g$  windows were taken to be 256 points (6.4 seconds) in length and the  $L_g$  windows were taken to be 512 points (12.8 seconds). Noise windows including 128 points (3.2 seconds) were also analyzed at the start of each record. The spectra were all corrected for the RSCP instrument response.

Figures 6 and 7 show the corrected  $L_g$  and  $P_g$  spectra for the four events; the corresponding pre-P noise spectra are superimposed on the plots. In general, the ground noise is well below the signals for frequencies above about 1 Hz. Unfortunately, however, the dynamic range of the recording system at RSCP is low; so the signal spectra are not good above about 10 Hz even though the Nyquist frequency is at 20 Hz. This dynamic range problem is somewhat apparent in the lower left  $L_g$  spectrum of Figure 6 which starts to flatten at 7 Hz well above the ground noise level. In any case, the useful frequency band for spectral analysis at RSCP is extremely limited. Out to 10 Hz we see little evidence in the blast signals of spectral scalloping which has been found for time-delayed shots in some areas (cf. Smith and Grose, 1987; Baumgardt and Ziegler, 1988); it seems likely that the limited frequency band may impede such observations at RSCP. The spectra do appear to show other differences between earthquakes and explosions. The  $L_g$  spectra in Figure 6 have apparent corner frequencies near 3 Hz. Above the corner the spectra for the blast signals appear to fall-off much more rapidly than the earthquake signals. For the  $P_g$  signals the corner frequencies are somewhat more difficult to identify, but again the spectral fall-off above 3 Hz is greater for the blasts than for the earthquakes. The observed behavior in the  $L_g$  spectra are analogous to the behavior seen by Murphy and Bennett (1982) and Bennett and Murphy (1986) in  $L_g$  signals from NTS explosions and nearby earthquakes although the mechanism responsible for this observation could be considerably different.

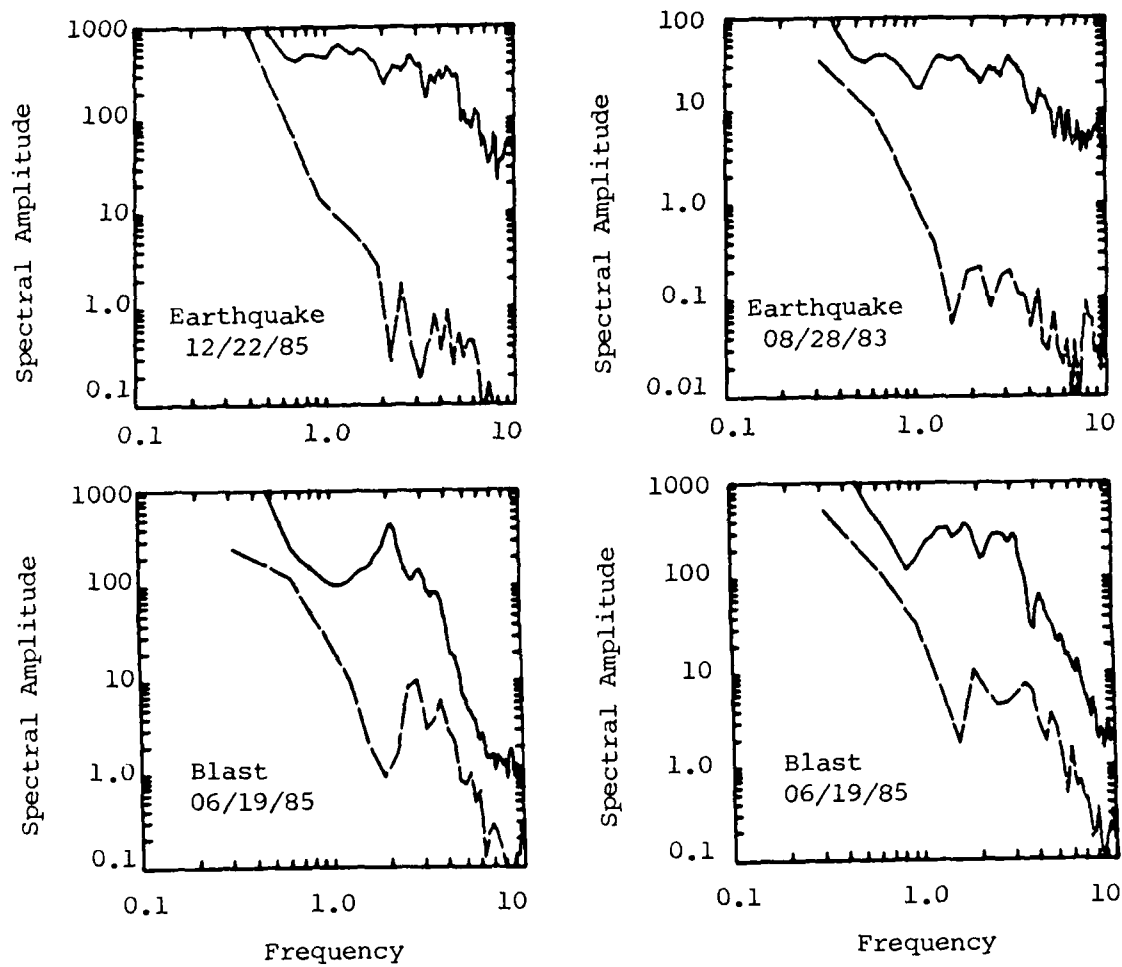


Figure 6.  $L_g$  spectra (solid line) and noise (dashed line) for the four events in Figure 5.

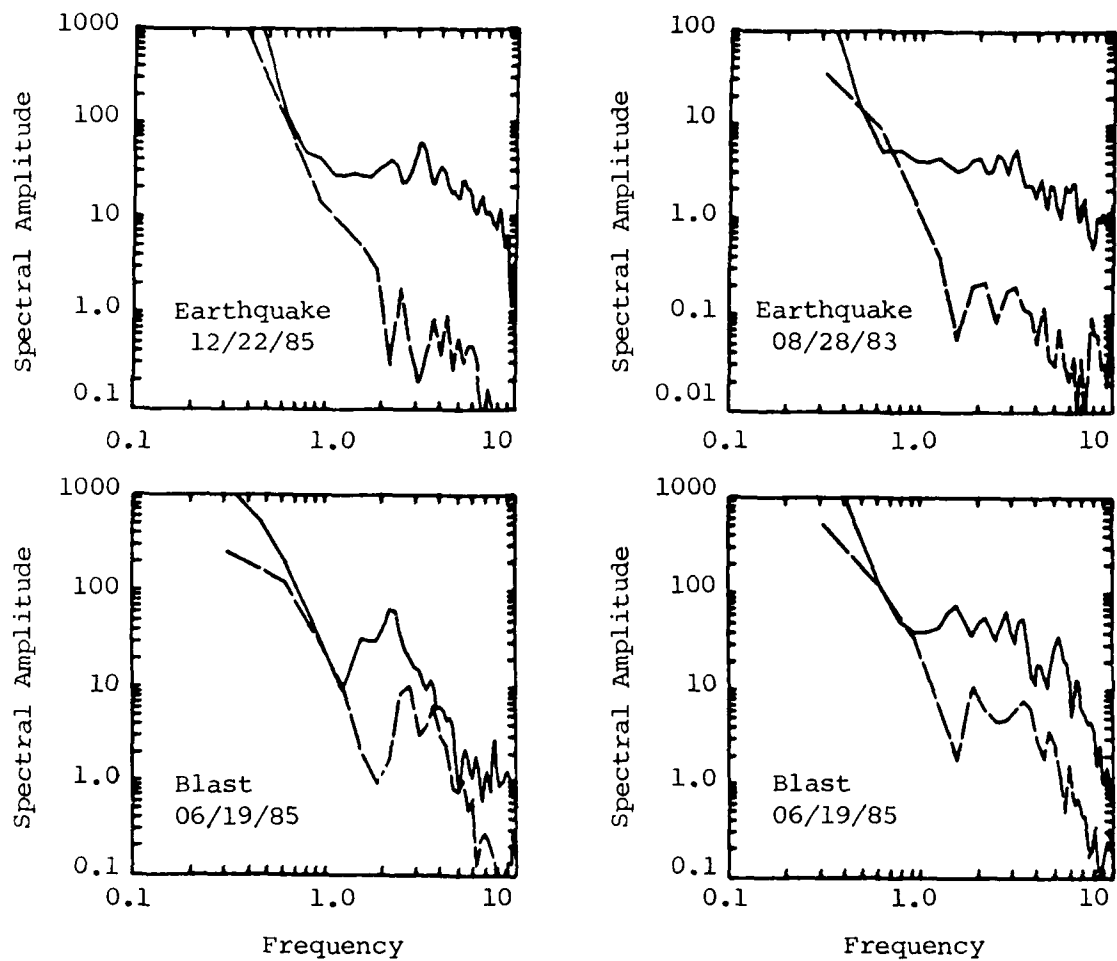


Figure 7.  $P_g$  spectra (solid line) and noise (dashed line) for the four events from Figure 5.

Figure 8 shows the vertical-component time histories for four additional events with ranges between about 270 km and 300 km from RSCP; the magnitudes are between 3.2 and 3.7  $m_b(L_g)$ . The top event is from the earthquake list, and the bottom three events are from the blast list.  $L_g$ ,  $P_g$  and noise spectra were computed for window lengths of 12.8 seconds, 6.4 seconds and 3.2 seconds, respectively; and the results, after correcting for instrument response, are plotted in Figures 9 and 10. The  $L_g$  spectra again show an apparent corner frequency near 3 Hz. Above this corner the  $L_g$  spectra for the bottom two events plotted in Figure 9 are observed to fall-off with frequency much more rapidly than for the top two events. A similar behavior is observed for the  $P_g$  spectra in Figure 10 although the corner frequencies are not so easily identified. A confusing aspect of these figures is that the top right spectrum in each of these figures corresponds to an event (Date 02/05/83) which had originally been identified as a blast in our tables, but the spectral behavior seems to be more comparable to the earthquake signal than to the blast signals. Reinvestigation of this event reveals that its identification as a blast in Table 1 was based on its assignment to a "blast" database by the Southeastern U.S. Seismic Network Bulletin. However, further investigation has revealed that, in addition to presumed mine blasts, this database included other unknown events from outside the geographical domain for which the Southeastern Network claims coverage. In fact, this event is identified in the St. Louis University Central Mississippi Valley Earthquake Bulletin as an earthquake with a felt report from Mississippi; and field studies by the Tennessee Earthquake Information Center (TEIC Quarterly Seismological Bulletin, January-March, 1983) confirm the earthquake identification. Concluding that this event was an earthquake, the  $L_g$  and  $P_g$  spectra in Figures 9 and 10 are again consistent with the previous observation that the earthquake spectra are relatively richer in higher frequencies than the corresponding blast spectra.

The spectral differences in regional phase signals between earthquakes and blasts is interesting but needs additional corroboration. It should be noted that the observations presented here correspond to a small number of events and that the propagation paths between comparable events do not coincide. As a result, path differences like attenuation or structural boundaries, which could affect the regional phase spectra, have not been taken into account. Other factors like changes in shooting practice between quarries or mines could also affect the  $P_g$  and  $L_g$  spectra. Considering the large number of

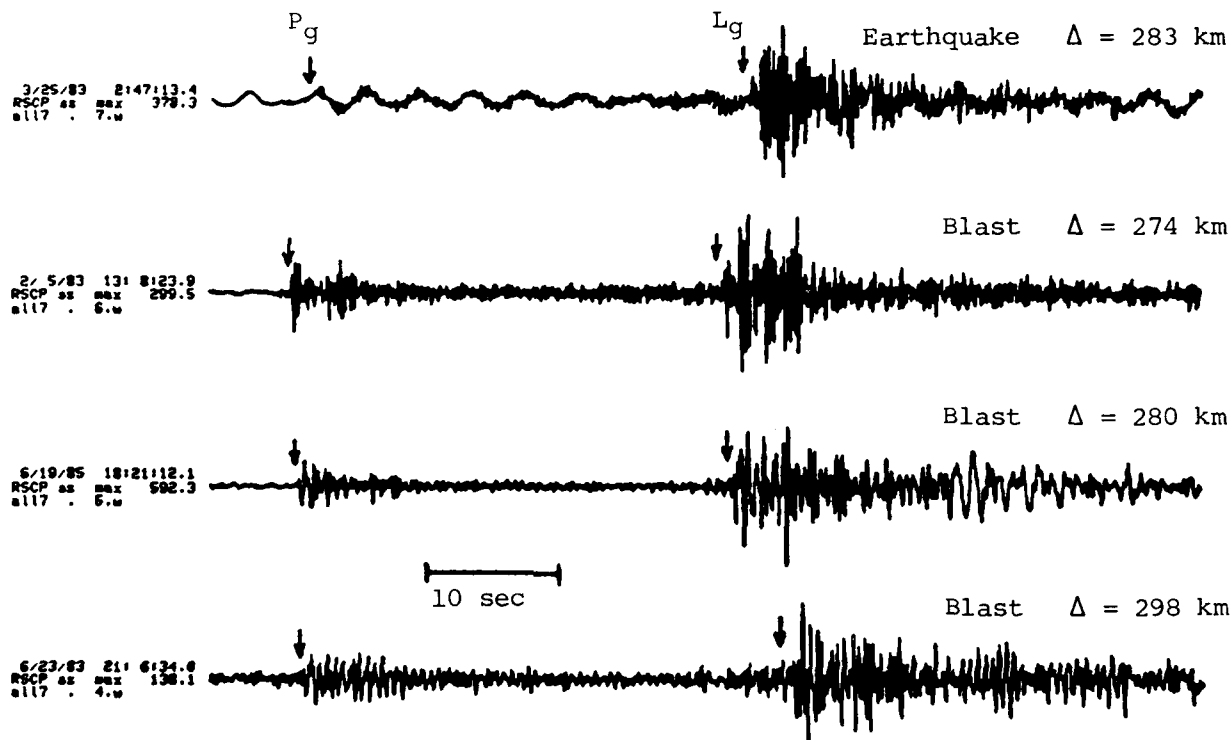


Figure 8. Vertical-component records for four other events recorded at RSCP.



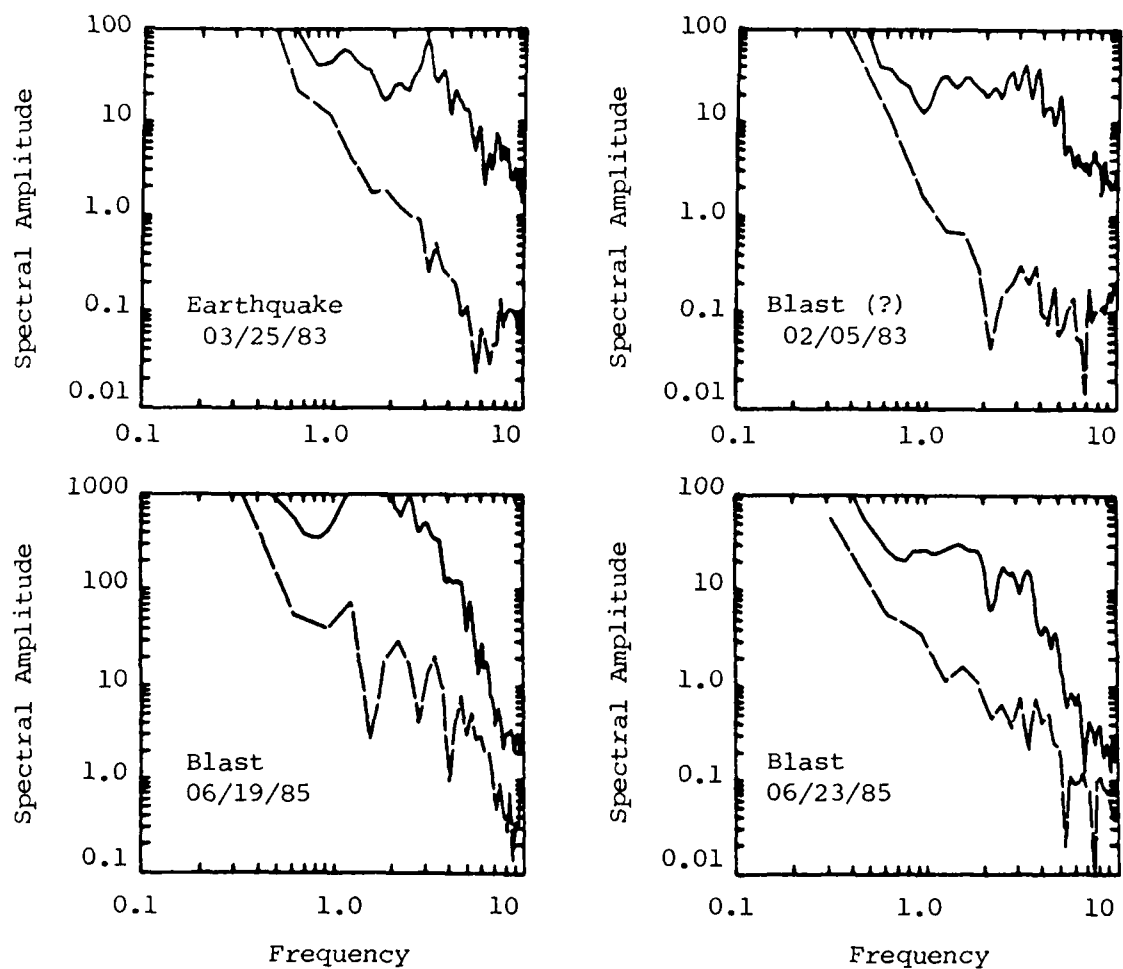


Figure 9.  $L_g$  spectra (solid line) and noise (dashed line) for the four events from Figure 8.

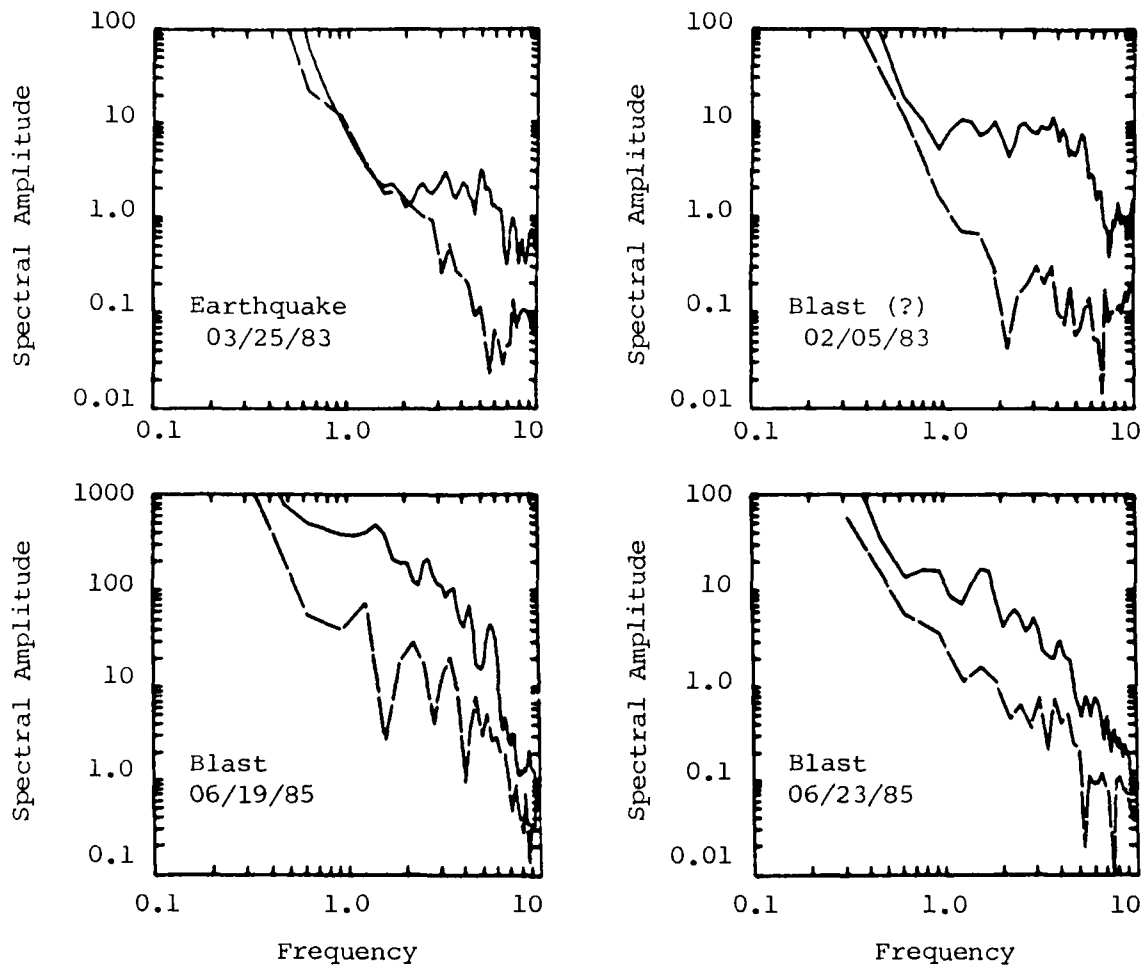


Figure 10.  $P_g$  spectra (solid line) and noise (dashed line) for the four events from Figure 8.

quarry blasts recorded on an almost daily basis by RSCP (and some of the other RSTN stations), the regional signals recorded by these stations appear to provide a good data source for investigating the distinctive characteristics of regional phases from quarry blasts in continental platform environments comparable to the Soviet Union.

### **2.3 Analysis of ECTN Data**

The Eastern Canadian Telemetered Network (ECTN) is a relatively-broadband, high-frequency dense network of high-quality stations located in a high-Q region. The network routinely records earthquakes and quarry blasts in the region up to a Nyquist frequency of 30 Hz. Typical events in the magnitude range of 2 to 3 may be recorded at several stations at distances less than 300 km. Therefore, this network provides a good research database to develop and test regional seismic monitoring procedures.

We have converted data for 36 events from ECTN data files to CSS format. The data were kindly provided by the University of Toronto. The 36 recovered events have magnitudes ranging from 0.1 to 5.1 and include 6 or 7 quarry blasts. There are on average about 10 stations recording each event.

Table 3 lists origin data provided by the University of Toronto. Events 20, 23, 34, 35, 36, and 37 were identified as probable quarry blasts. We suspect that event 7 may also be a blast based on the assigned depth of 1 km. Only 8 of the 37 origins have unconstrained depths. The rest of the depths have been assigned by a "Geophysicist". The magnitudes are a mix of "MB", "ML", and "MN". "MB" is the teleseismic  $m_b$  magnitude, "MN" is an  $L_g$  magnitude, while "ML" is a local Richter magnitude. Eleven of the events have been studied by Chun *et al.* (1987) with the two station  $L_g$  method and Chun *et al.* (1989) give additional  $L_g$  magnitude calibration information for 12 of the events.

The ECTN instruments are relatively broadband instruments recording at 60 samples per second, except GAC which is recording at 30 samples per second. Instrument responses are shown in Figure 11 for the ECTN Mark-I, Mark-II stations (vertical only) and the GAC installation (three components). The station locations are provided in Table 4.

**Table 3**  
**Origins for Available ECTN Data**

DATE				O.T.	N-LAT.	E-LONG.	H(KM)	MAG	#
Oct	04	1983	17:18:40.		43.45	-79.8	2G	3.1MN	1
Oct	07	1983	10:18:46.		43.94	-74.26	13G	5.1MB	2
Oct	07	1983	10:39:39.		43.95	-74.26	8G	3.5MB	3
Oct	11	1983	04:10:55.		45.20	-75.75	14G	4.1MB	4
Oct	16	1983	03:00:47.		45.62	-75.05	12.	3.1MB	5
Oct	16	1983	03:00:47.		45.62	-75.05	12.	3.1MB	6
Oct	24	1983	01:00:06.		48.14	-77.97	1G	3.1MB	7
Oct	03	1983	12:14:15.		44.14	-74.34	18G	2.8MB	8
Nov	01	1983	10:16:52.		45.67	-73.90	18G	3.4MB	9
Nov	16	1983	12:13:56.		47.00	-66.60	5G	3.2MB	1
Nov	17	1983	15:32:18.		47.00	-66.60	5G	3.7MB	11
Nov	18	1983	10:28:40.		47.00	-66.60	5G	3.0MB	12
Nov	27	1983	09:49:24.		46.80	-78.77	18G	2.8MB	13
Dec	04	1983	10:48:25.		45.19	-69.10	18G	3.1MB	14
Dec	08	1983	12:23:05.		45.11	-67.19	7.	3.0MB	15
Dec	09	1983	05:45:14.		44.48	-56.59	18G	3.6ML	16
Dec	09	1983	05:45:14.		44.48	-56.59	18G	3.6ML	17
Dec	01	1983	02:58:58.		44.53	-73.41	18G	2.7MN	18
Dec	01	1983	07:43:55.		45.70	-74.77	11.	2.8MN	19
Dec	11	1983	05:53:42.		45.12	-72.11	1G	2.4MN	20†
Dec	11	1983	01:52:03.		46.70	-76.27	18G	3.1MN	21
Dec	19	1983	20:00:36.		45.24	-66.77	5G	2.1MN	22
Dec	21	1983	15:04:44.		45.21	-73.96	10G	3.0MN	23†
Dec	28	1983	12:24:22.		47.07	-76.28	18G	3.5MN	24
Jan	15	1984	00:49:55.		46.54	-72.10	18G	2.5MN	25
Jan	15	1984	00:49:55.		46.54	-72.10	18G	2.5MN	26
Jan	02	1984	01:52:44.		47.53	-70.03	5.	0.1ML	27
Feb	02	1984	11:15:34.		44.66	-56.38	18G	4.2ML	28
Feb	11	1984	04:27:46.		46.49	-70.03	8.	1.0ML	29
Feb	11	1984	04:27:46.		46.49	-70.03	8.	1.0ML	30
Feb	13	1984	08:23:12.		46.91	-71.42	20G	2.2ML	31
Feb	13	1984	10:23:10.		46.88	-71.35	18G	2.1MN	32
Feb	15	1984	07:34:29.		47.50	-70.05	12.	0.7ML	33
Jul	07	1984	10:20:01.		46.88	-83.17	1G	2.9MN	34†
Jul	21	1984	09:28:00.		49.79	-82.31	1G	2.8MN	35†
Jul	21	1984	09:36:00.		47.94	-80.67	1G	2.8MN	36†
Sep	25	1984	04:00:00.		46.01	-71.37	1G	3.1MN	37†

† Probable Blasts

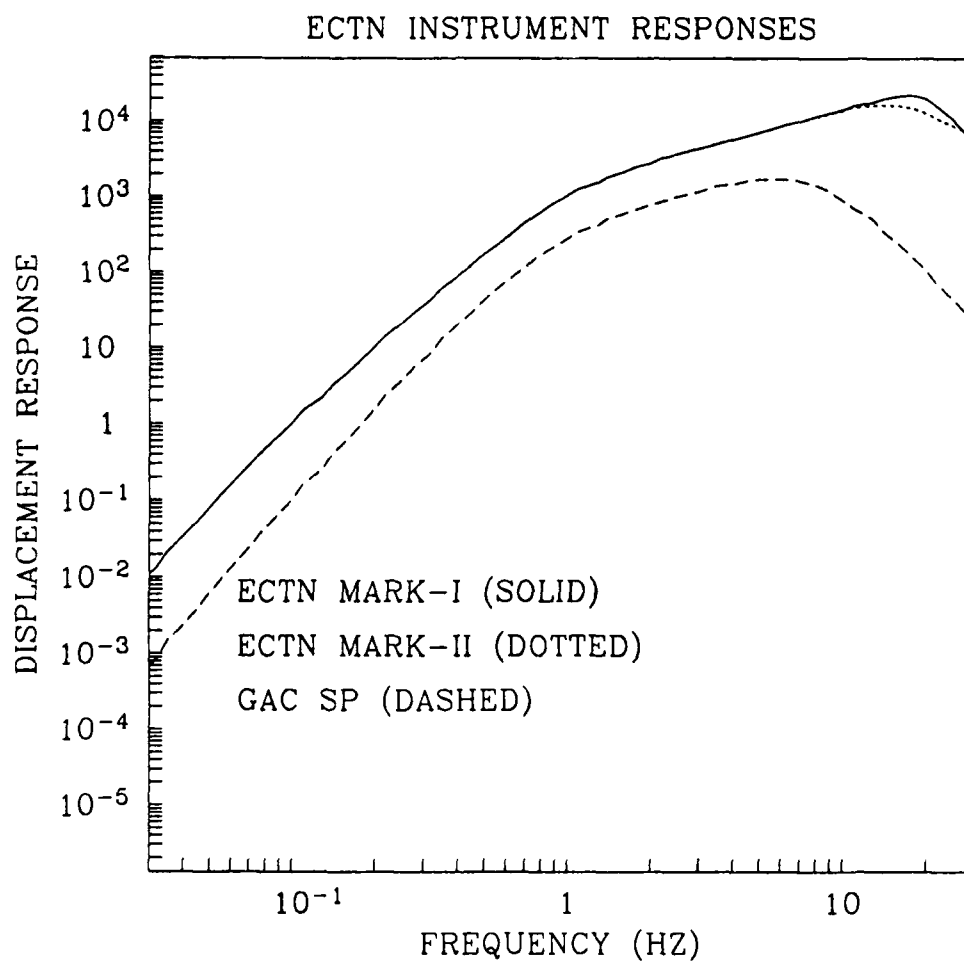


Figure 11. Instrument responses for the MARK-I, MARK-II and GAC systems at ECTN.

**Table 4**  
**ECTN Station Locations**

STA	N-LAT	E-LONG	ELEV(M)	LOCATION
CKO	45.9940	-77.4500	190	CHALK RIVER ONTARIO
EBN	47.4620	-68.2420	195	EDMONSTON N. B.
EEO	46.6411	-79.0733	398	ELDEE ONTARIO
GAC	45.7030	-75.4779	62	GLEN ALMOND QUEBEC
GGN	45.1170	-66.8220	30	ST. GEORGE N. B.
GNT	46.3628	-72.3722	10	GENTILLY QUEBEC
GRQ	46.6067	-75.8600	290	GRAND-REMOUS QUEBEC
GSQ	48.9142	-67.1106	398	GROSSES-ROCHES QUEBEC
HTQ	49.1917	-68.3939	123	HAUTERIVE QUEBEC
JAQ	53.8022	-75.7211	366	LA GRANDE-3 QUEBEC
JBQ	53.6103	-75.6053	381	LA GRANDE-3 QUEBEC
KAQ	53.9833	-73.5230	472	LA GRANDE-4 QUEBEC
KLN	46.8433	-66.3717	411	MCKENDRICK LAKE N. B.
LMN	45.8520	-64.8060	363	CALEDONIA MTN N. B.
LPQ	47.3408	-70.0093	126	LA POCATIERE QUEBEC
MNQ	50.5333	-68.7744	610	MANICOUAGAN S. QUEBEC
MNT	45.5025	-73.6230	112	MONTREAL S. QUEBEC
OTT	45.3939	-75.7158	83	OTTAWA S. ONTARIO
SBQ	45.3783	-71.9263	265	SHERBROOKE QUEBEC
SUO	46.4027	-81.0068	252	SCIENCE N. SUDBURY ONTARIO
TRQ	46.2222	-74.5556	858	MONT-TREMBLANT QUEBEC
VDQ	48.2300	-77.9717	305	VAL-D OR QUEBEC
WBO	45.0003	-75.2750	85	WILLIAMSBURG ONTARIO
WEO	44.0186	-78.3744	149	WELCOME ONTARIO
SCP	40.7950	-77.8650	352	STATE COLLEGE PA. (DWWNSSN)
RSNY	44.5483	-74.5300	357	ADIRONDACK N.Y. (RSTN)
RSON	50.8589	-93.7022	357	RED LAKE ONTARIO (RSTN)

A map is shown in Figure 12 with station and event locations. Stations are indicated with triangles and the three stations SCP, RSNY, and RSON are plotted for reference. Events are plotted as crosses and the probable quarry blasts are indicated with a circle around the cross.

Among the various issues that we wished to address with this data, was the reliable estimation and interpretation of cepstra to be used in discrimination between earthquakes and quarry blasts. Several researchers in recent years have reported the detection of ripple-firing in recordings of quarry blasts (c.f. Baumgardt and Ziegler, 1988; and Smith 1988b). In addition, Alexander and Borkowski (1988) report the use of cepstral methods to estimate pP-P and sP-P times from regional seismograms. With the exception of Alexander and Borkowski, most cepstral analysis has been performed on a single station or a small array of stations. With its density of coverage in a high-Q area, the ECTN has the capability of giving multiple estimates of cepstra and allowing us to gauge the robustness of single station estimates. Also of interest is the bandwidth of the network since cepstral analysis requires the maximum available bandwidth. The ECTN stations have a Nyquist frequency 50 percent higher than the RSTN, DWWSSN, or NORESS array stations. Although the NORESS high-frequency station has a greater sampling rate than the ECTN, it is only one station.

First, we review cepstral analysis and some of the statistics of the estimation procedure. We make several observation about the process of cepstral estimation,

- Cepstral analysis is not an objective model independent analysis.
- There are no published criteria for judging the statistical significance of a cepstral peak.
- Bandwidth is critical to cepstral analysis and most data available does not have enough bandwidth to resolve the smallest time delays associated with ripple firing.

Given these considerations, we derive some statistical criteria for the evaluation of the significance of cepstral peaks and show that there is a maximum likelihood estimator for the combination of network data. The network stacking method of Alexander and Borkowski is related to this maximum

# ECTN EVENTS AND STATIONS

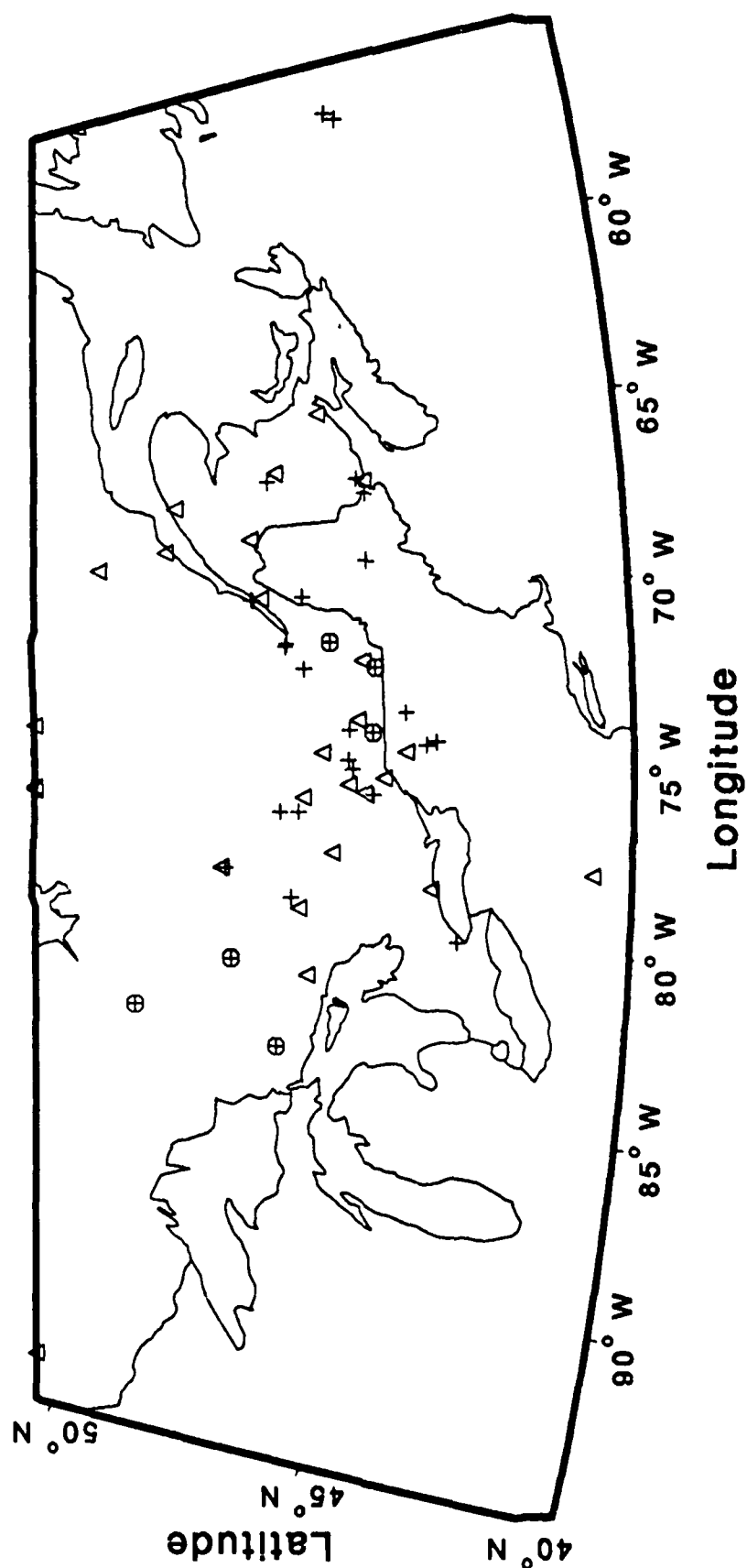


Figure 12. Map of ECTN stations and events. Stations indicated with triangles, events with crosses, and probable quarry blasts with circled crosses.



likelihood network estimator. Given that cepstral estimation is a model dependent procedure, we propose a procedure that balances bandwidth resolution against model dependence by use of a well-defined smoothing operator. Finally, the results for several probable quarry blasts and earthquakes are shown and discussed.

### 2.3.1 A Review of Cepstral Theory

The cepstrum is defined as the Fourier transform of the log of the power spectrum of the signal (Oppenheim and Schaffer, 1975). If  $s(t)$  is the time domain signal and  $P(f)$  is its power spectrum then the cepstrum,  $C(\tau)$ , is the spectrum of  $\ln(P(f))$ . If we write the Fourier transform operator as  $F[.,f]$  and the time domain taper as  $\theta(t)$  then we have that

$$P(f) = |F[\theta(t)s(t), f]|^2 = |\Theta(f) \times S(f)|^2$$

$$C(\tau) = F[\ln(P(f)), \tau] = F[\Pi(f), \tau]$$

where  $\times$  is the convolution operation. The intent of cepstral estimation is to analyze the modulation of the power spectrum. With the use of some algebra, simple identities related to Fourier spectra, and a Taylor series expansion for  $\ln()$ , it can be shown (see Flinn *et al.*, 1973) that if the signal contains an echo of relative amplitude  $b$  with time delay  $\tau_0$  described by

$$s(t) = a(t) + b a(t + \tau_0),$$

then the cepstrum is

$$C(\tau) = F[\ln(P(f)), \tau] + F[\ln(1 + b^2 + 2b\cos(2\pi f\tau_0)), \tau]$$

$$\approx F[\Pi(f), \tau] + 2bF[\cos(2\pi f\tau_0), \tau]$$

$$\approx \pi(\tau) + 2b\delta(|\tau - \tau_0|).$$

Therefore  $C(\tau)$  will have a peak located at  $\tau = \tau_0$  and  $\tau = -\tau_0$ . The size and resolution of the peak will be determined by the relative amplitude of the

echo,  $b$ , and the shape of the log-power spectrum  $\pi(\tau) = F(\Pi(f), \tau)$ . This interfering term is the Fourier component of the shape of the log-power spectrum without the echo. Since we are usually interested in small time delays, we are concerned with the shape of the spectrum over large bandwidths. Since no realistic seismic signal has a flat spectrum, it is necessary to remove any trends and general shape of the log-power spectrum prior to estimating the cepstrum. Some model for  $\Pi(f)$  is assumed (or fit) in order to remove the interfering effects of the broadband shape of the log-power spectrum. This is analogous to a trend removal and taper in the time domain prior to estimating the power spectrum. As the analogy suggests, this pre-whitening of the log-power spectrum introduces artifacts into the cepstrum just as tapering affects the estimation of the power spectrum. For example, smoothing of the log-power spectrum will introduce a multiplicative response into the cepstrum. We can not escape the fact that the processing at this step is nonlinear and model dependent.

To be precise, we may either add (or subtract) a correcting function,  $\zeta(f)$ , to the log-power spectrum, multiply (or divide) the log-power spectra by a correcting function,  $\kappa(f)$ , or convolve a smoothing operator,  $\gamma(f)$ , with the log-power spectra. The result of adding a correction is,

$$\begin{aligned}\tilde{C}(\tau) &\approx F[(\zeta(f) + \ln(P(f)) + 2b\cos(2\pi f\tau_0)), \tau] \\ &\approx Z(\tau) + \pi(\tau) + 2b\delta(|\tau - \tau_0|).\end{aligned}$$

The result of applying a multiplicative correction is,

$$\begin{aligned}\hat{C}(\tau) &\approx F[\kappa(f)(\ln(P(f)) + 2b\cos(2\pi f\tau_0)), \tau] \\ &\approx K(\tau) \times [\pi(\tau) + 2b\delta(|\tau - \tau_0|)].\end{aligned}$$

And the result of convolving a smoothing operator is,

$$\begin{aligned}C'(\tau) &\approx F[\gamma(f) \times (\ln(P(f)) + 2b\cos(2\pi f\tau_0)), \tau] \\ &\approx \Gamma(\tau)[\pi(\tau) + 2b\delta(|\tau - \tau_0|)].\end{aligned}$$

In practice, all three things are done to the power spectrum in order to prepare it for cepstral estimation and we have,

$$C(\tau) \approx \Gamma(\tau)K(\tau) \times [Z(\tau) + \pi(\tau) + 2b\delta(|\tau - \tau_0|)].$$

Generally, the log-power spectrum is pre-whitened by the removal of a trend which is equivalent to assuming the power spectrum is proportional to frequency raised to some power,  $f^{-a}$ , where  $-a$  is the slope of the log-power spectrum. Since most seismic spectra have this form at high frequencies, this may be a good model. However, since most seismic log-spectra are also concave downward (due to corner frequency and attenuation), the effect of a simple slope correction is to introduce a cepstral signal with broad bandwidth and significant cepstral power at low quefrequency. If a signal with 20 Hz Nyquist and 10 Hz corner frequency is subjected to a detrending, a 10 Hz modulation will remain in the log-power spectrum and show up as a 0.1 sec quefrequency peak in the cepstrum. This will be true even if the bandwidth from 0 to 20 Hz has infinite signal-to-noise ratio.

The effects of limited bandwidth are even more subtle. If signal-to-noise ratio is such that the bandwidth is limited to a simple window in the frequency domain, such as  $f_1$  to  $f_2$ , then the cepstrum will contain the Fourier transform of the spectral bandwidth (boxcar from  $f_1$  to  $f_2$ ) and a false peak may occur at  $1/|f_2 - f_1|$ . For example, suppose the 20 Hz Nyquist signal is limited to 2 to 15 Hz, then we can only expect to resolve quefrequencies longer than 1/13 seconds. A number of researchers have attributed quefrequency peaks shorter than 0.2 seconds to multiple sources with data limited to a 20 Hz Nyquist and bandwidths significantly less than 0 to 20 Hz.

An additional misconception may arise due to padding in the frequency domain. The power spectrum is defined from  $-f_N$  to  $f_N$  and the cepstrum is computed using a total bandwidth of  $2f_N$  that implies an apparent resolution of  $\delta\tau = 1/2f_N$ . In fact this is misleading, since the power spectrum contains the symmetry,  $P(f) = P(-f)$ , and the doubling of the power spectrum is only equivalent to a sinc interpolation. The best possible resolution is limited to  $\delta\tau = 1/f_N$ . As the previous discussion makes clear, practical resolution is limited to the reciprocal of a spectral window for which we have adequate signal-to-noise

ratio,  $\delta\tau = 1/|f_1 - f_2|$ . Furthermore, it is well known that Fourier estimation of low frequencies is a very difficult problem unless the window includes two or more cycles. These low frequencies (quefrequencies in this case) are very sensitive to the de-trending algorithm and leakage from other quefrequencies. Consequently, it is unwise to take much stock in detections of quefrequencies less than  $3/f_N$ . For a 20 Hz Nyquist signal this is 0.15 second quefrequency or 0.1 second for a 30 Hz Nyquist.

Since pre-whitening is necessary, the procedure is model dependent and the model assumptions must be examined as part of the procedure. It is possible to view the detection of multiple shots as a fitting procedure to the spectra. This is in effect proposed by Smith (1988b) who claims that bandwidths of at least 35 Hz will be required in order to make reliable detections of ripple firing with group delays of 100 to 200 milliseconds. From the point of view of cepstral analysis, this amounts to the  $\tau > 3/f_N$  criteria stated above.

Finally, we can examine the detection of cepstral peaks using extensions of statistical methods traditionally applied to the detection of spectral peaks in power spectra. Assuming that the pre-whitening model has been applied correctly then we have  $\Pi(f) = \ln(P(f)) + W(f)$  where  $W(f) = \ln(w(f))$  is the deterministic pre-whitening correction. We note that  $P(f)w(f)$  is distributed  $\chi^2$  with two degrees of freedom assuming that  $w(f)$  correctly pre-whitens the spectrum (Shumway, 1988). Therefore  $\Pi(f) = \ln(P(f)w(f))$  is zero-mean normal with unit variance except for any modulation due to the interference of multiple sources. Then  $|C(\tau)|^2$  is the power spectrum of a Gaussian white-noise process plus the spectrum of the modulation. We can establish a 95 percent detection criteria for peaks of  $C(\tau)$  assuming that  $|C(\tau)|^2$  is distributed  $\chi^2$  with 2 degrees of freedom in the absence of modulation due to multiple sources. Any peak greater than the 95 percent significance level is considered to be true modulation of the log-power spectrum.

Now in order to pre-whiten the log-power spectra, we choose to subtract a correction spectra derived from the convolution of a smoothing operator (low-pass filter) with the log-power spectrum. In this way we try to minimize the model errors associated with the pre-whitening of the log-power spectrum. We give up resolution of the smallest quefrequencies to attain a better (unbiased) estimate of the cepstra for  $\tau > \tau_L$ . We choose  $\tau_L$  to be in the neighborhood of  $3/f_N$ .

Figure 13 shows a flow chart that describes the process. The smoothing operator (low-pass filter),  $\gamma(f)$  is applied so that the cepstral estimator is given by,

$$C(\tau) = F[2\ln(|F[s(t)\theta(t)], f|) \times (1 - \gamma(f)), \tau],$$

$$= F[2\ln(|S(f) \times \Theta(f)|) \times (1 - \gamma(f)), \tau],$$

$$= F[2\ln(|S(f) \times \Theta(f)|), \tau](1 - \Gamma(\tau)).$$

$\Gamma(\tau)$  decays to zero for  $\tau > \tau_L$  such that the cepstra above  $\tau_L$  are undisturbed.

We have discarded the lowest frequencies as unreliable. These frequencies are expected to be diagnostic of the ripple firing usually associated with delays measured in the 0.1 to 0.01 second range. However, if we reexamine the tapered signal as a sum of  $N$  subsignals of size  $b_k$  with time delays  $\tau_k$  then

$$s(t) = \theta(t) \sum_{k=1} t_0 N b_k a(t + \tau_k)$$

$$P(f) = |\Theta(f) \times A(f)|^2 (1 + 2 \sum_{k=1} t_0 N b_k \cos(2\pi f \tau_k) + \sum_{k,j=1} t_0 N b_k b_j \cos(2\pi f(\tau_k - \tau_j)))$$

$$\Pi(f) = \ln(P(f)) \approx 2\ln(|\Theta(f) \times A(f)|)$$

$$+ 2 \sum_{k=1} t_0 N b_k \cos(2\pi f \tau_k)$$

$$+ \sum_{k,j=1} t_0 N b_k b_j \cos(2\pi f(\tau_k - \tau_j)) + \dots$$

$$C(\tau) \approx F[2\ln(|\Theta(f) \times A(f)|), \tau](1 - \Gamma(\tau))$$

$$+ 2(1 - \Gamma(\tau)) \sum_{k=1} t_0 N b_k \delta(\tau - \tau_k)$$

CEPSTRAL ESTIMATION WITH CONVOLUTIONAL PRE-WHITENING  
AND SIGNIFICANT PEAK DETECTION

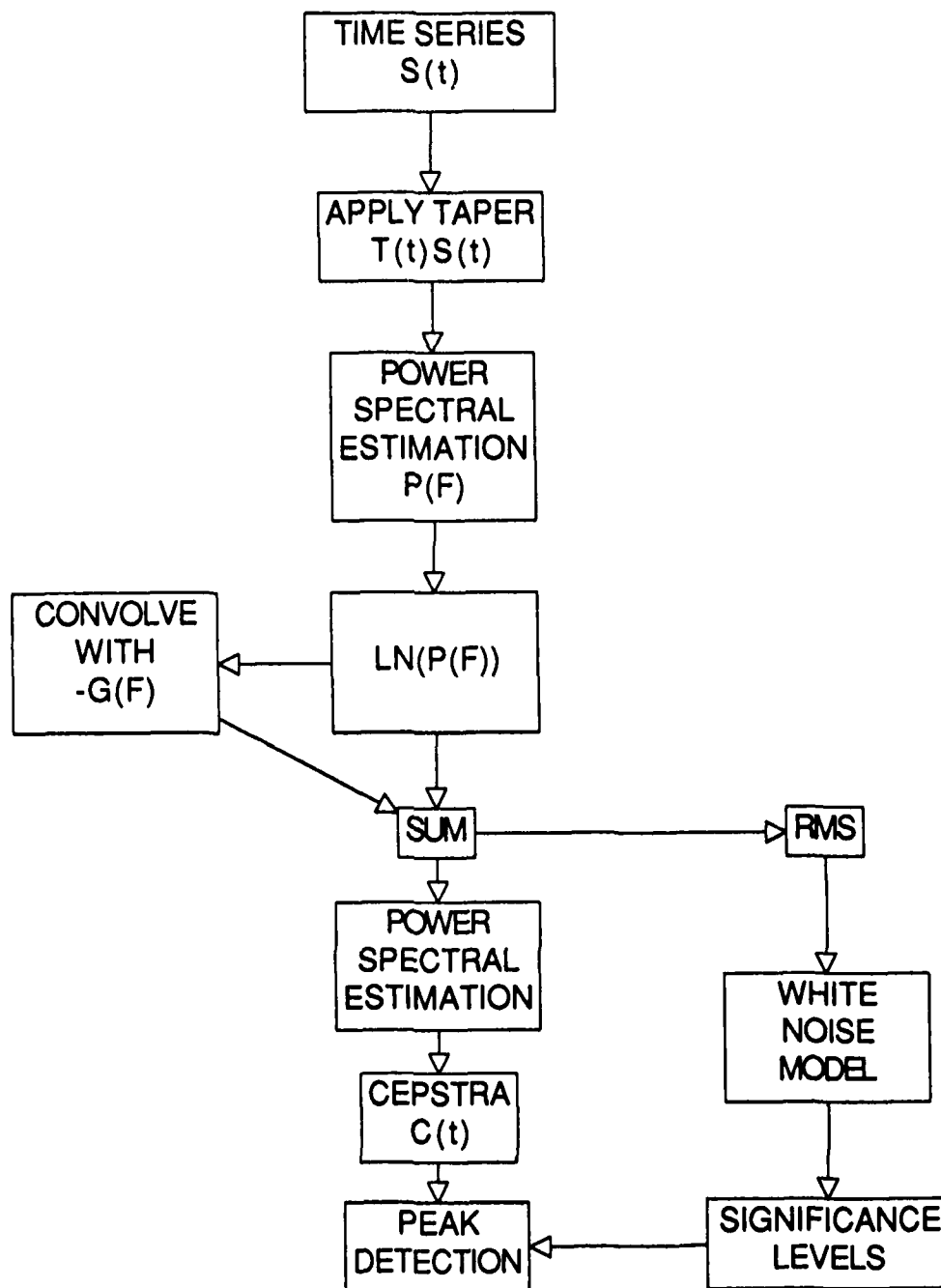


Figure 13. A flow chart describing the estimation of cepstra using a low-pass smoother  $\gamma(f)$  to derive a baseline log-power spectrum to prewhiten the log-power spectra prior to estimation of cepstra.

$$+ (1 - \Gamma(\tau)) \sum_{k,j=1} t_0 N b_k b_j \delta(|\tau - (\tau_k - \tau_j)|) + \dots$$

Depending upon the shot array  $(\tau_1, \dots, \tau_N)$  the last term may make significant contributions for delays approaching the duration of the shot array. Since the shot arrays are often designed to "stretch-out" the shot duration (Dowding, 1985) in order to minimize high-frequency near-field accelerations, the contribution to the cepstrum of all of the delay differences can not be ignored. A synthetic example is shown in Figure 14 (left). The synthetic shot array consists of 100 shots, 10 rows of 10 shots each. Rows and columns are detonated at 50 msec intervals and a 5 msec standard deviation is assumed for each blasting cap (Dowding page 242). The cepstra are "perfect" in that they do not include any blurring effects due to limited bandwidth, tapering, spectral smoothing, or incoherence between shots that may occur if the individual explosion sources are not identical. Note that significant cepstral peaks occur at multiples of the 50 msec delay between shots. However, a shot pattern may be chosen that shows no isolated peaks. A synthetic 10x10 shot array with 30 and 50 msec delay times is shown in Figure 14 (right). Note the absence of isolated cepstral peaks. Isolated cepstral peaks by themselves may not be sufficient to identify ripple firing.

In order to verify that peaks in the cepstra are significant most researchers have either examined cepstra from different stations or different phases at the same station. Baumgardt and Ziegler (1988) using NORESS data examined the cepstra of different phases. Alexander and Borkowski (1988) used several regional stations and stacked the cepstra from independent stations within the network. Alexander and Borkowski used both a linear (mean) and a non-linear (product) stacking procedure for the cepstra. Given that the cepstra are distributed  $\chi^2$ , which is approximately log-normal, the geometrical mean of the network is an appropriate averaging procedure. The geometrical mean would constitute a maximum likelihood estimate under these assumptions. Alexander and Borkowski used the product of the cepstra without taking the n'th root as would be required for a geometrical mean. As presented, the cepstral peaks in the work of Alexander and Borkowski are probably misleading with their apparent large signal-to-noise figure. In the following analysis, we compare stacking of the cepstra versus stacking of the power spectra. We find that stacking of the detrended power spectra from the network appears to give a

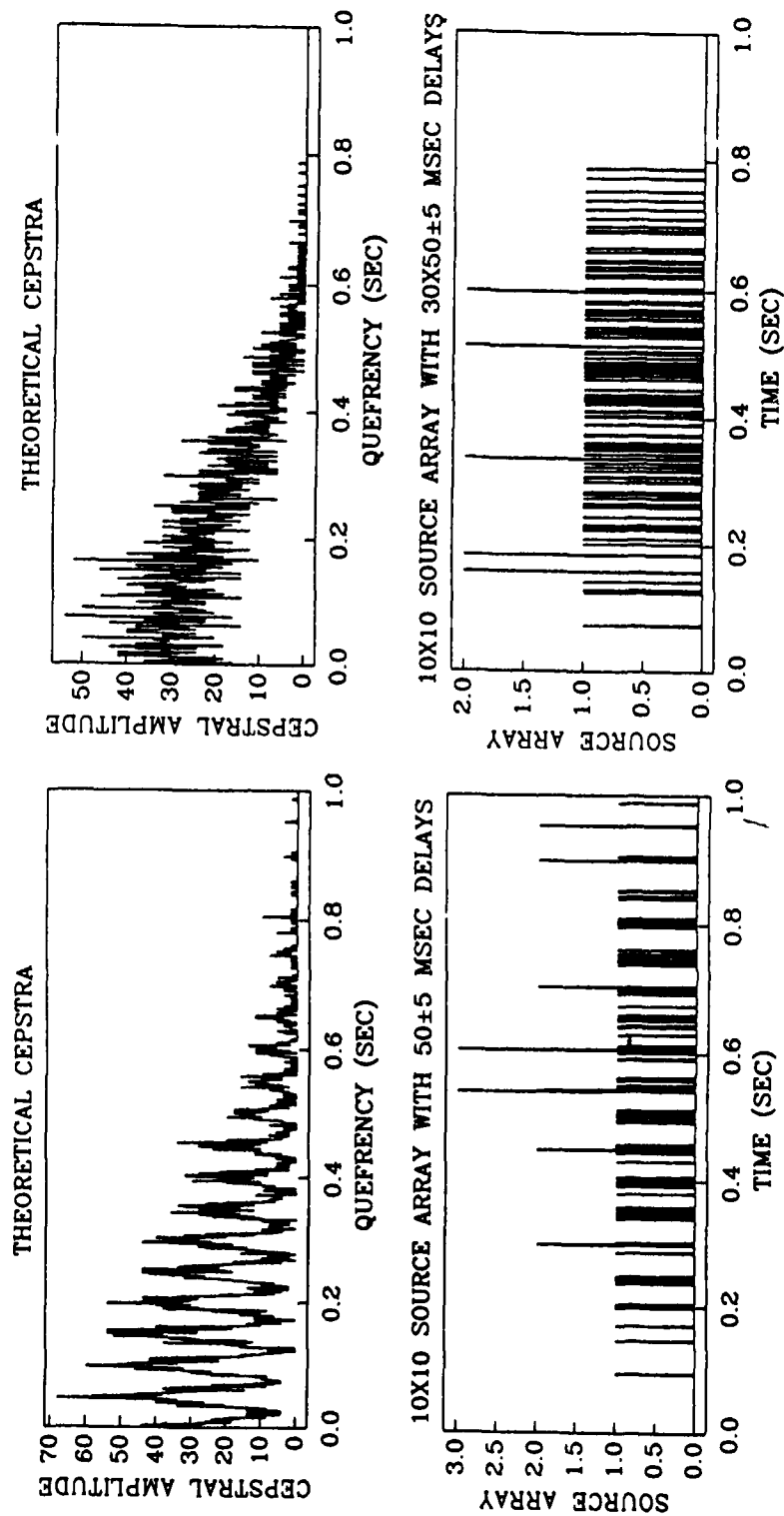


Figure 14. A synthetic rectangular source array of 10 by 10 shots with delays of 50 msec in both orthogonal directions (left) and delays of 50 msec and 30 msec in the two orthogonal directions (right) with 5 msec standard deviation assumed for the blasting caps. The ideal source is shown at the bottom and the theoretical cepstra at the top.



better estimate of the cepstra.

### 2.3.2 Cepstral Analysis of ECTN Data

Four events were chosen for preliminary analysis, two probable quarry blasts and two earthquakes. The four events had numerous good recordings at a range of distances and azimuths. Preliminary spectra indicated that the P and  $P_n$  signals had good signal-to-noise ratios above 20 Hz. The  $L_g$  and/or  $S_n$  had less predictable high frequency signal-to-noise ratios, so it was decided to concentrate on the P and  $P_n$  waveforms.

The average P-wave spectra for the four events are shown in Figure 15A, B, C, and D. The spectra from each station were adjusted to give the same average spectral level in the 4 to 7 Hz bandwidth and log-averaged. The standard deviation of the individual spectra are shown. Note that each network average spectrum appears to have somewhat regular spectral nulls. The earthquakes have corner frequencies in the 5 to 10 Hz range. While, the 12/21/83 quarry blast could be characterized with a corner frequency in the 5 to 10 Hz band, the 09/25/84 event has a broad minimum at 2 Hz and a broad maximum between 5 and 6 Hz. The detrended network average P-spectra are shown in Figures 16A, B, C, and D. They show the modulations apparent in the original network averaged spectra.

We have formed network estimates of the cepstra in two ways. We illustrate these two slightly different procedures with the 12/21/83 event. In the first way, analogous to the procedure of Alexander and Borkowski, we compute the cepstra for each station and then take a geometrical mean of the cepstra. Figure 17 shows the individual cepstra at the bottom and the geometrical mean above. For comparison, the "scaled" product of the cepstra (dashed line) is compared to the geometrical mean. As pointed out above, the product appears to have significant peaks but is deceptive in that it over emphasizes the three largest local maxima. Note the scatter in the individual station cepstra shown below. The 95 percent confidence level is established from the 95 percentile of a cepstrum computed from a Gaussian white-noise log-power spectrum with the same rms level as the individual detrended log-power spectra.

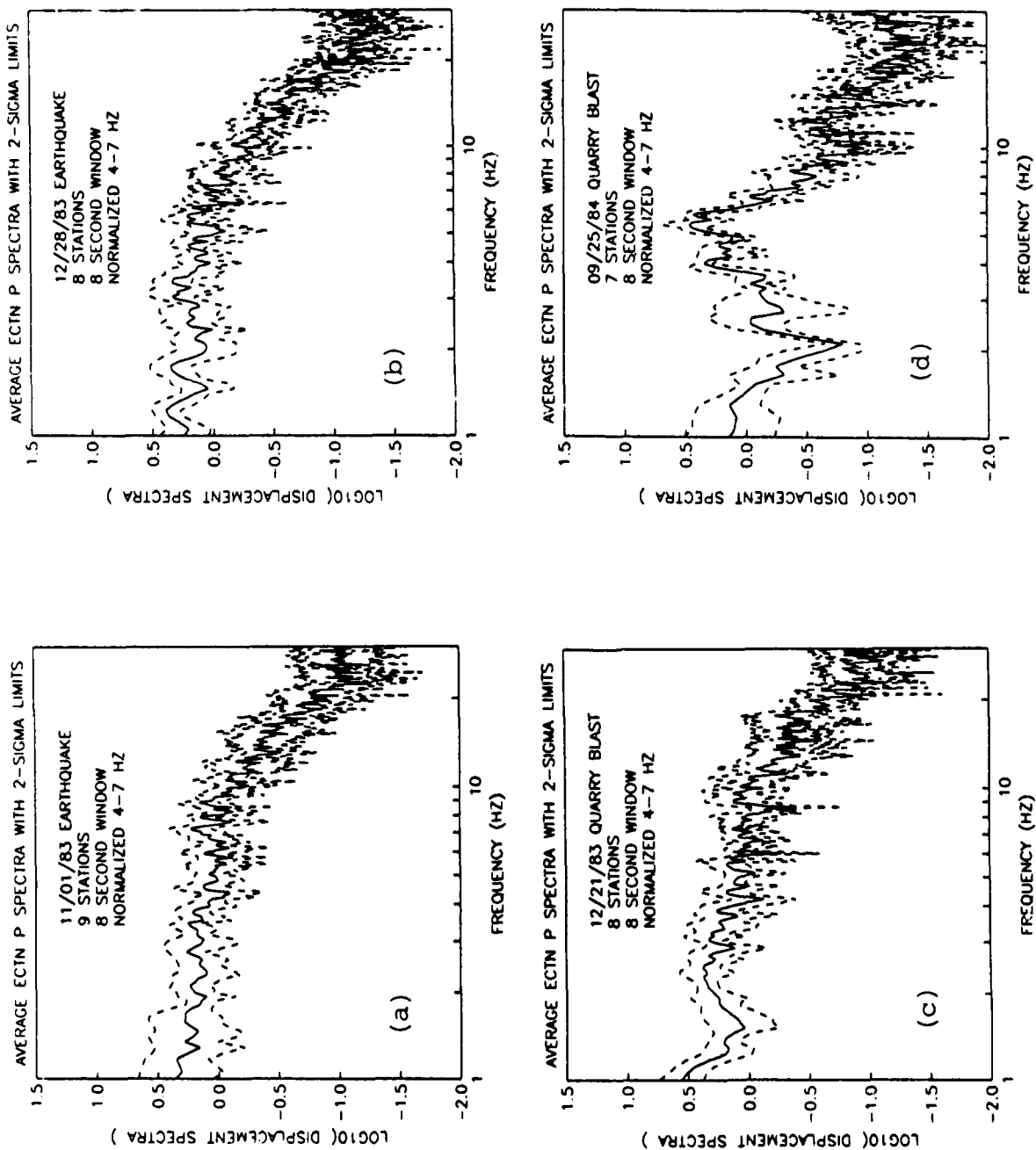


Figure 15. Network-averaged P-wave spectra for events of 11/01/83 (a), 12/28/83 (b), 12/21/83 (c), and 09/25/84 (d). Spectra were normalized in 4-7 Hz passband prior to averaging. Dashed lines indicate  $\pm$  one sigma bounds.

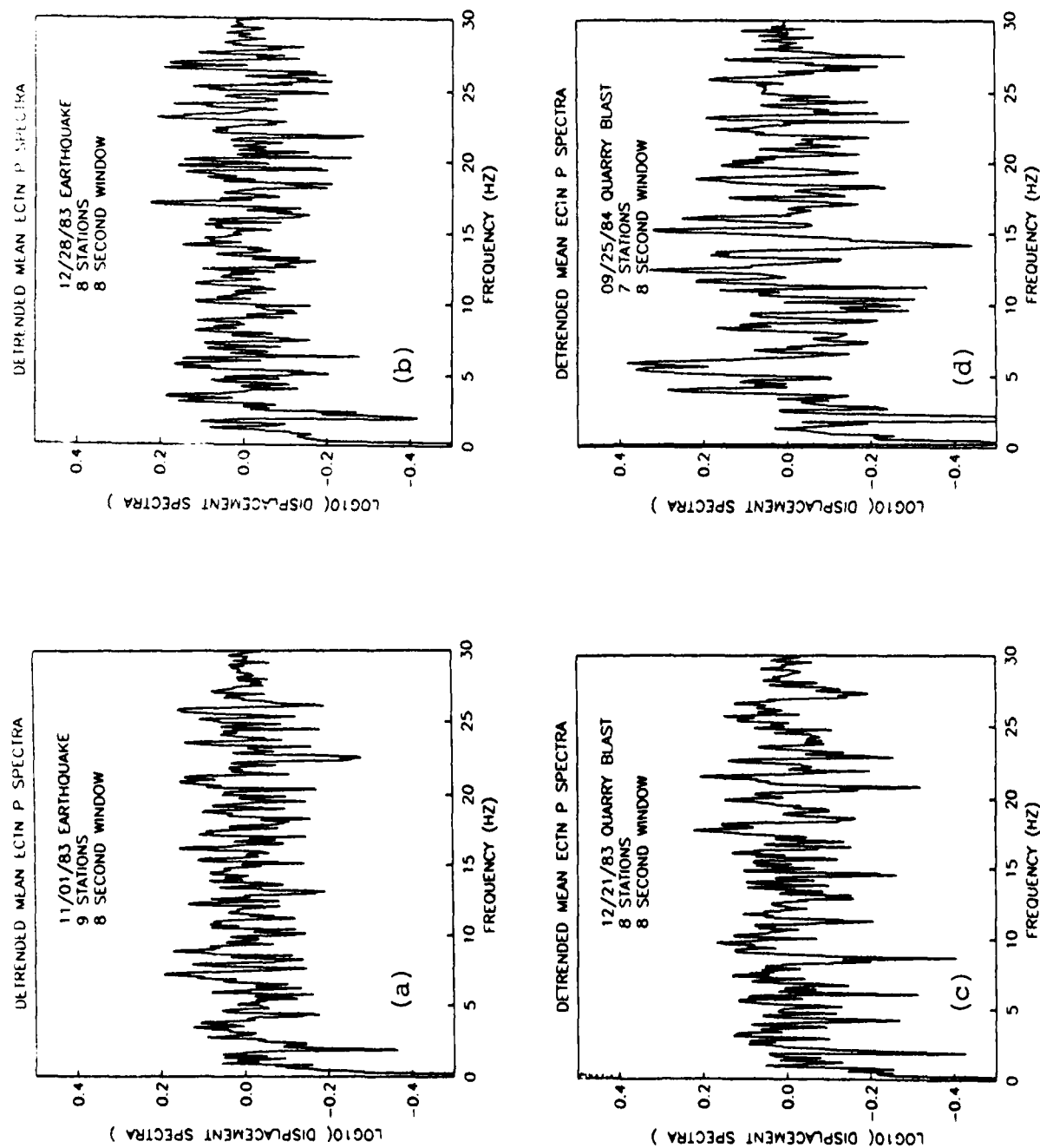


Figure 16. Detrended average P-wave spectra for events from Figure 15.

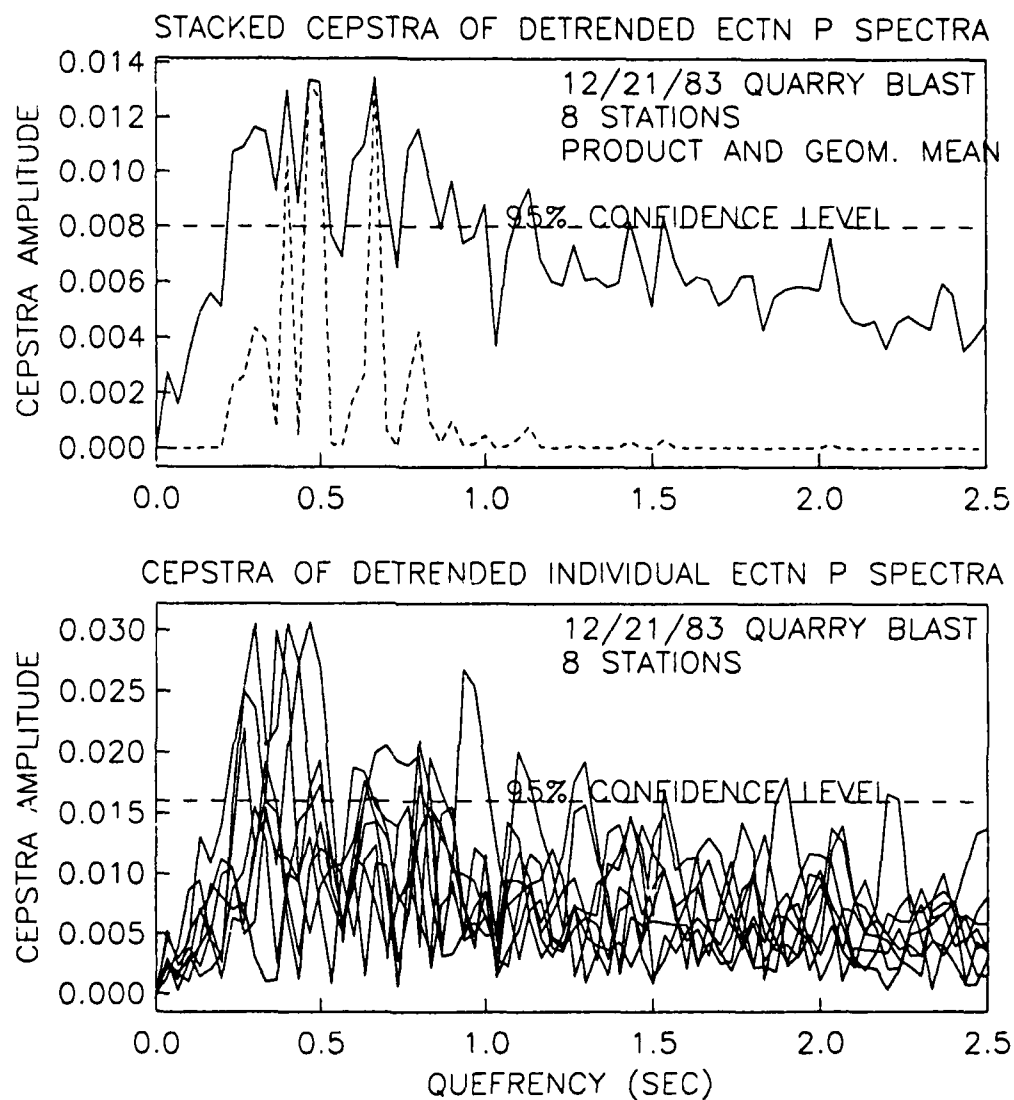


Figure 17. Individual cepstra for 8 different stations for the 12/21/83 event (bottom). Geometric mean of the 8 cepstra (solid line) and a "scaled" version of the product of the individual cepstra (dashed line) (top).

As an alternative procedure, log-power spectra are averaged and then the cepstrum is computed. This network cepstral estimate is compared with the stacked cepstral estimate in Figure 18. The cepstrum of the stacked spectra (solid line) shows one very large peak at 0.5 seconds and numerous other well defined peaks at the 95 percent confidence level. The same peaks are apparent in the stacked cepstral estimate (dashed line) although the peaks appear to be broader and the background level is higher. There are no strong reasons at this point to prefer one of the two methods over the other; however, the second procedure appears to have a lower background level over a broader quefreny. The log-averaging of the individual power spectra appears to be more stable and lead to a more prewhitened log-power spectrum than the detrending of the individual log-power spectra. This would suggest that the second procedure is better.

Figures 19A, B, C, and D show the network cepstral estimates for the four events (two earthquakes and two probable quarry blasts). Note that all four events exhibit peaks at the 95 percent confidence level.

The two earthquakes have constrained depths of 18 km, and as such would be expected to have cepstral peaks with quefrenies of 5 or 6 seconds if the P+pP were responsible for the spectral modulation. The time window used to analyze the P waves was chosen to be 8 seconds, so we would not expect to reliably detect periodicity within the P waveform with quefrenies longer than 4 seconds. These events would have to be quite shallow to have periodicities caused by pP and sP with quefrenies near 1 second. It is not clear at this time what is responsible for these periodicities in the P waveforms. These periodicities are particularly puzzling, since the spectral modulations are present for a number of stations at different distances and azimuths from the event. Reverberations in the crustal structure could not be expected to be coherent across the network. It is possible that each P-wave path exhibits crustal periodicity and that these cepstral peaks then combine in a fashion not properly modeled by the statistical model proposed above. The null hypothesis that was used to define a significance level assumes that detrended log-power spectra are Gaussian white-noise time series in the absence of source multiplicity. The periodicities may be in the propagation paths. It may be that the proper null hypothesis more correctly assumes that each path has a set of randomly chosen periodicities with a spectrum defined by the range of crustal

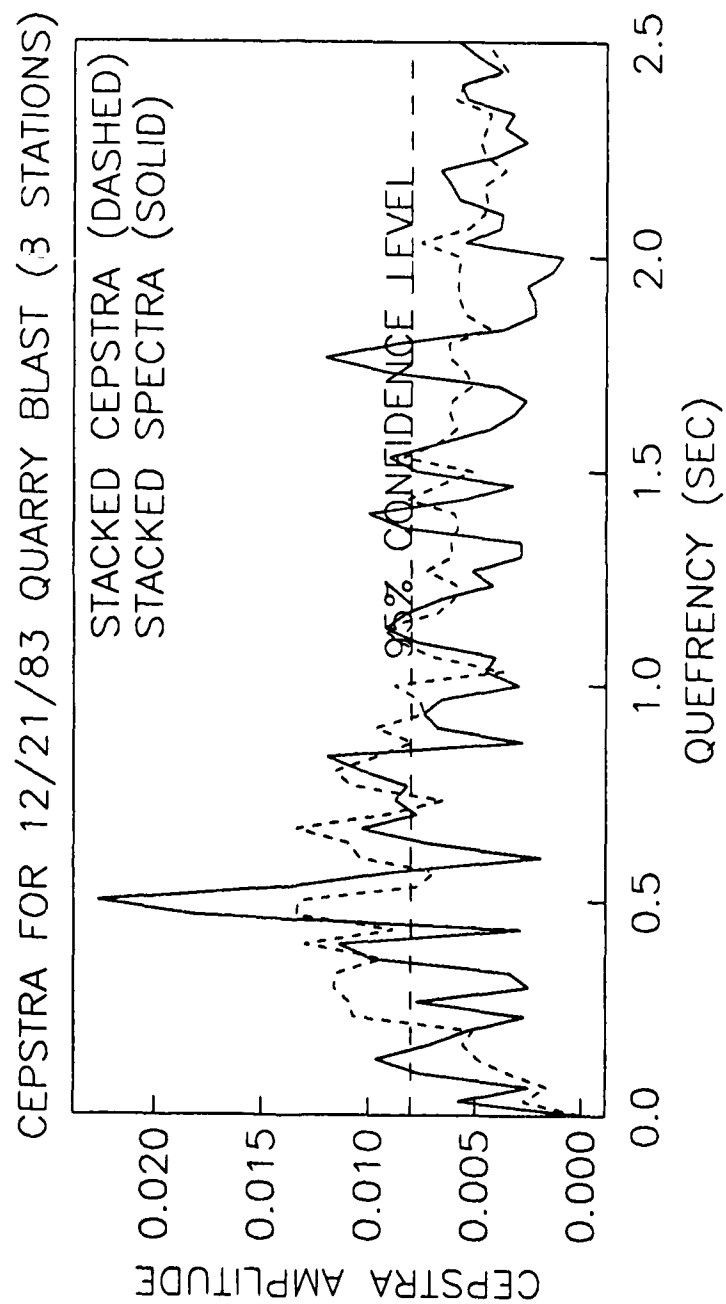


Figure 18. Comparison of the stacked cepstra from Figure 17 (dashed line) with the cepstra derived from the stacked log-power spectra (solid line).

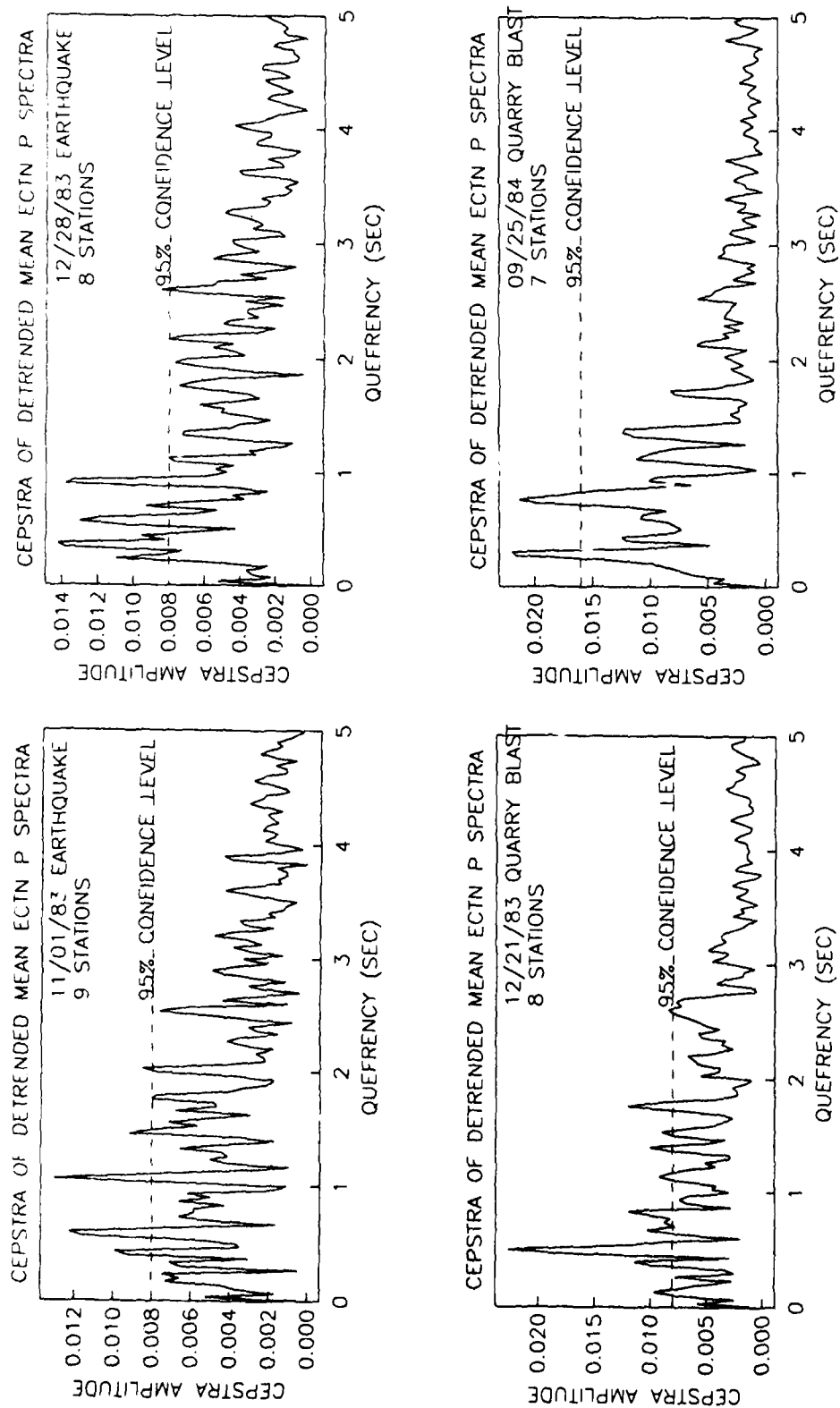


Figure 19. Cepstra from the detrended stacked log-power spectra of Figure 16 for events of 11/01/83 (a), 12/28/83 (b), 12/21/83 (c) and 09/25/84 (d).

structures in the region. One way to evaluate this hypothesis and establish confidence levels will require examination of synthetic P and  $P_n$  waveforms for a range of acceptable crustal models.

In summary, both earthquakes and probable quarry blasts recorded by the ECTN show evidence for deterministic modulation of the spectra as detected in cepstra. This spectral modulation requires a repetitive nature for both source types with quefrequencies in the 0.2 to 1.0 second range. The cepstral peaks are observed at multiple stations in the network at a range of distances. Since the earthquakes had corner frequencies above 5 Hz, it is unlikely that these periodicities are related to source processes and are rather due to propagation effects. The null hypothesis used to test the significance of the cepstral peaks may be in error. An alternative hypothesis may be that crustal reverberations lead to spectral modulation that mimics multiple sources. This hypothesis could be explored with synthetic seismograms generated for a range of crustal structures.

In the light that false alarms are quite *likely* in cepstral analysis, the routine use of cepstral estimation may have limited utility for discrimination. The presence of cepstral peaks in the 0.2 to 1.0 second quefrequency range is not in itself a *reliable* discriminant.



### III. IDENTIFICATION OF SEISMIC SOURCES IN THE SOUTHERN SOVIET UNION

#### 3.1 Regional Observations from Soviet Events

To be considered truly reliable, regional discrimination procedures need to be tested on events from areas where the identification procedures are to be applied or, at least, calibrated for those areas. As noted above in Section II, regional seismic data have generally not been available for events in the Soviet Union. A few authors (e.g., Nuttli, 1986; Ringdal, 1988) have systematically measured  $L_g$  signal amplitudes at far-regional distances from East Kazakh underground nuclear explosion and used the results to compute  $L_g$  magnitudes for correlation with the explosion yield. However, in nearly all cases the paths to the stations used in these studies have been extremely long or tectonically complex resulting in very weak signals and requiring some assumptions about  $L_g$  propagation which may not be warranted for the paths involved. In particular, Ruzaiкин *et al.* (1977) suggested that  $L_g$  signals were effectively blocked, and not normally attenuated, in crossing some of the tectonically active zones to the south of the Soviet test site. In previous work at S-CUBED, we reviewed the quality of regional phase signals including  $L_g$  recorded at SRO and other stations outside the southern Soviet border and concluded that the signals from Soviet explosions in both the East Kazakh and Caspian regions were weak and barely above noise level for most of the events. However, there was evidence that events from the same source regions typically produced stronger  $L_g$  signals at larger regional distances to stations in Scandinavia and northern Europe, even though the regional phases themselves were typically highly dispersed and not distinct.

It seems clear from these studies that the observed behavior of the signals and the propagation paths are atypical of the conditions which are anticipated for future in-country monitoring with regional seismic networks or stations. As pointed out above in Section II, the stable continental platform areas interior to the Soviet Union are expected to provide highly efficient propagation environments for regional phases, and particularly  $L_g$ , comparable to conditions in eastern North America. Highly efficient  $L_g$  transmission in Soviet platform

areas is certainly suggested by the far-regional observations in Scandinavia and northern Europe by Nuttli and Ringdal, which were cited above. However, the far-regional measurements do not truly represent normal regional monitoring which typically utilizes stations at ranges less than 2000 km and more often ranges less than 1000 km.

Only recently high-quality seismic data recorded at normal regional distance ranges from events near the Soviet East Kazakh test site have started to become available. These data are from two sources: the Chinese Digital Seismic Network (CDSN) and the joint Soviet/Natural Resources Defense Council (NRDC) temporary network surrounding the East Kazakh test site. The former has recorded numerous Soviet underground nuclear explosions and earthquakes at comparable magnitudes and ranges while the latter recorded mainly a large number of Soviet commercial blasts of small magnitude at nearer ranges. The data provide a good source for investigating the characteristics of regional phase propagation in more representative tectonic environments and for assessing the capabilities and problems which may arise for future in-country regional seismic monitoring around East Kazakh.

### **3.2 Analysis of Regional Signals from the CDSN**

In analyzing the regional signals from underground nuclear explosions and earthquakes recorded by the CDSN, we focused on observations at station Urumchi (WMQ) which is the nearest station to the principal Soviet test site in East Kazakh (cf. Figure 20). Preliminary review of data from the WMQ site (cf. Bennett *et al.*, 1988) had indicated the potential of this station for recording good regional signals, including  $L_g$ , from East Kazakh explosions ( $R \approx 970$  km) and earthquakes at comparable ranges. Installation of the high quality digital station at WMQ in 1986 greatly enhanced the station's capability and made the waveform data easily accessible for analysis. In this study we attempted to recover the digital seismic signals from all East Kazakh underground nuclear explosions which occurred since the installation of the digital station. After reviewing the digital data from some of the earlier explosions, we found that there appeared to be a problem with station triggering which caused the recording system to shut off prior to arrival of  $L_g$  and not restart at the time of  $L_g$  even though the signal level was much higher than the background noise at the time of shutdown. As a result the  $L_g$  signals were missed. This was most

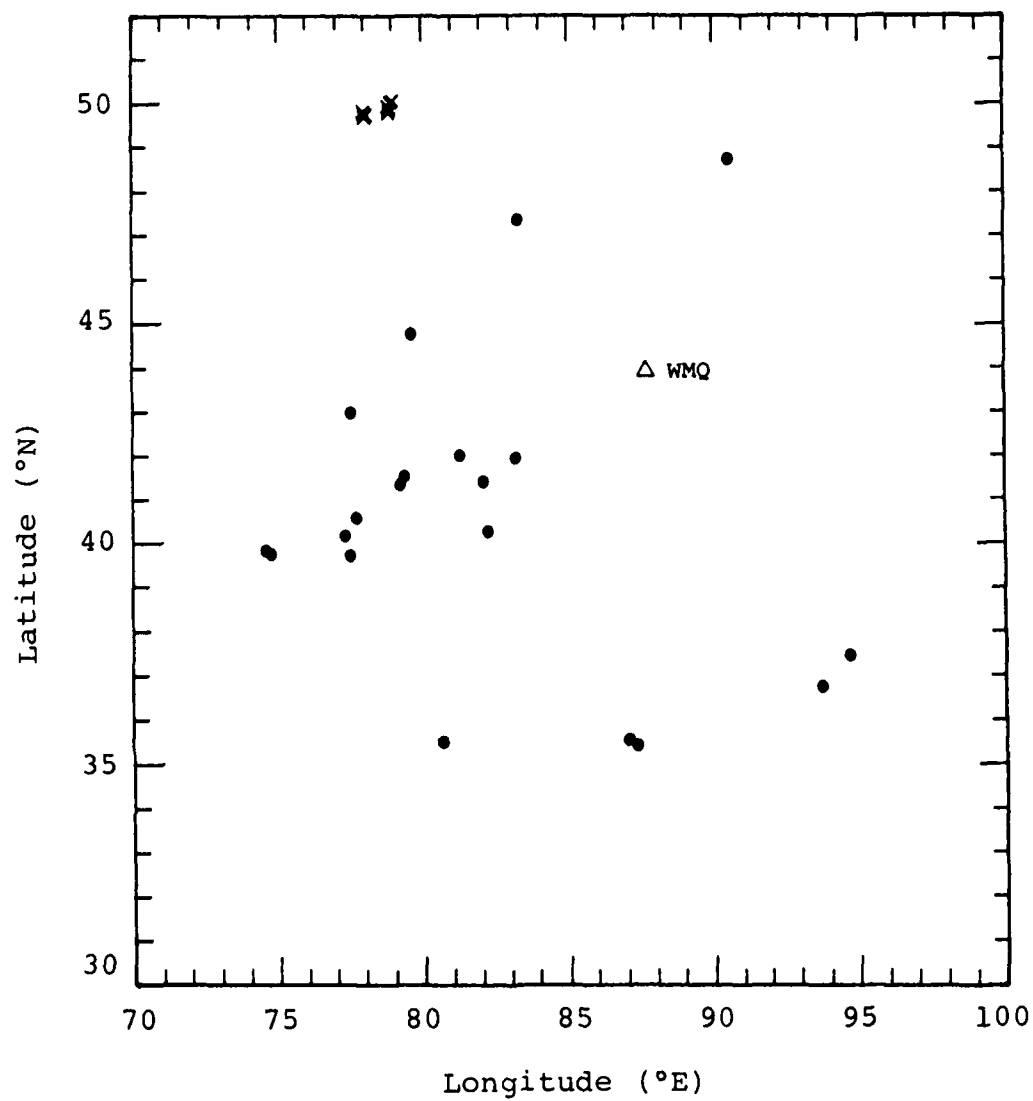


Figure 20. Locations of East Kazakh nuclear explosions (x) and regional earthquakes (•) in WMQ database.

problematic for the high sampling rate channels (40 samples/sec); in many cases the intermediate sampling rate channel (20 samples/sec) included the  $L_g$  signal window for these same events although even there the system occasionally shutdown before the end of the  $L_g$  signal. This triggering problem was ameliorated to some extent by a change to the detection algorithm, but we decided to use the intermediate channel in these analyses. We found that the intermediate channel provided a somewhat more complete event sample and still recovered most of the useful frequency band where signal-to-noise level was adequate at the ranges involved.

Figure 20 shows the locations of 12 underground nuclear explosions at East Kazakh for which the regional recordings at WMQ were analyzed. Table 5 provides the source information on these events. The magnitudes were between 4.7 and 6.2  $m_b$ . The range of the explosions from WMQ was from 945 to 992 km with the nearer events located at Shagan River and the farther at Degelen Mountain. To develop a comparable earthquake sample, we searched the National Earthquake Information Service (NEIS) event list for events since the time that WMQ was converted to digital recording. In this search we attempted to identify earthquakes with magnitudes comparable to those of the explosions and located at distances from WMQ which encompass the distance range for the explosions. It is well known that the area surrounding the East Kazakh test site is virtually aseismic, so comparable earthquakes were not available which would have transmission paths close to those of the explosions. We were, therefore, forced to select from a more diffuse set of events. Figure 20 shows the locations of the 20 earthquakes for which regional signals from WMQ were recovered. The source information on these earthquakes is summarized in Table 6. The earthquakes had magnitudes between 4.5 and 5.9  $m_b$ , and the distances from WMQ were between 423 and 1176 km.

Figure 21 shows representative examples of the vertical component records obtained at station WMQ for four explosions and four earthquakes. The regional records from both source types normally show strong, complex P and  $L_g$  phases. At this distance range the P waves from the explosions are typically dominated by early, high-frequency P phases which apparently correspond to paths in the deep crust or upper mantle. The  $P_g$  phase is not particularly distinct, appearing as a segment of increased amplitude coda

Table 5

## East Kazakh Underground Nuclear Explosions

Date	Origin Time	Lat. (°N)	Lon. (°E)	$\Delta$ (km)	$m_b$
03-12-87	01:57:17.3	49.93	78.78	956	5.4
04-03-87	01:17:08.0	49.93	78.83	956	6.2
05-06-87	04:02:05.7	49.83	78.13	989	5.6
06-06-87	02:37:07.0	49.86	78.10	992	5.3
06-20-87	00:53:04.8	49.91	78.74	956	6.1
08-02-87	00:58:06.8	49.88	78.92	945	5.9
12-20-87	02:55:06.3	49.83	78.00	996	4.7
02-13-88	03:05:05.9	49.95	78.91	956	6.1
04-03-88	01:33:05.7	49.89	78.96	945	6.0
04-22-88	09:30:06.7	49.79	78.11	987	4.9
05-04-88	00:57:06.8	49.92	78.76	956	6.1
06-14-88	02:27:06.4	50.02	78.99	956	4.9

Table 6  
Regional Earthquakes Recorded at WMQ

Date	Origin Time	Lat. (°N)	Lon. (°E)	Δ (km)	m <sub>b</sub>
12-14-86	03:19:16.7	47.31	83.31	517	5.0
12-20-86	23:08:16.5	36.75	93.66	940	5.3
01-05-87	22:52:46.5	41.96	81.32	578	5.9
01-24-87	08:09:21.3	41.53	79.32	732	5.9
01-24-87	13:40:40.3	41.44	79.25	742	5.2
03-05-87	02:33:39.3	35.41	87.39	934	4.5
04-09-87	07:25:35.7	35.50	87.07	926	4.8
04-09-87	20:01:19.5	35.51	80.65	1102	4.9
04-30-87	05:17:37.0	39.76	74.57	1168	5.7
06-08-87	13:30:32.8	39.75	74.62	1176	5.1
08-05-87	10:24:21.1	41.36	82.11	534	4.8
12-03-87	23:51:42.9	39.66	77.48	967	4.7
12-06-87	16:20:45.2	37.44	94.61	912	4.7
12-17-87	12:17:25.6	41.94	83.20	423	5.1
01-02-88	22:02:36.0	40.06	77.34	956	4.9
03-25-88	02:07:55.8	44.71	79.60	656	4.5
05-02-88	02:13:26.3	40.26	82.20	600	4.9
05-25-88	00:05:22.8	40.57	77.62	912	4.9
06-17-88	13:30:45.0	42.94	77.50	834	5.3
07-23-88	07:38:09.9	48.72	90.51	589	5.5

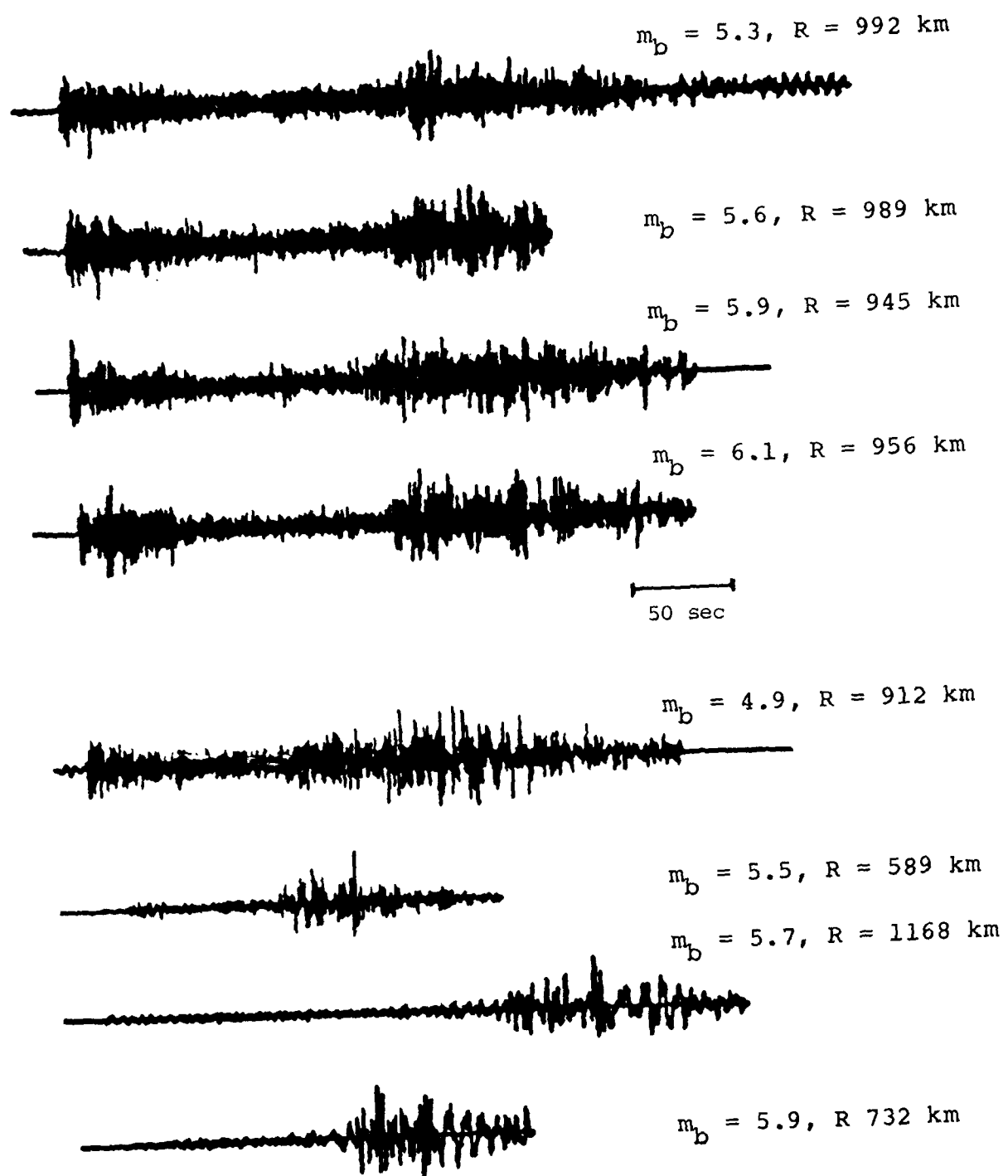


Figure 21. Vertical-component records at WMQ from four nuclear explosions (top) and four regional earthquakes (bottom).

trailing the earlier P arrivals.  $L_g$  appears as a long-duration, complex phase with a peak amplitude which is frequently as large as the P phase on these broad-band recordings from the explosions. For the earthquakes the P phases are generally smaller in amplitude than the  $L_g$  phases, and multiple phases are frequently apparent depending on the epicentral distance.  $L_g$  signals are strong and of long-duration for the earthquakes and in some cases are preceded by an  $S_n$  phase which wasn't apparent in the explosion signals.

We made peak amplitude measurements of P and  $L_g$  signals from the broadband records of the explosions and earthquakes at WMQ. Figure 22 shows the  $S_{max}/P_{max}$  and  $L_g/P_g$  peak amplitude ratios for these events. The  $S_{max}/P_{max}$  ratio compares the peak amplitudes before and after  $S_n$  arrival time while  $L_g/P_g$  compares peak amplitudes in the appropriate group velocity windows (i.e., near 6 km/sec for  $P_g$  and less than 3.6 km/sec for  $L_g$ ). In nearly all cases the  $S_{max}$  corresponded to the  $L_g$  peak, but as noted above  $P_{max}$  seldom corresponded to  $P_g$ . The ratio measurements provide fairly good separation between event types with generally larger ratios for earthquakes than for explosions. In order to clarify and possibly enhance these differences, we performed a band-pass filter analysis using a suite of seven narrow-band filters. The filter passbands were 0 to 1 Hz (center frequency  $f_c = 0.5$  Hz), 0.5 to 2 Hz ( $f_c = 1.25$  Hz), 1 to 3 Hz ( $f_c = 2$  Hz), 2 to 4 Hz ( $f_c = 3$  Hz), 3 to 6 Hz ( $f_c = 4.5$  Hz), 4 to 8 Hz ( $f_c = 6$  Hz), and 6 to 12 Hz ( $f_c = 9$  Hz). Above and below the corners the filter response dropped off at 48 dB per octave. After filtering we recomputed the  $S_{max}/P_{max}$  ( $L_g/P_{max}$ ) amplitude ratios for the various events as a function of the center frequency of the bandpass filter. Figure 23 shows the results of those measurements for the individual events. The  $L_g/P_{max}$  ratios in all cases start out well above 1.0 at low frequencies, but the ratios rapidly decay toward higher frequencies. The ratio measurements for both types of events start to level off at higher frequencies with the earthquakes leveling off at higher ratios. As a result, the ratios are observed to be somewhat intermingled with respect to event type at frequencies below about 2 Hz but completely separated at higher frequencies. The  $L_g/P_{max}$  ratios for the earthquakes are generally much higher than for the explosions above about 3 Hz. Figure 24 shows the average  $L_g/P_{max}$  ratios for the two event types as a function of frequency. Superimposed on these curves are the 95 percent confidence bounds on the means which were estimated using the data from Figure 23. The only area where the confidence bounds overlap is for the lowest center frequency



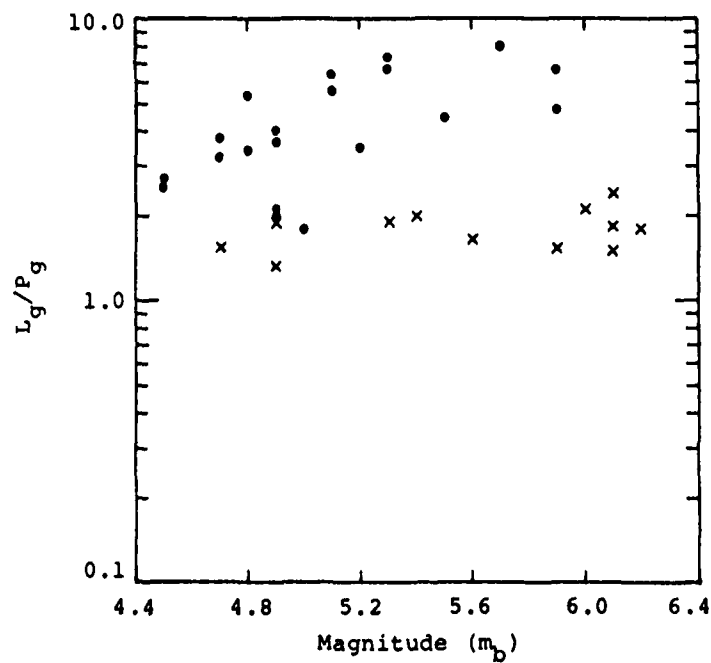
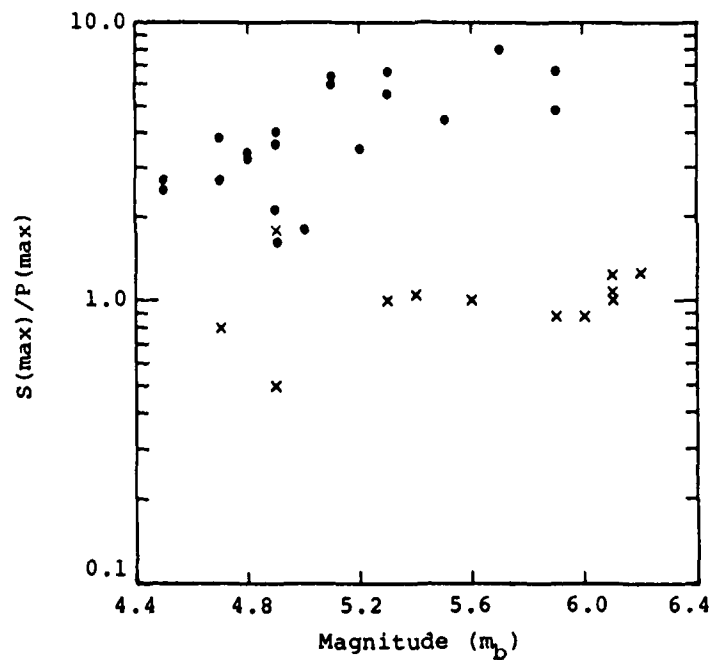


Figure 22. Peak amplitude ratios for  $S_{\max}/P_{\max}$  (top) and for  $L_g/P_g$  (bottom) measured from broad-band recordings at WMQ.

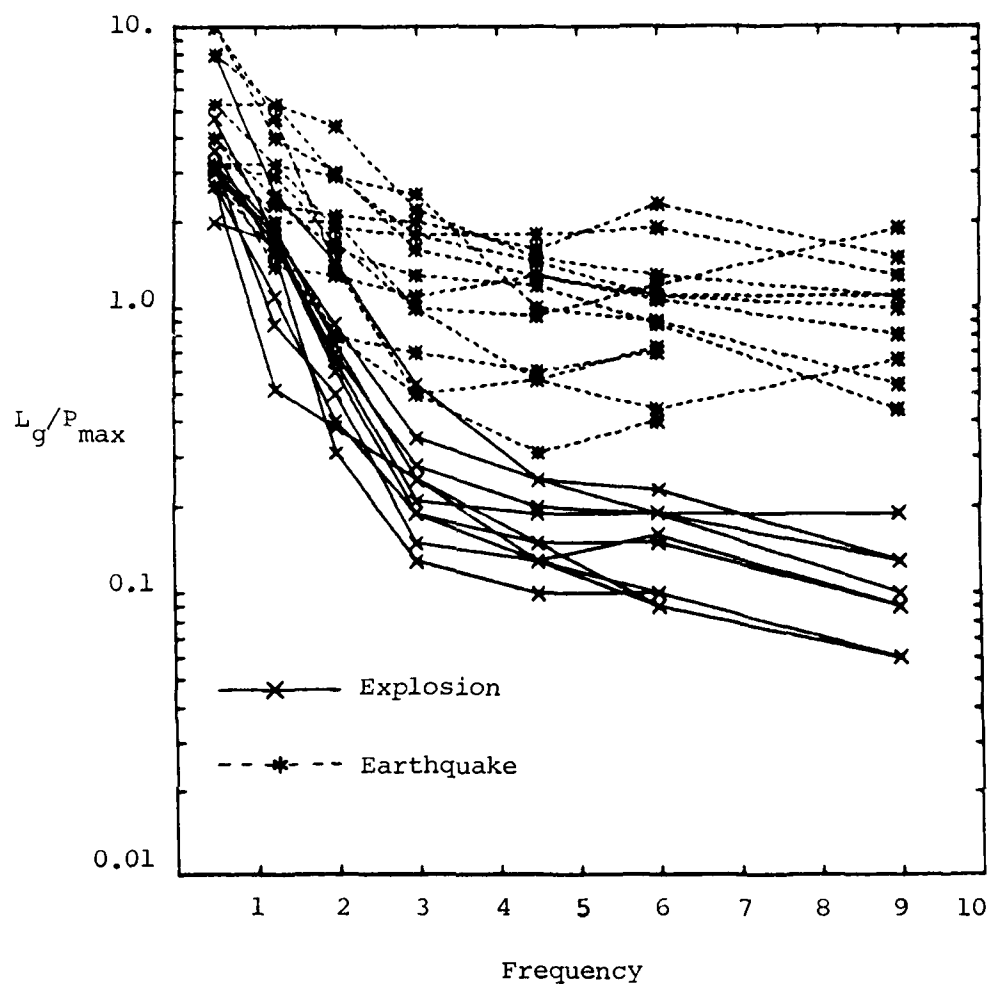


Figure 23.  $L_g/P_{max}$  ratios as a function of frequency for explosions and earthquakes recorded at WMQ.

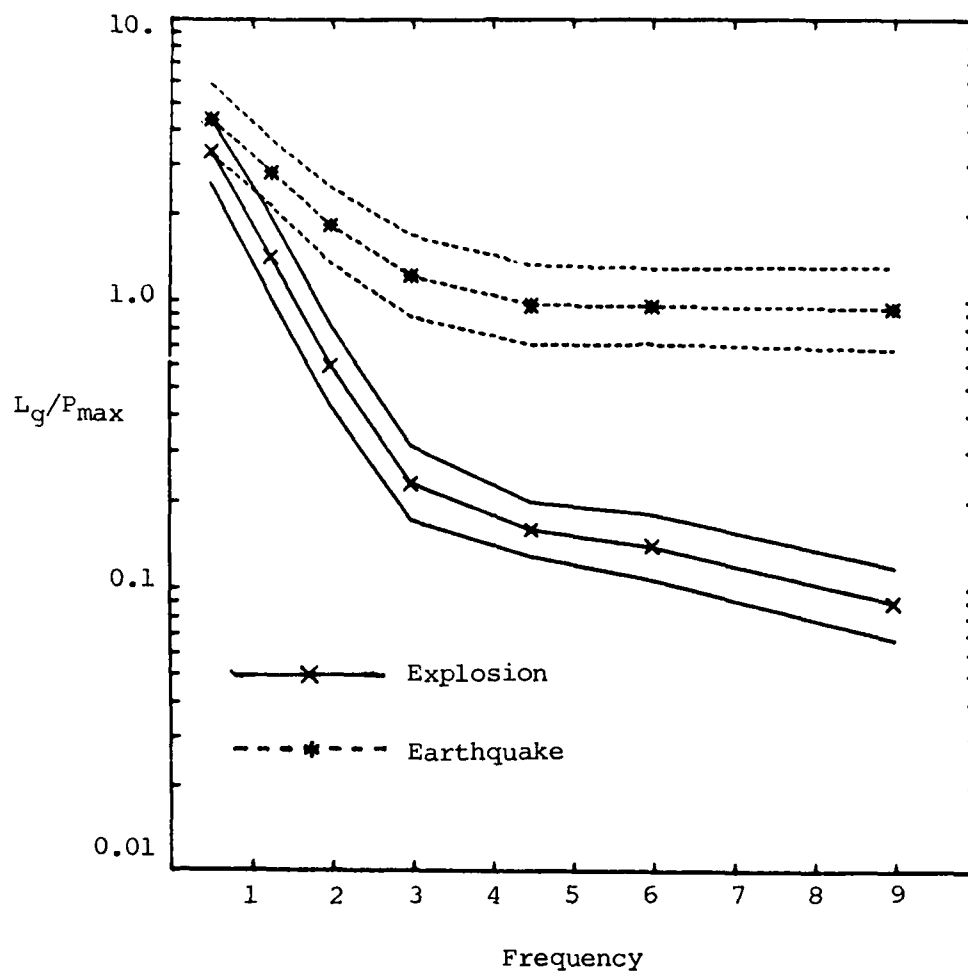


Figure 24. Average  $L_g/P_{max}$  ratios as a function of frequency for explosions and earthquakes recorded at WMQ.

(viz 0.5 Hz); at 1 Hz and above the  $L_g/P_{\max}$  amplitude ratios are completely separated at the 95 percent confidence level. Furthermore, it appears that the separation between the measurements tends to increase toward higher frequencies. At the low-frequency end the average  $L_g/P_{\max}$  ratio is about 4.4 for the earthquakes and about 3.3 for the explosions. The average earthquake curve levels off at a value near 1.0 above about 3 Hz. The average explosion curve falls off more rapidly out to 3 Hz and continues to fall off, at a somewhat slower rate, at higher frequencies. As a result, the average amplitude ratios are separated by almost an order of magnitude at higher frequencies.

Figures 25 through 27 show comparisons of the S/P amplitude ratio in two different frequency bands for various combinations of regional phases. Since the S measurement in virtually all cases corresponded to  $L_g$ , the different figures actually represent comparisons of the excitation of the different P phases relative to  $L_g$ . Figure 25 shows the  $S_{\max}/P_{\max}$  ratios for filter passbands of 3 to 6 Hz (top) and 0 to 1 Hz (bottom). The ratios are completely intermingled for the low-frequency band but well-separated for the high-frequency band. There is no apparent trend in the amplitude ratios with respect to magnitude. The results point out a need for care in dealing with observations obtained from seismic systems with sharply peaked response characteristics. Discriminants which rely on differences in a limited frequency band could provide false identifications at other frequencies. Figure 26 shows a similar plot for  $L_g/P_n$  ratios, where  $P_n$  is taken as the first arrival. In this figure the arrows indicate that the measurements represent either upper or lower limits on the actual ratios; in most cases this is only an artifact of the measurement procedure and could have been corrected by scaling the time histories differently. In any case, we again see some intermingling at the low frequencies and complete separation at high frequencies. It is interesting that for the lower-frequency passband the separation is actually better for the  $L_g/P_n$  ratio than for the  $S_{\max}/P_{\max}$  ratio in the previous figure. For the earthquakes the initial low-frequency P is normally quite small, and there is a tendency for P-coda phases to be somewhat larger. As a result the  $L_g/P_n$  ratios will tend to be larger than the  $S_{\max}/P_{\max}$  ratios for the earthquakes. This may also hold to some extent for the higher-frequency passband measurements. Finally, Figure 27 shows the same kind of plot for the  $L_g/P_g$  ratios. For the low-frequency (0 to 1 Hz) band the  $L_g/P_g$  peak amplitude ratios are about the same for earthquakes and explosions, but for the 3 to 6 Hz band the  $L_g/P_g$  amplitude ratios

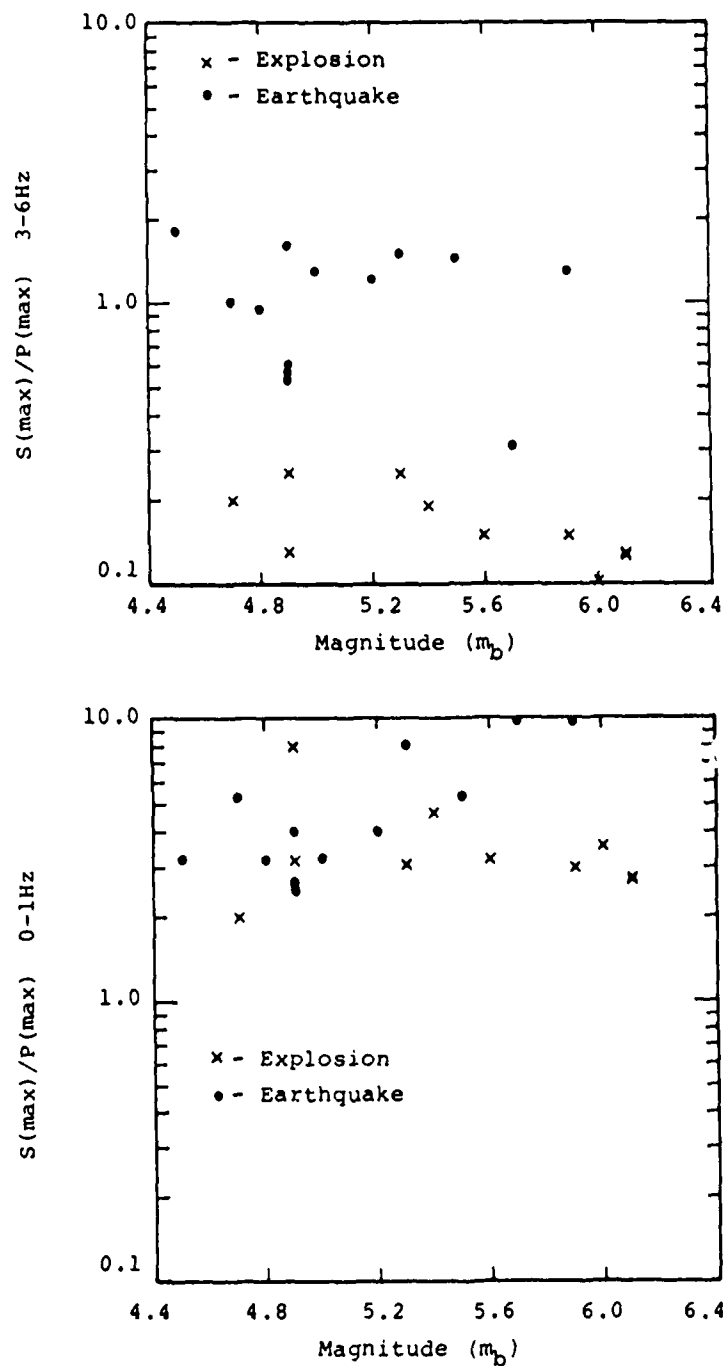


Figure 25. Comparison of  $S_{\max}/P_{\max}$  ratios at WMQ for 3-6 Hz passband (top) and 0-1 Hz passband (bottom).

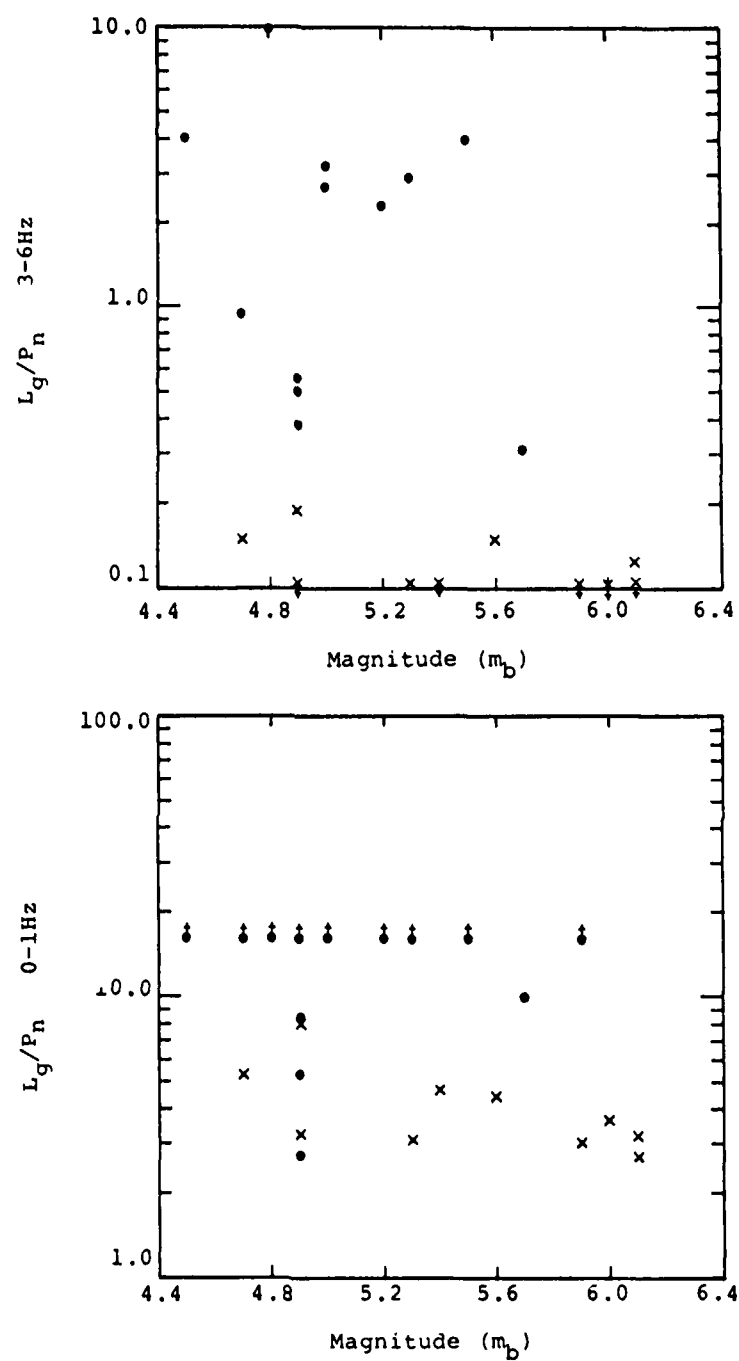


Figure 26. Comparison of  $L_g/P_n$  ratios at WMQ for 3-6 Hz passband (top) and 0-1 Hz passband (bottom).

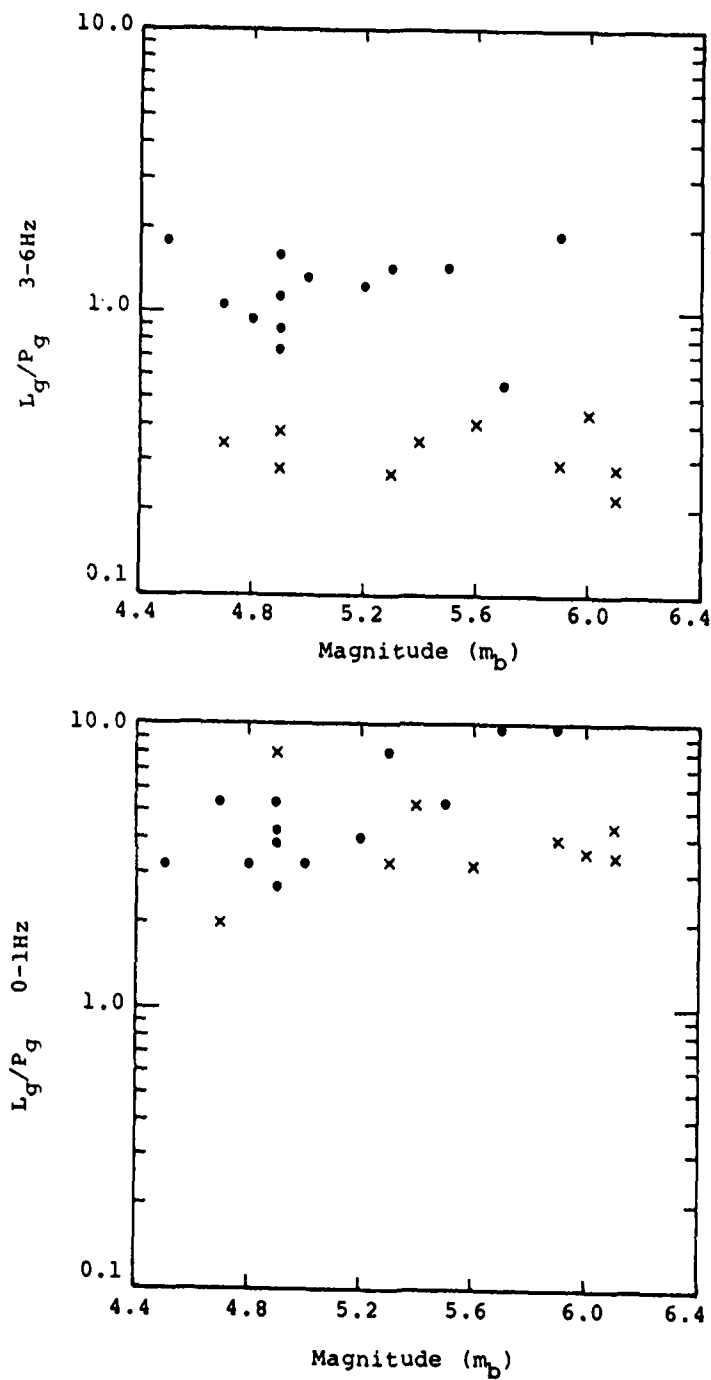


Figure 27. Comparison of  $L_g/P_g$  ratios at WMQ for 3-6 Hz passband (top) and 0-1 Hz passband (bottom).

are larger for the earthquakes. At low frequencies the  $P_g$  signal is quite small for both earthquakes and explosions resulting in the large  $L_g/P_g$  ratios. At high frequencies the ratios are smaller and we have separation of the event types; but the measured signal in the  $P_g$  window may correspond to coda from earlier P phases and not the normal  $P_g$ . Again in Figure 27 there is no apparent trend in the ratio measurements with respect to magnitude.

One final comparison of the high- and low-frequency passband amplitude ratios is presented in Figure 28. Here we present the  $S_{\max}/P_{\max}$  ratios as a function of the epicentral distance at which the measurement was obtained. It was thought that this could be important because the explosions were concentrated in a very limited distance range from WMQ while the earthquake distances were more variable. First, for the lower-frequency passband there is little evidence of any dependence of the amplitude ratio on epicentral distance. The  $S_{\max}/P_{\max}$  ratios at all distances scatter about a mean value near four. For the high-frequency band there does appear to be some tendency for the  $S_{\max}/P_{\max}$  peak-amplitude ratios to decrease with epicentral distance. Focusing on the earthquake measurements, the ratios are generally greater than 1.0 at distances less than 800 km and show an overall decrease toward larger distances. However, the explosion  $S_{\max}/P_{\max}$  ratios would still fall well below any trend through the earthquake observations. So that even if the earthquake amplitude ratios were adjusted to a common range with the explosions using some average trend, the  $S_{\max}/P_{\max}$  ratios would still be separated by about a factor of four. One further caveat, which requires additional study, is that attenuation along the propagation path to East Kazakh may be different from the regional trend based on the earthquakes in Figure 28. We will return to this in subsequent discussions.

Our initial interpretation of the observed frequency dependence in the  $S_{\max}/P_{\max}$  amplitude ratio was that the observation was consistent with previous findings from the western U.S. Those studies (cf. Murphy and Bennett, 1982; Bennett and Murphy, 1986; Bennett *et al.*, 1988a) indicated that the earthquake  $L_g$  signals were richer in high frequencies than the comparable explosions, but the  $P_n$  signals had equivalent spectral content for explosions and earthquakes. Thus, the  $L_g/P_n$  amplitude ratios for those events would be expected to fall off more rapidly toward high frequencies for explosions than for earthquakes. Based on this interpretation it would then be anticipated that the



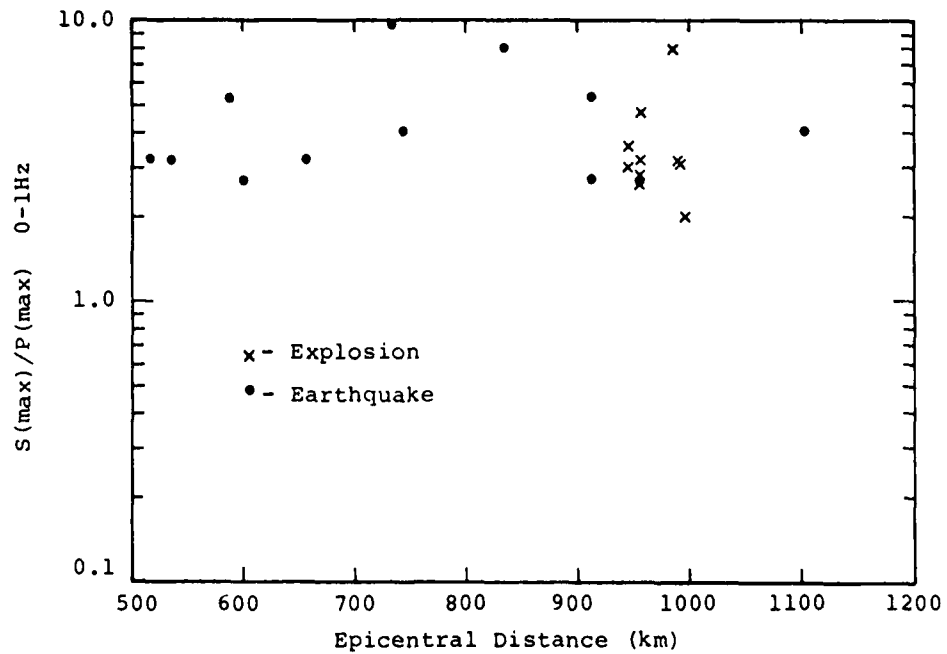
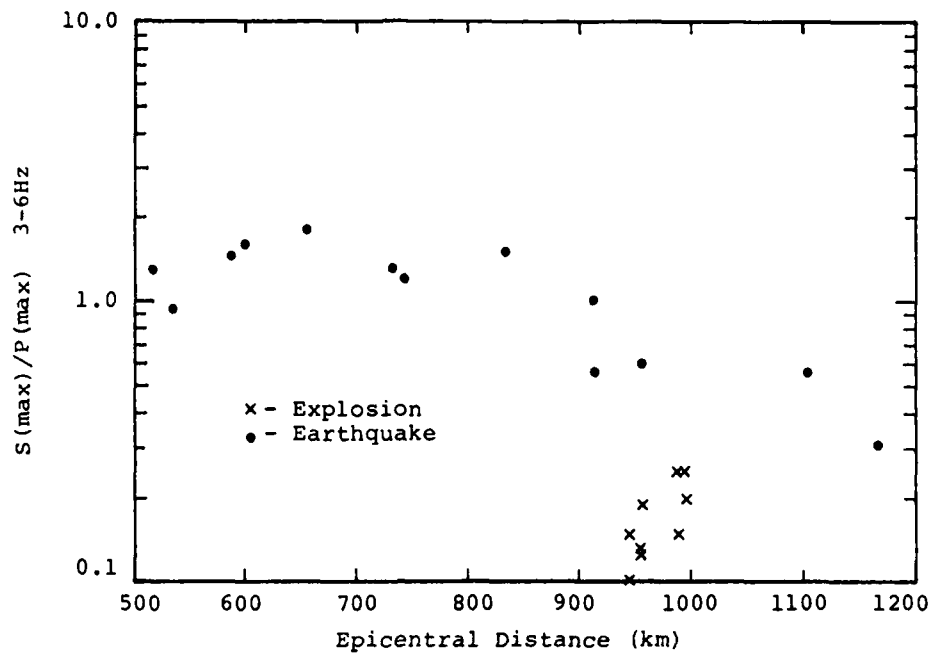


Figure 28. Dependence of  $S_{\max}/P_{\max}$  ratios at WMQ on epicentral distance for 3-6 Hz passband (top) and 0-1 Hz passband (bottom).

$L_g$  spectral ratio discriminant might work on the events recorded at WMQ. To test this hypothesis we computed the  $L_g$  spectra for selected events from the WMQ database including seven explosions and seven earthquakes. The explosion magnitudes were between 4.7 and 6.1  $m_b$  and the earthquake magnitudes were between 4.5 and 5.9  $m_b$ . Epicentral distances were between 945 and 996 km for the explosions and between 732 and 1168 km for the earthquakes. Figure 29 shows the  $L_g$  spectra for the seven explosions after correcting for instrument response. The spectra show a nearly flat portion at lower frequencies and a relatively steep decay above an apparent corner frequency in the range from 0.6 to 1.0 Hz. In general, the corner frequency increases with decreasing magnitude as expected from simple source theory. The earthquake  $L_g$  spectra also showed a flat low-frequency segment and strong spectral decay above a corner frequency, but corner frequencies were somewhat more erratic with respect to magnitude. The apparent corner frequencies for the earthquakes were in all cases lower than the corner frequencies for the explosions with comparable magnitudes. Figure 30 shows schematic representations of the observed  $L_g$  spectra for the explosions and earthquakes observed at WMQ. Some of the variability in the low frequency level for the earthquakes may be attributed to epicentral distance differences; no correction has been applied for attenuation. However, in general the low-frequency  $L_g$  spectral level appears to be higher for the earthquakes than for the comparable explosions. If events with the same  $m_b$  are scaled to have comparable low-frequency spectral levels, then the explosions have higher corner frequencies and appear relatively richer in high frequencies. On the other hand, looking beyond the corner frequencies, the explosions appear to show a slightly steeper spectral decay than the earthquakes. Admittedly the latter is not a particularly strong difference and attenuation variations between the earthquake and explosion paths could be affecting the observations.

To obtain additional insight into the significance of potential attenuation differences on the  $L_g$  spectra, we applied Q corrections to the  $L_g$  spectra from a few selected events. The Q correction was applied in the form of a  $t^*$  operator,  $e^{\pi t^*}$ , where  $t^* = t/Q$ ;  $t$  is the travel time which we just took to be the epicentral distance divided by the  $L_g$  group velocity (approximately 3.5 km/sec). It is well known that Q varies significantly in the crust depending on the tectonic environment (cf. Nuttli, 1981, 1986). As a first approximation to Q for the path from East Kazakh to WMQ, we used the value determined by Bennett *et al.*

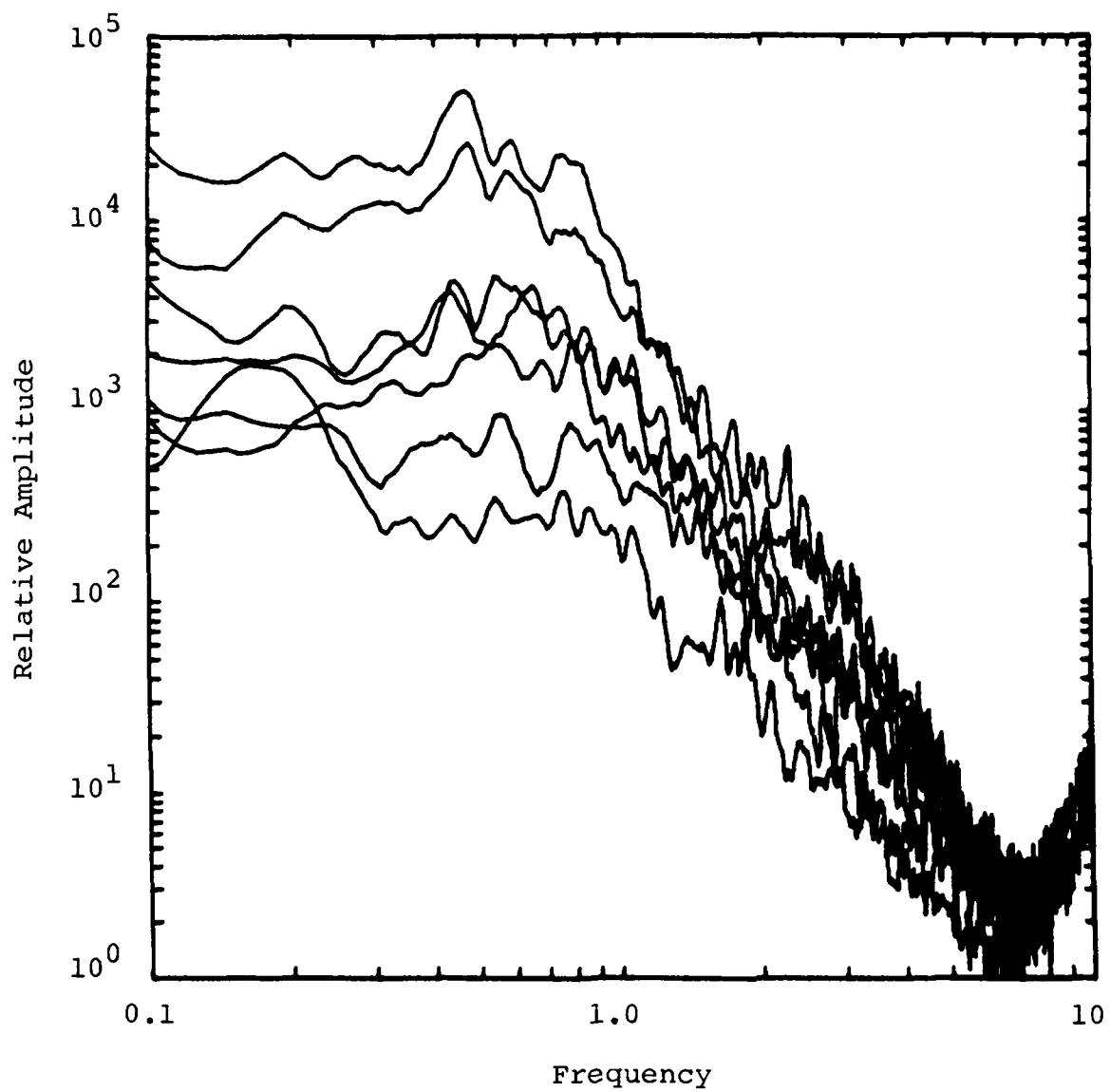


Figure 29.  $L_g$  spectra for seven East Kazakh underground nuclear explosions measured at WMQ.

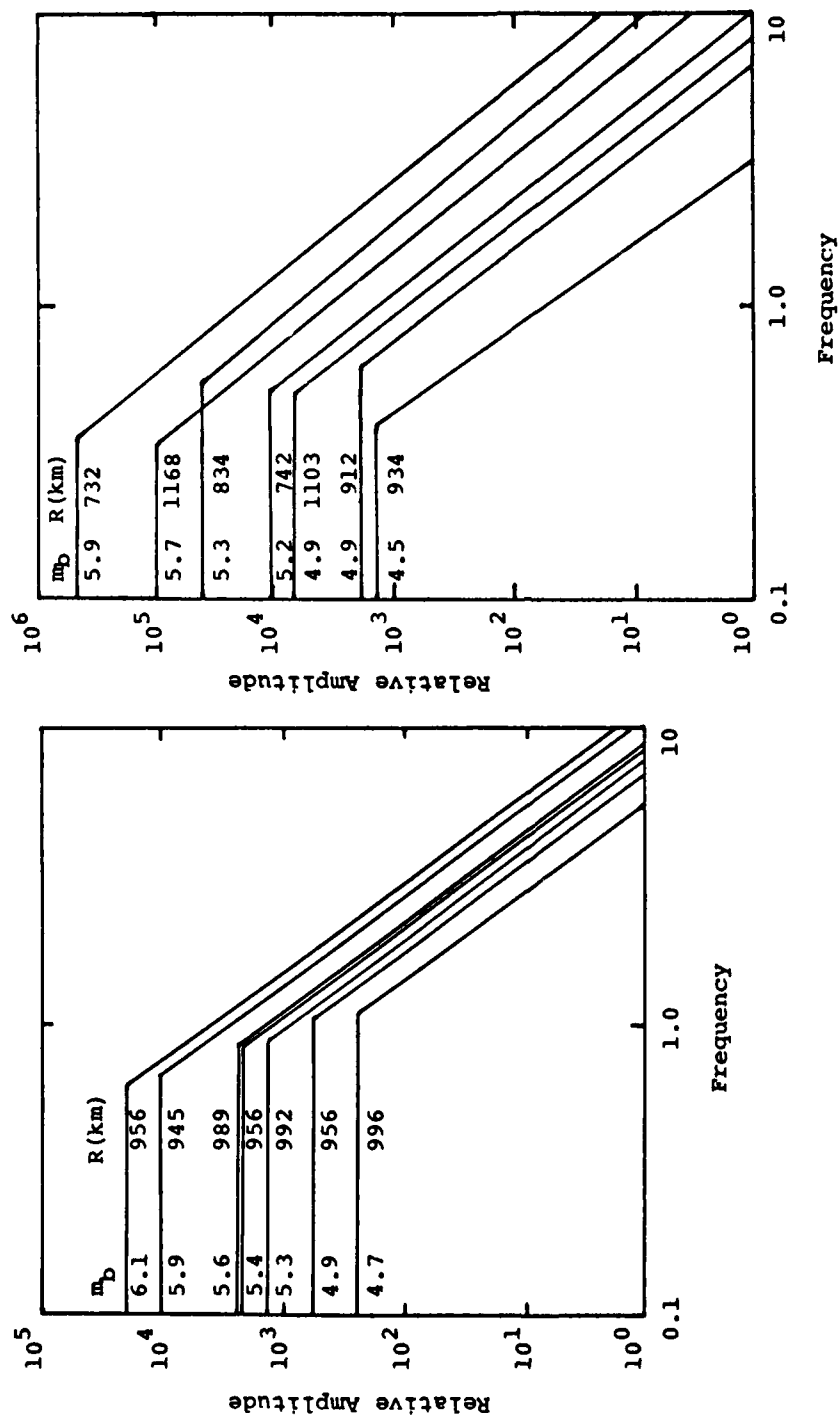


Figure 30. Comparison of schematic Lg spectra observed at WMQ for seven East Kazakh explosions and seven regional earthquakes.

(1988b) for the region around East Kazakh. They found an effective  $Q$  of 2000 for  $L_g$ . This  $Q$  value is considered fairly high, representative of a relatively efficient propagation path such as found in platform regions. It is believed that higher attenuation and lower  $Q$  values are appropriate in regions with increased tectonic activity, so that lower  $Q$  values may be more representative of the paths from many of the earthquake epicenters to WMQ. Figure 31 shows an example of the  $Q$ -corrected  $L_g$  amplitude spectrum for a magnitude 5.9 explosion at East Kazakh and a magnitude 5.9 earthquake. The earthquake range was 732 km. We applied the  $Q$  correction and then normalized the spectra to have equivalent values at 1 Hz. The plot on the left assumes that the explosion and earthquake had equivalent- $Q$  paths with  $Q = 2000$ ; while the plot on the right assumes the  $Q$  for the explosion path was 2000 but the  $Q$  for the earthquake path was only 1000. Comparing the spectral decays above the corner frequency, we see that for the equivalent  $Q$  assumption the slope of the spectral decay is practically the same for the explosion and earthquake. However, under the alternate assumption of a lower  $Q$  path for the earthquake, the slope is less steep for the earthquake. Figure 32 shows the same procedure applied to magnitude 5.3 events. The decay above the corner frequency is again seen to be about the same when the path  $Q$ 's are assumed to be equal, but the decay is somewhat steeper for the explosion when a lower  $Q$  path is assumed for the earthquake. It seems reasonable from tectonic considerations to assume that the path to the earthquakes has lower  $Q$ . If this is in fact the case, it would follow that the  $Q$  corrected  $L_g$  spectra for the earthquakes would be relatively richer in high frequencies than the explosions with similar amplitude levels at 1 Hz. However, the precise  $Q$  corrections for the various source/station paths are unknown at this time and would require considerable effort to develop. Procedures exist for determining station-specific  $Q$  corrections to  $L_g$  (cf. Nuttli, 1986), but those have not yet been implemented for the paths involved here. One other interesting feature of the  $L_g$  spectra in Figures 31 and 32 is that the earthquake spectra at frequencies below 1 Hz appear to be relatively richer in low frequencies. This observation appears to conflict with  $L_g$  spectral observations from NTS (cf. Murphy and Bennett, 1982; Bennett and Murphy, 1986; Bennett *et al.*, 1988a; Taylor *et al.*, 1988), but it is unclear to what extent the spectral amplitudes at low frequencies can be relied on. Additional insight into the spectral behavior in this lower-frequency band might be gained from analysis of the  $L_g$  signals from a channel with better low-frequency response.

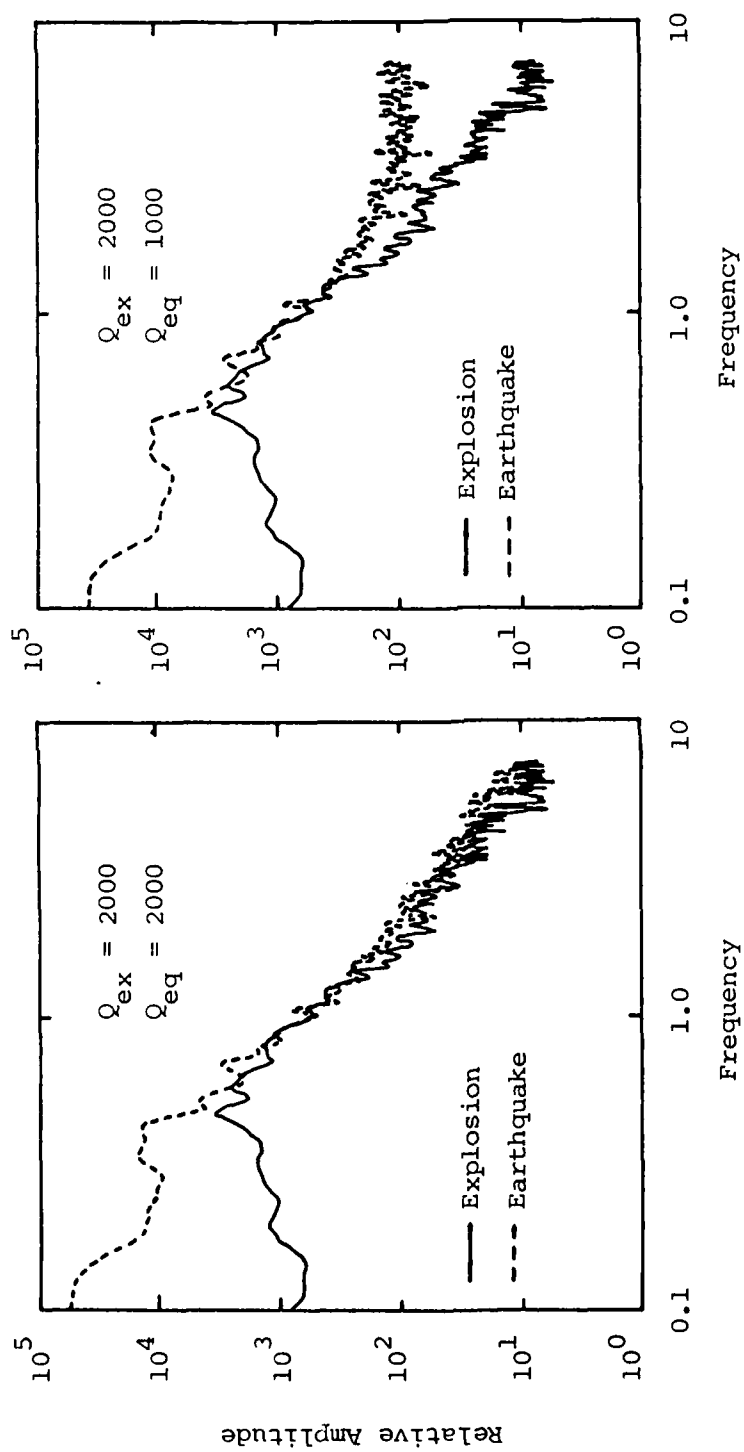


Figure 31. Comparison of Lg spectra at WMQ after Q correction for magnitude 5.9  $m_b$  explosion and earthquake.

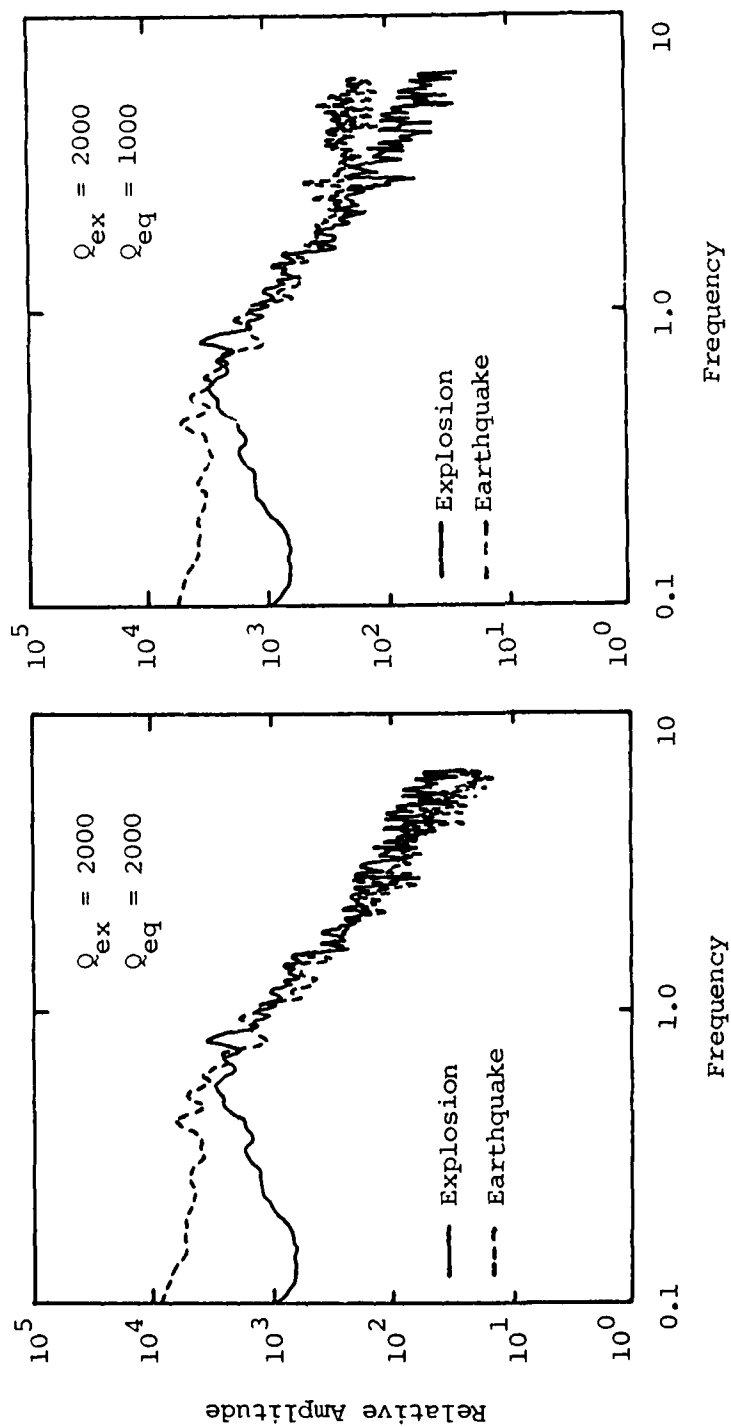


Figure 32. Comparison of Lg spectra at WMQ after Q corrections for magnitude 5.3  $m_b$  explosion and earthquake.

In summary, the CDSN observations from East Kazakh explosions and regional earthquakes indicate some new possibilities for regional discrimination. Regional phases including  $L_g$  and several P phases are strong at this distance range and should provide useful signals for comparing different source types. Comparison of  $L_g$  to P excitation as a function of frequency appears to provide a promising discrimination method for these events, but additional investigation is needed to determine the significance of path differences on the measurements.

### **3.3 Identification of Events from the Vicinity of the East Kazakh Test Site Recorded by the Soviet/NRDC Network**

The Soviet/NRDC seismic network in East Kazakh was installed during the summer of 1986 and monitoring continued episodically through early September of 1987. Seismic instrumentation in the network during the monitoring period was upgraded at several stages. In this report we will consider observations made during Phase II monitoring starting in March, 1987, which included both surface and borehole three-component seismometer installations at each of three stations surrounding the Soviet test site. Figure 33 shows the locations of the three stations at Karkaralinsk (KK), Bayanaul (BA), and Karasu (KS); the station locations in each case were hardrock sites (cf. Leith, 1987). The installations had a high digitizing rate of 250 samples per second enabling analysis of very high frequency signals although the frequency band was limited to frequencies below about 80 Hz by an antialiasing filter. Observations from the Soviet/NRDC network have been described in several previous reports (cf. Berger *et al.*, 1987, 1988; Bennett *et al.*, 1988b; Priestley and Walter, 1988; Smith, 1988a). In our previous report (cf. Bennett *et al.*, 1988b), we focused primarily on utilization of the teleseismic data to define P-wave bias of the region relative to NTS and on analysis of regional event signals to estimate attenuation and effective Q of the earth's crust in that area. The present analysis concentrates on the identification problem for the regional events recorded by the network.

Figure 33 also shows the locations of 362 regional events (including three network calibration explosions) which were located by CSS analysts in the region surrounding the test site using three-component single-station location methods. The stations were shut down, by prior agreement, during Soviet



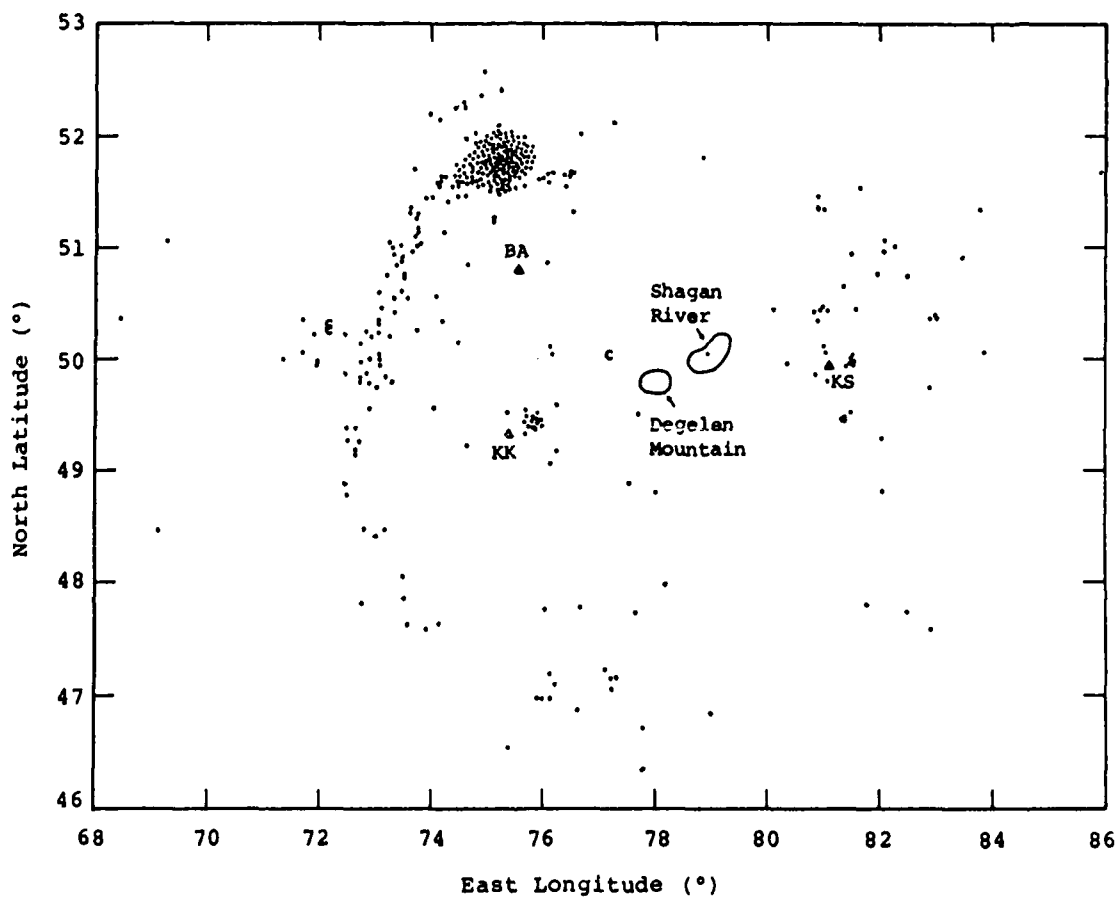


Figure 33. Locations of presumed mine blasts in East Kazakh recorded by the Soviet/NRDC network.

underground nuclear tests. As a result, the observations during Phase II, which extended from March 19, 1987 to September 5, 1987 actually included only 79 days of available data.

The observation of four to five locatable events per day of unknown origin in the region was initially somewhat surprising considering that the area around the East Kazakh test site is generally regarded as being naturally aseismic or as having a very low level of natural earthquake activity. This issue was clarified to some extent by Bennett *et al.* (1988b) who concluded that the majority of these events were probably blasts related to mining or construction activity in the area. This conclusion was based primarily on the fact that 92 percent of the events were concentrated during an eight-hour period of the time of day, suggesting a tendency to blast during daylight hours, which is similar to mining practice in the United States. We can also see in Figure 33 that many of the events tend to be clustered in specific areas (e.g., near 51.5°N, 75.0°E, near 49.8°N, 72.5°E, and near 49.4°N, 75.9°E). Several of these areas (e.g., Ekibastuz at 51.8°N, 75.3°E and Karaganda at about 50.0°N, 73.0°E) are centers of coal fields which are being actively strip-mined (Leith, 1988). However, except for the three calibration shots, we have no particular knowledge of the individual events in this sample, so it's possible that some of the events may not have been commercial blasts. This situation is comparable in many ways to that which we described above in Section II for eastern North America with regional stations detecting a large number of unknown events which would need to be identified if some low-level monitoring threshold were established.

In this study we have not attempted to conduct a comprehensive analysis of all 362 regional events in the database; however, we have sought to identify some of the salient features in the regional seismic signals from these events which may be useful in distinguishing them from other sources in the region. The signals recorded by the Soviet/NRDC network stations from these events frequently included strong  $P_g$ ,  $L_g$ , and short-period fundamental-mode Rayleigh waves,  $R_g$ , to ranges of 400 km or more indicating efficient propagation paths for these small magnitude events. Figures 34 to 37 show several examples of the vertical-component signals at different ranges recorded at stations BA and KK from sources in two different zones: one to the north near Ekibastuz and a more diffuse zone to the south (locations around 47.0°N, 76.5°E). Although

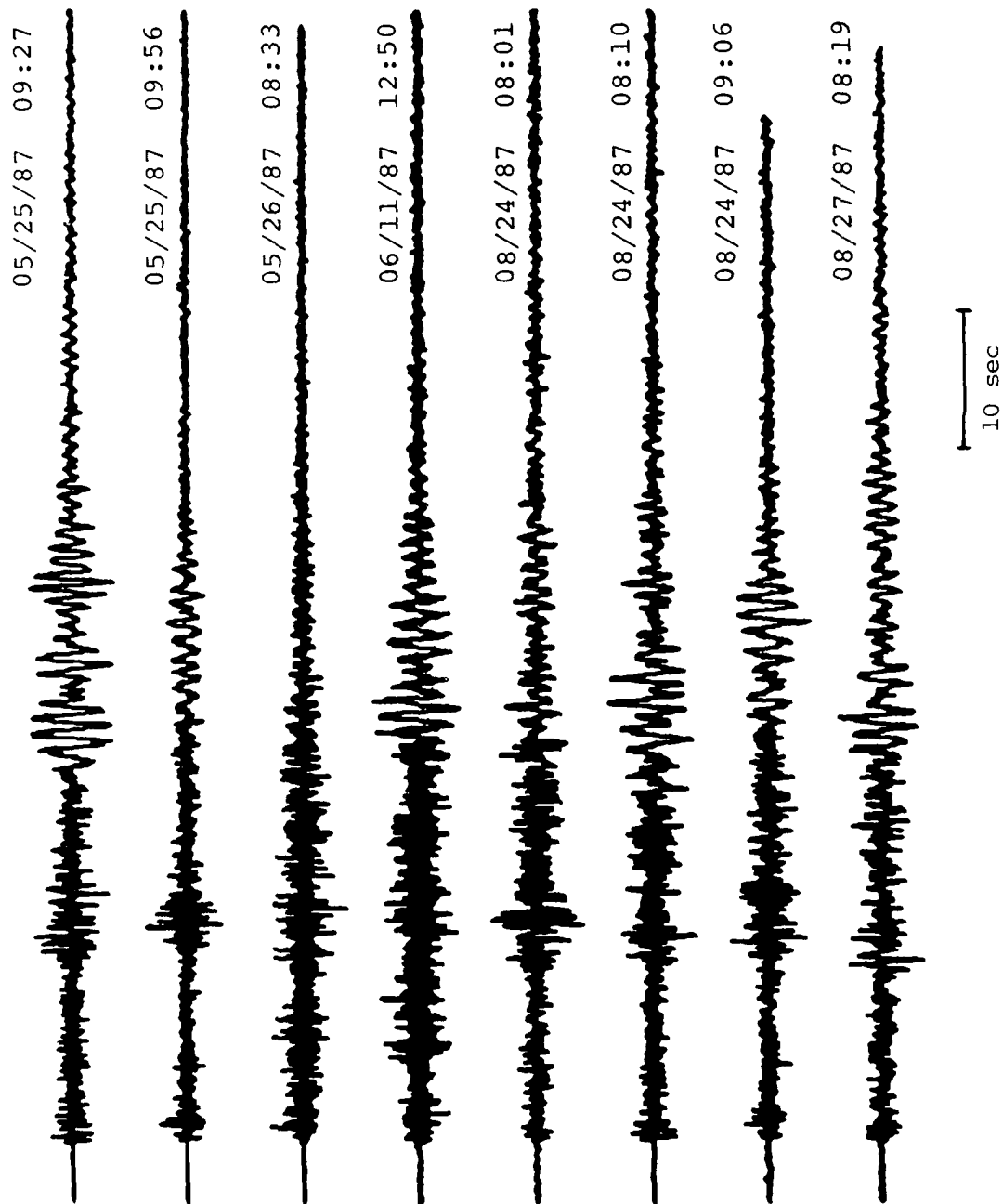


Figure 34. Vertical-component records at station BA from eight presumed mine blasts near Ekibastuz ( $R \approx 100$  km).

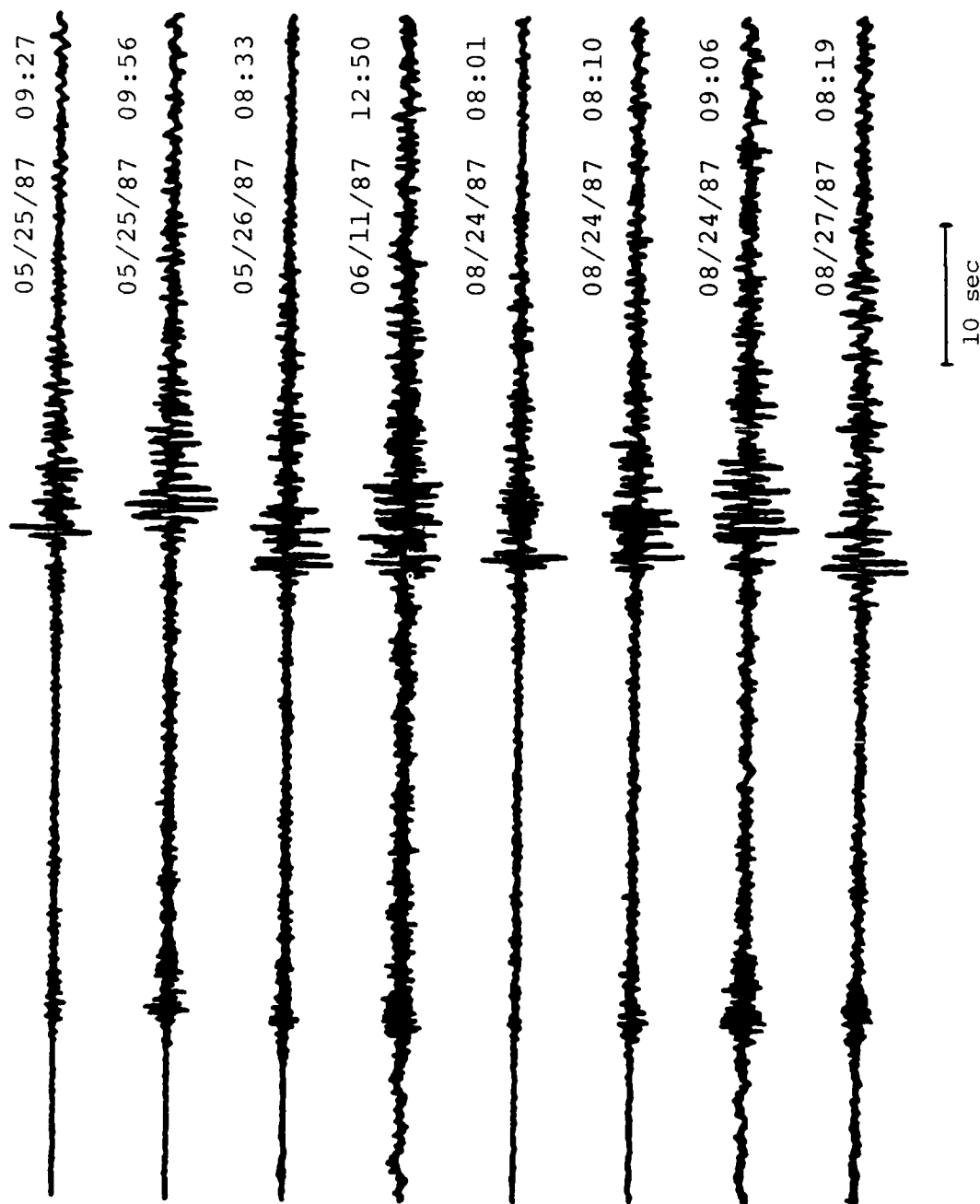


Figure 35. Vertical-component records at station KK from same eight presumed mine blasts near Ekibastuz ( $R \approx 270$  km).

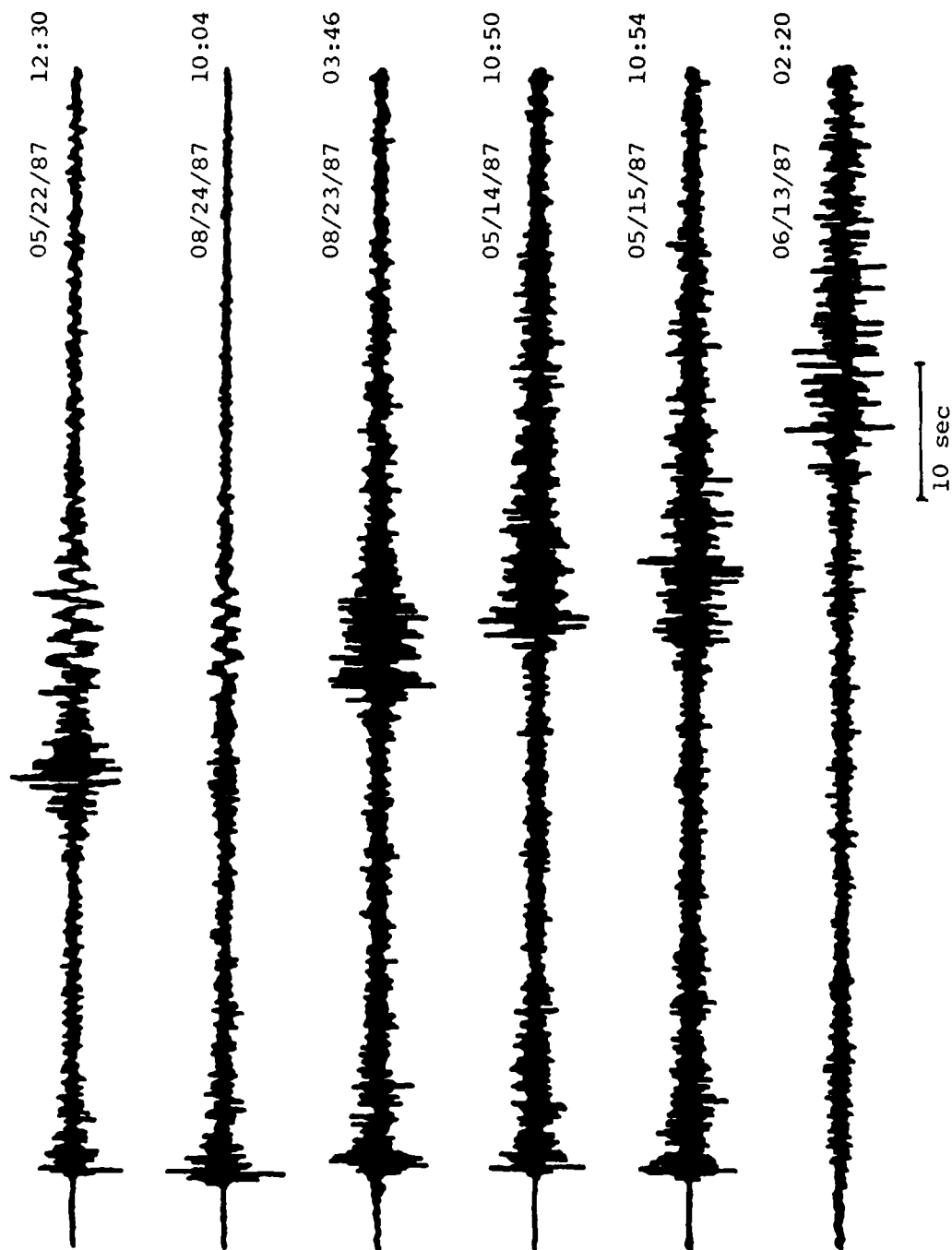


Figure 36. Vertical-component records at station KK from six presumed mine blasts from vicinity of 47.0°N, 76.5°E.

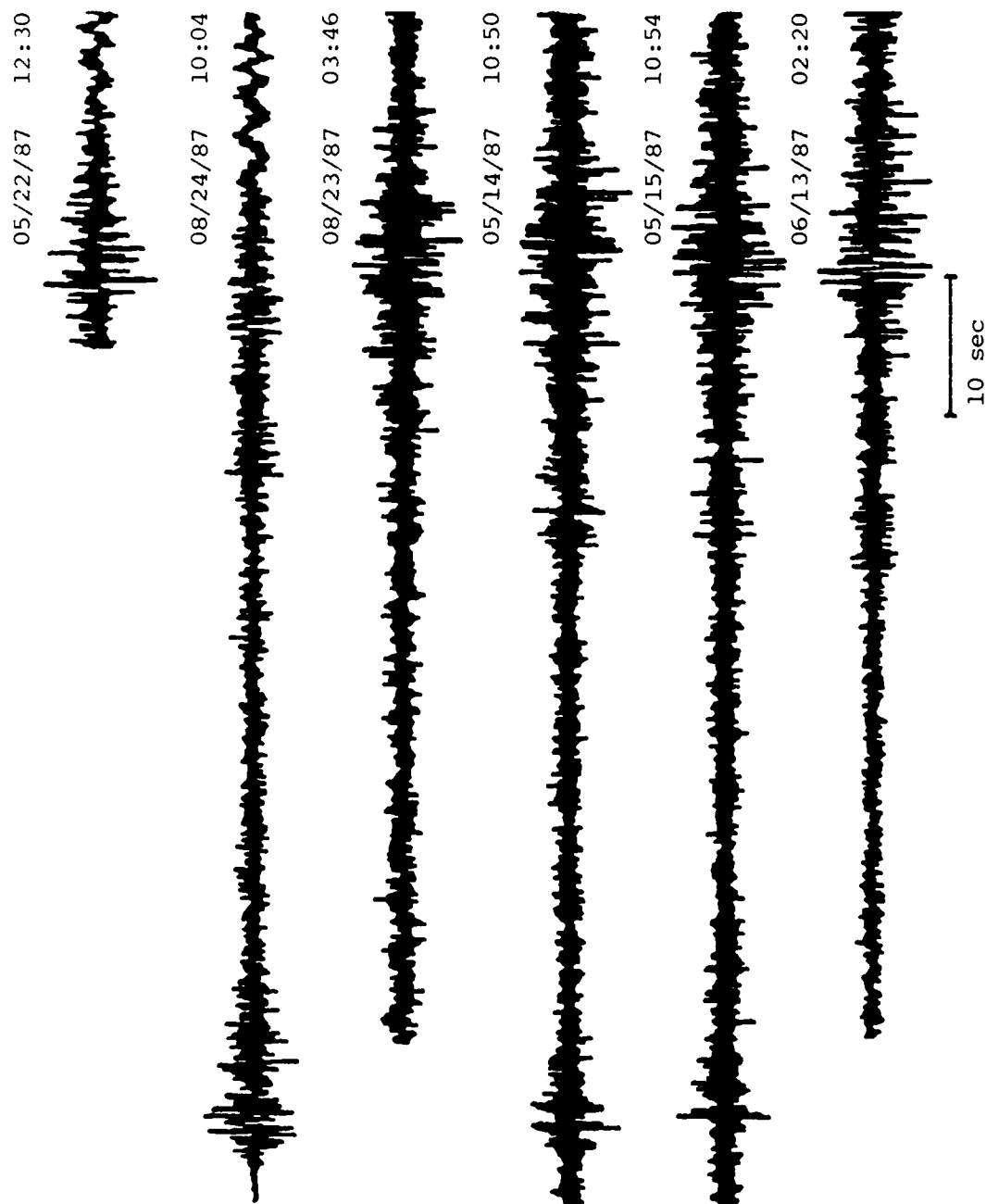


Figure 37. Vertical-component records at station BA from same six presumed mine blasts from vicinity of 47.0°N, 76.5°E.

the relative amplitudes of the  $P_g$  and  $L_g$  signals vary somewhat from event-to-event, the  $P_g$  signal amplitudes are generally less than or about equal to those of the  $L_g$  signals on the broad-band records. Furthermore, the signals from events in specific source zones have remarkable consistency from event-to-event. A notable exception in this regard can be seen by comparing the top two events in Figure 36. The 05/22/87 event has an  $L_g$  signal much larger than the  $P$  while the 08/24/87 event has an  $L_g$  signal much smaller than the  $P$ . Although the events within this source zone were clearly not all located at the same spot, the locations of the 05/22/87 event and the 08/24/87 event were essentially the same within the uncertainty of the single-station location method. Aside from the relative amplitude differences, the signals are quite similar in appearance for the  $P$ ,  $L_g$  and  $R_g$  wave segments. Assuming that these two events were blasts located in close proximity, it seems reasonable to conclude that the differences in the relative amplitudes of  $P$  and  $L_g$  are most likely indicative of some change in shooting practice. This conclusion would imply that the effects of such changes in shooting practice on the relative amplitudes of  $P$  and  $L_g$  need to be understood before much reliance can be placed on such comparisons for discrimination.

Short-period, fundamental-mode Rayleigh waves,  $R_g$ , were frequently quite prominent on the Soviet/NRDC records from the presumed mining blasts in the East Kazakh region. These signals were particularly strong at the nearer distance ranges. Figure 38 shows three-component records at station KK for three presumed mining blasts at a range of 25 to 30 km. The  $R_g$  phase is strong on the vertical and E-W components and has a dominant frequency between 1.0 and 1.5 Hz. A similar fundamental-mode Love wave which is also controlled by the near-surface, low-velocity waveguide appears as a strong phase on the N-S component records for these blasts. Figure 39 shows similar  $R_g$  and Love wave phases recorded at station BA for two different presumed mine blasts, in this case located at ranges of 100 km. As noted above in Section II, these strong, short-period, fundamental-mode phases are associated with the seismic excitation of the low-velocity layer at the earth's surface by shallow-focus events. Unfortunately, we don't know whether any of the events surrounding the East Kazakh test site, which are in the Soviet/NRDC database, are earthquakes. Some of the events certainly produce somewhat weaker  $R_g$  signals, but this could also be caused by differences in shooting practice or attenuation which could be strong if the

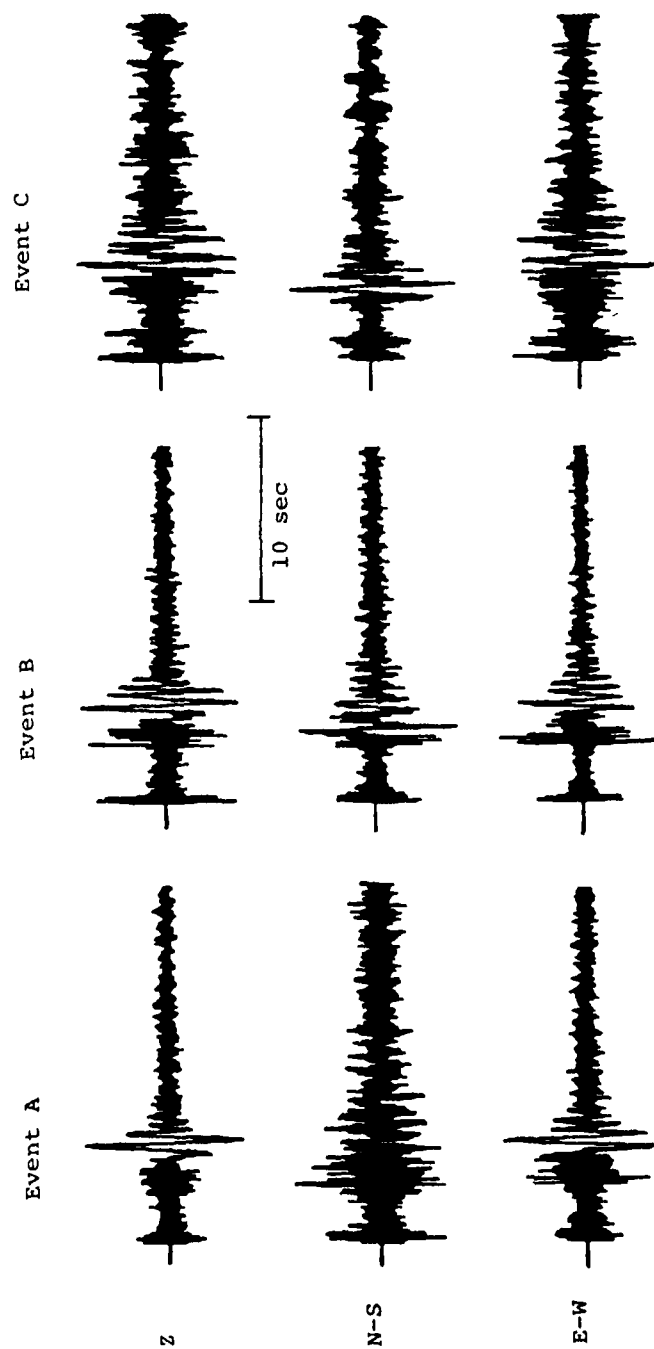


Figure 38. Three-component records at station KK for three presumed mine blasts located 25-30 km to the east.



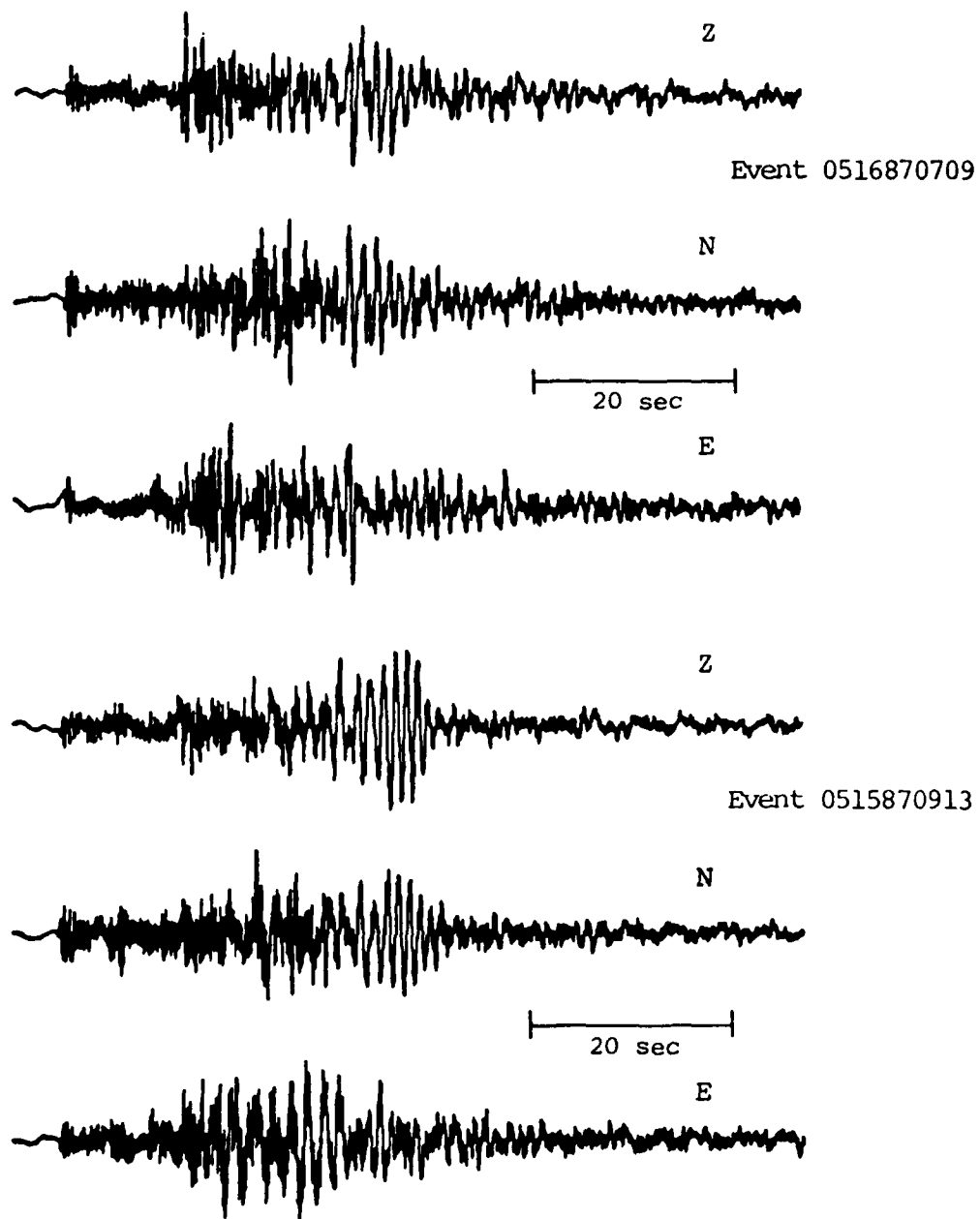


Figure 39. Three-component records at station BA for two presumed mine blasts located near Ekibastuz ( $R \approx 100$  km).

waveguide is not continuous. So the lack of  $R_g$  cannot be regarded as an unambiguous indication of source depth which could be used to distinguish earthquakes from blasts.

On the other hand, the simple  $R_g$  waveforms observed for some of the presumed blasts recorded by the Soviet/NRDC network could be quite valuable for investigating regional crustal structure. To demonstrate this capability we analyzed the observed  $R_g$  signals recorded at station KK from the mine blasts located just east of the station at a range of 25 to 30 km. As shown above in Figure 38, these blasts produced strong, uncomplicated  $R_g$  signals at these relatively short ranges. It is well known from previous studies (cf. McEvilly, 1964; Herrmann, 1969; Kafka and Reiter, 1987) that the dispersed  $R_g$  wavetrain produced by such blasts is strongly dependent on the velocity structure in the upper few kilometers along the propagation path. Murphy (1981) and Murphy and Shah (1988) represented the near-surface explosion source as an axisymmetric vertical pressure acting on the surface of a multilayered half-space. They found for this source that the ground motion displacement was dominated by low-frequency, surface-wave components and that the Rayleigh-wave ground motion could be reasonably approximated as an Airy phase provided the source corner frequency,  $f_c$ , is less than the dominant frequency,  $f_o$ , associated with the site response. While we recognize that the individual shots in mine blasting are likely to have relatively high, source corner frequencies, it is believed that shot delays as well as non-linear interaction at the mine blast source will tend to lengthen the source duration and decrease  $f_c$ . Furthermore, although the actual mechanism of the mine blast is no doubt more complex than the model, the simplicity of the observed waveforms suggested that some insight could be gained from the relatively simple source description. Therefore, in analyzing the Rayleigh waves recorded at station KK from the mine blasts, we followed the approach of Murphy and Shah (1988) and assumed that  $f_c$  is less than  $f_o$ . Under this assumption Murphy and Shah found that the displacement spectral amplitude was sharply peaked primarily due to the Rayleigh wave site response term and that it could be represented as the product of a site response term, a propagation term and the source function all evaluated at  $f_o$  with

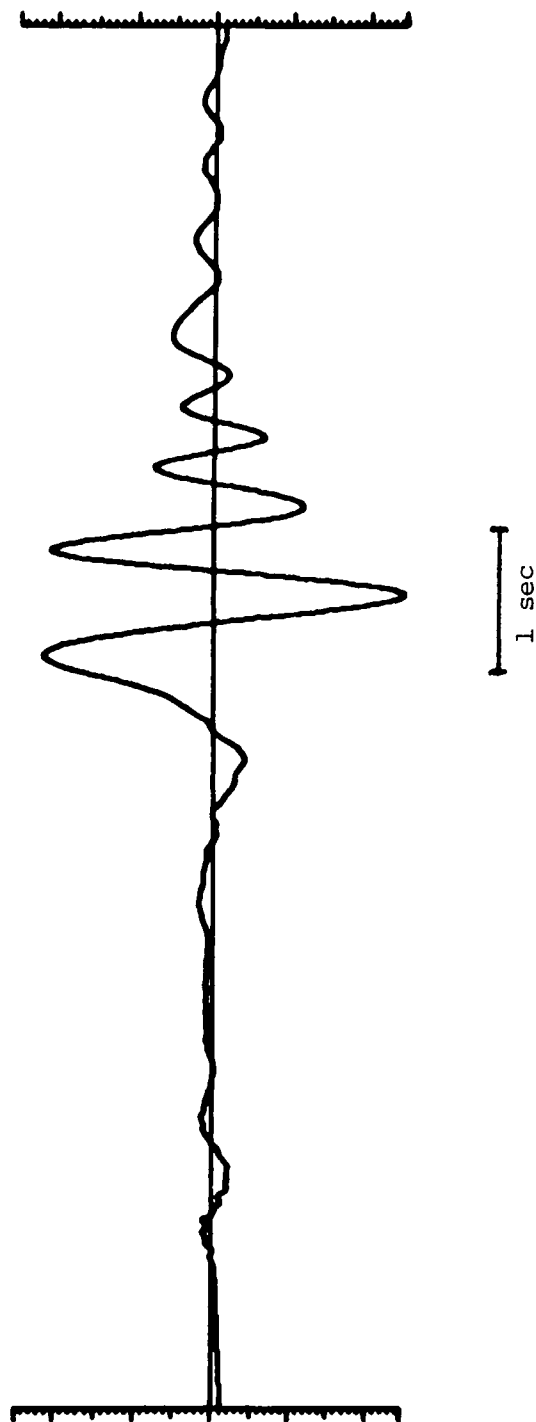
$$f_o = \frac{\bar{\beta}}{2.3H}$$

where  $\bar{\beta}$  is the average shear-wave velocity above the first significant discontinuity in velocity at depth  $H$ . Then, for the vertical component Rayleigh wave, the peak amplitude of the ground motion was found to decrease as shear velocities in the structure increase, and the duration of the motion increased as the ratio of the shear velocity below to above the interface increased.

Figure 40 shows the vertical-component, displacement time history, corrected for instrument response, for a blast recorded on 05/23/87 at station KK. The signal is dominated by a somewhat weakly dispersed Rayleigh wave with a dominant frequency near 1.3 Hz. By comparison of the observed signal duration in Figure 40 with the results reported by Murphy and Shah for the dependence of the duration on the shear-velocity ratio, it appears that a velocity ratio with  $\beta_2 / \beta_1 \approx 2$  matches closely the observed behavior. We therefore take  $\beta_c / \bar{\beta} = 2$  where  $\beta_c$  is the shear velocity in the deeper crustal rock (i.e., half-space). Now, according to Leith (1987) the compressional velocity of crustal rock in the region is about 5.4 km/sec. Assuming a Poisson's ratio  $\sigma$  of 0.25,  $\beta_c = 5.4/\sqrt{3} = 3.12$  km/sec. Thus,  $\bar{\beta} = 1.56$  km/sec, and using the relation  $f_0 = \bar{\beta}/2.3H = 1.3$  Hz, we estimate  $H$  to be about 0.5 km. Murphy and Shah (1988) proceeded to show that the Rayleigh-wave vertical displacement time history for the model could be approximately represented by

$$W(r, \tau) = \frac{A_p e^{-\alpha \tau^2}}{r^{\frac{5}{6}}} \cos \omega_0 \tau$$

where  $\tau$  is time relative to the surface wave peak which has an amplitude  $A_p$ ,  $\omega_0 = 2 \pi f_0$ , and  $\alpha$  is a parameter representing the decay in the wavetrain envelope with time. For the blast in Figure 40, we estimated  $\alpha$  to be 0.89; then, the waveforms at the bottom of Figure 40 show the comparison between the Airy phase approximation to the blast Rayleigh wave and the observed signal. Obviously, the match is good near the peak and in adjacent cycles but not as good later as the signal becomes more dispersed. We conclude from this preliminary analysis that the dominant part of the vertical Rayleigh wave signal is adequately represented by the simple blast source for a layer over a half-space model. In the model the layer thickness is about 0.5 km, and the shear-wave velocity is 1.56 km/sec in the layer and 3.12 km/sec in the half-space. It seems clear that in a more exact treatment, we could probably do a



Airy Phase Approximation

$$\frac{A_0 e^{-\alpha \tau} \tau^{3/2}}{r^{5/6}} \cos \omega_0 \tau$$

$$\text{with } f_0 = \frac{\omega_0}{2} = 1.3 \text{ Hz}$$

$$\alpha = 0.89$$



Figure 40. Vertical-component displacement at station KK from presumed mine blast near East Kazakh (top). Comparison of observed  $R_g$  (solid line) and Airy phase approximation (dots) for an explosion source (bottom).

better job of matching some of the observed signal characteristics (e.g., dispersion). Nevertheless, the fact that the simple model agrees with the observations fairly well suggests that at least some signal characteristics may not be strongly influenced by the details of the blast mechanism. This could be demonstrated by analyzing observations from additional mine blasts with different shooting practices. Analyses of the dispersion characteristics of the short-period Rayleigh waves for the mine blasts in the other areas around East Kazakh might provide additional insight into variations in the near-surface geology across the region.

A final observation relating to discrimination of mine blasts using the Soviet/NRDC network data is the presence in the signals of characteristic indications of source multiplicity. It is well known that commercial explosions frequently consist of a series of delayed shots designed to reduce damaging vibrations and increase rock fracturing. Frantti (1963) and Willis (1963) provided some early insights into the potential influences of shot delays on seismic signals, but their studies focused on observations made fairly close to the source. Until recently little effort has been made to identify such effects in more distant seismic signals. This is partly because shot delays are rather short; and, therefore, the effects should be strongest at high frequencies, but seismic instrumentation has generally not been adequate in the past to investigate such effects. Simple theory indicates that the spectra of seismic signals from multiple shots will include a series of holes and another series of lobes at frequencies related to the delay times between shots. Dick *et al.* (1983) indicate that in surface blasting shot delays are normally between 25 and 100 msec, and similar practice is thought to extend worldwide. In order to resolve the spectral effects of these kinds of shot delays, it would be necessary to have fairly broad-band recording instruments with signal spectra extending from low frequencies to several tens of Hertz. In Section II above we noted that the frequency band of signals recorded at RSCP from mine blasts in the eastern U. S. was probably inadequate to identify such spectral scalloping. However, recent studies by Baumgardt and Ziegler (1988) and Smith (1988b) using broad-band seismic systems have found evidence of delayed shooting in some mine blast recordings at regional distances in Norway and northern North America.

Since the Soviet/NRDC network had a fairly high digitizing rate and the signal-to-noise level extended to high frequencies for many of the larger events, it is reasonable to expect that the regional signals from the mine blasts would show some evidence of the expected spectral scalloping. Figure 41 shows uncorrected spectra obtained at stations BA ( $R = 100$  km) and KK ( $R = 270$  km) for the  $L_g$  signal windows from one of the larger presumed mine blasts in the northern source zone near Ekibastuz ( $51.6^\circ\text{N}$ ,  $75.0^\circ\text{E}$ ). We show the spectra out to 100 Hz although it appears that the spectrum at the more distant station has fallen to the noise floor at a lower frequency. At the nearer station BA, the  $L_g$  spectrum is seen to consist of a sequence of peaks and troughs which we interpret to correspond to the expected scalloping. The spectral lobes are rather broad, but the holes seem to be relatively sharp. The most obvious hole occurs at 11.5 Hz and we observe a sequence of successive holes positioned at odd multiples of the initial hole with intervening lobes as would be predicted by simple theory. Since the spectral scalloping is presumed to be related to the shot delays in the source, the theory would predict that the same scalloping should be observed at the other station. Although the holes are less definitive, we certainly see evidence of their presence at some of the expected frequencies. Again following the simple theory, the shot delay required to produce a hole at 11.5 Hz, and at the successive odd multiples, is just equal to the reciprocal of twice that frequency, or about 43 msec. Unfortunately, as noted earlier, we lack specific information on the shooting practice in these presumed blasts. The shot-delay explanation for the observed spectral behavior seems reasonable, but alternate causes may also be possible. Furthermore, it's clear from the spectrum at the more distant station in Figure 41 that the spectral scalloping in the regional signals may not be easy to discern at larger ranges except for much larger events. It is also clear in principle that variations in shot delays could complicate the spectrum to an extent that the regularity in the pattern expected from delayed shooting might go unnoticed. Therefore, detection of delay shooting characteristics in regional phase spectra from mine blasts may be useful for identifying some events but may not provide the panacea which will be required to eliminate the large number of commercial blasts at lower threshold levels.

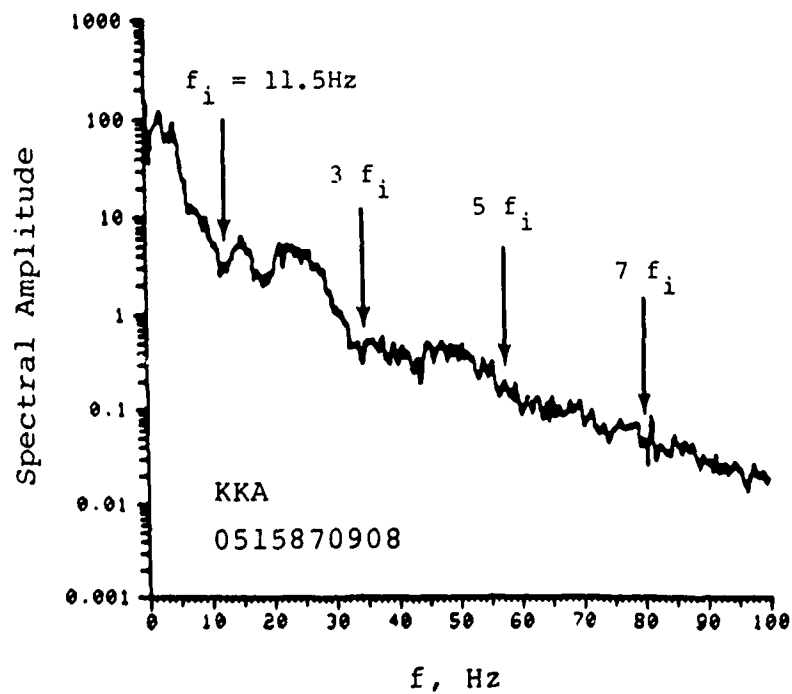
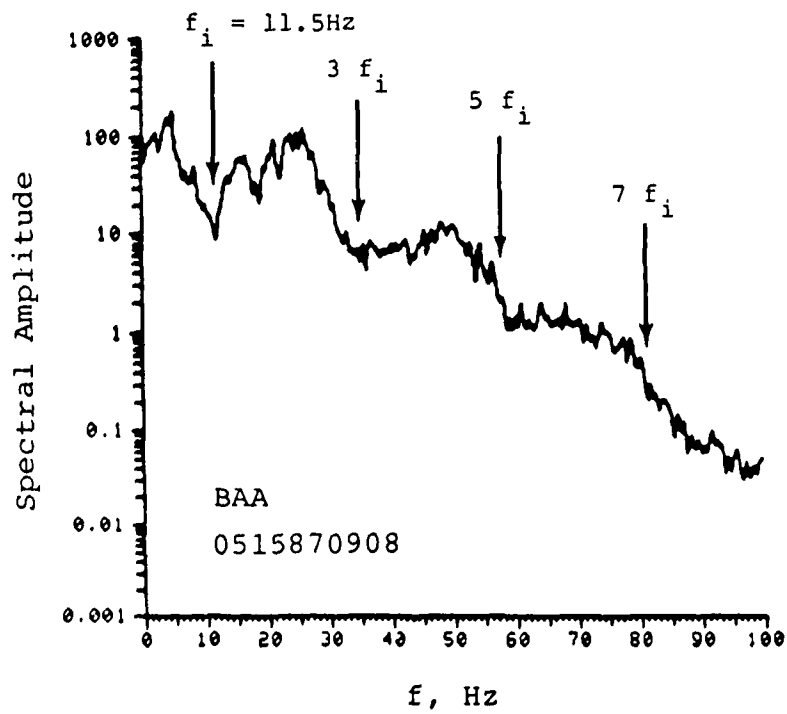


Figure 41. Evidence of notches in  $L_g$  spectra from presumed mine blast near Ekibastuz.

## **IV. NTS UNDERGROUND NUCLEAR EXPLOSIONS AND COMPARABLE EARTHQUAKES**

### **4.1 Empirical Derivation of Techniques for Regional Discrimination of Nuclear Explosions**

It is well known that the excitation and propagation of regional seismic signals is strongly dependent on the crustal properties of the source and receiver region. Therefore, a true test of regional discrimination capability in the Soviet Union should involve determination of the seismic signal differences between Soviet underground nuclear tests and nearby earthquakes of comparable magnitude. Several factors have precluded satisfactory empirical testing of this kind; these include, in particular, the general lack of natural seismicity in the Soviet platform region where most nuclear explosion tests have been conducted and the unavailability (prior to CDSN and the new IRIS sites) of data from seismic stations at regional distances from Soviet tests. This lack of a suitable database for testing regional discrimination in the Soviet Union has forced many previous investigators to take a more hybrid approach. This approach utilizes empirical results from regional seismic measurements for U.S. nuclear tests and comparable earthquakes and infers how source or propagation differences might influence the measurements in areas of intended application (viz the Soviet Union). An important feature in this methodology is the utilization of a controlled set of sources enabling analysis of the sensitivity of the measurements to a variety of source conditions.

Blandford (1981) found that, after careful correction for attenuation differences, the amplitude ratio of the regional signals before and after the predicted S times separated U.S. underground nuclear explosions from earthquakes with locations throughout the eastern and western U.S. However, Murphy and Bennett (1982) and Bennett and Murphy (1986) found considerable intermingling of small NTS explosions and nearby earthquakes when the relative amplitudes of  $P_n$ ,  $P_g$  and  $L_g$  signals were compared using measurements at equivalent ranges from regional VELA array stations; but those studies also produced evidence of spectral differences in the regional phases from the explosions and earthquakes. Recent studies by Taylor *et al.* (1986,1988) and Glaser



et al. (1986) have investigated a wide variety of regional discriminant measures and found that some discriminants were more effective than others in separating the source types when applied to NTS explosions and earthquakes spread throughout the western U.S. Taylor et al. (1988) and Patton (1988) demonstrated sensitivity in the  $L_g$  signals from explosion sources to certain source parameters including depth of burial, material properties and spall. Because of the significance of using a controlled source sample to establish empirical regional discrimination techniques, a part of our efforts in this research has focused on analysis of a data sample from NTS underground nuclear explosions and western U.S. earthquakes. Our data sources in this phase of the research were primarily selected events from the Lawrence Livermore National Laboratory (LLNL) seismic network and several additional events recorded at greater regional distances at the RSTN station RSSD. These stations provided high-quality digital data with relatively high sampling rates.

#### **4.2 Analysis of LLNL Data**

In previous reports (cf. Bennett et al., 1987a,b), we described the results of analyses of the amplitude and spectral characteristics of the regional phases recorded by the LLNL network stations from a small sample of four underground nuclear explosions and four nearby earthquakes. Those data have subsequently been supplemented with records from six additional NTS explosions and four additional earthquakes with epicenters less than 100 km from NTS. The earthquake sample was selected from the larger LLNL database so as to minimize propagation differences by choosing those earthquakes with epicenters closest to NTS. The explosion sample was selected to provide events from a single source area (Yucca Flat) with depths both above and below the water table and with at least some explosions having equivalent magnitudes to the earthquakes which were being compared. The data themselves were generously supplied by Dr. Steven Taylor with the assistance of others at LLNL. Figure 42 shows the event locations relative to the LLNL network stations, and Table 7 summarizes the event source information. The explosions were all at Yucca Flat at ranges of about 225 km from MNV (Mina, Nevada), 290 km from KNB (Kanab, Utah), 310 km from LAC (Landers, California), and 400 km from ELK (Elko, Nevada). The magnitudes of the explosions in the sample were between 4.2 and 5.5  $M_L$ ; and the source depths were from 0.3 to 0.7 km.

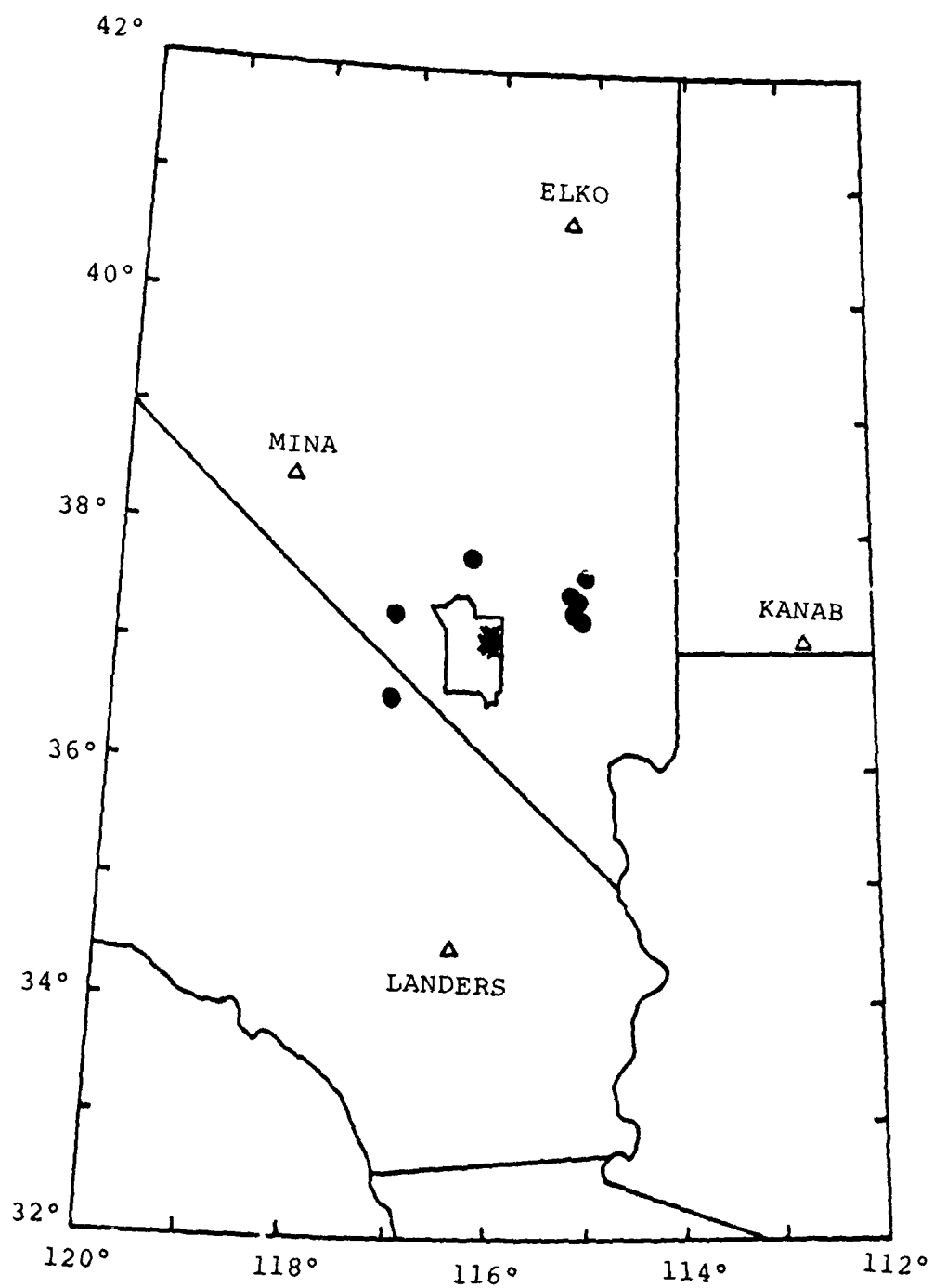


Figure 42. LLNL station locations and event sample from vicinity of NTS.

Table 7  
LLNL Data Sample

<u>NTS EXPLOSIONS</u>							
Date	Time	Lat. (°N)	Lon. (°W)	Depth (km)	M <sub>L</sub> (BRK)	m <sub>b</sub>	
03-31-84	14:30:00.0	37.15	116.08	0.32	4.2	4.1	AGRINI
08-11-83	14:00:00.1	37.00	116.00	0.32	4.2	4.4	SABADO
08-03-83	13:33:00.1	37.12	116.09	0.33	4.3	4.2	LABAN
01-31-84	15:30:00.0	37.11	116.12	0.39	4.4	4.1	GORBEA
09-27-78	17:00:00.0	37.08	116.05	0.44	5.0	5.0	DRAUGHTS
09-13-84	14:00:00.0	37.09	116.07	0.48	5.0	5.0	BRETON
04-14-83	19:05:00.1	37.07	116.05	0.53	5.5	5.7	TURQUOISE
04-27-77	15:00:00.1	37.09	116.03	0.59	5.1	5.4	BULKHEAD
03-23-78	16:30:00.2	37.10	116.05	0.64	5.5	5.6	ICEBERG
04-05-77	15:00:00.2	37.12	116.06	0.69	5.5	5.6	MARSILLY

<u>EARTHQUAKES NEAR NTS</u>							
Date	Time	Lat. (°N)	Lon. (°W)	Depth (km)	M <sub>L</sub>	m <sub>b</sub> (L <sub>g</sub> )	
08-12-79	11:31:19.7	37.26	115.08	3	3.6	-	
08-16-79	03:37:44.9	37.25	115.06	3	3.7	-	
07-06-82	02:10:43.5	37.69	115.05	3	4.2	-	
06-04-83	11:37:40.9	37.39	115.21	4	3.6	2.9	
05-12-82	19:29:24.5	37.27	115.08	7	4.0	3.3	
10-25-80	00:30:59.0	37.79	116.28	8	3.8	-	
12-25-79	14:17:10.8	37.27	117.06	8	4.2	-	
03-16-82	07:08:13.1	36.60	117.07	9	3.5	-	

Earthquake locations surrounded the Test Site with ranges between 160 and 300 km from MNV, between 200 and 395 km from KNB, between 250 and 385 km from LAC, and between 340 and 485 km from ELK. The earthquake magnitudes were between 3.5 and 4.2  $M_L$ , and the depths were between about 3 and 9 km.

In previous reports Bennett *et al.* (1987a,b) presented representative vertical component time histories for the smaller explosions in the database and several nearby earthquakes. Figure 43 shows representative time histories for several of the events from the LLNL database. The general characteristics of the regional phases from these events were described in the previous reports. The  $P_n$ ,  $P_g$ , and  $L_g$  phases in most cases appear as clear signals except at those ranges less than the  $P_n$ - $P_g$  crossover distance where  $P_n$  is buried in the  $P_g$ . The explosions are more repetitive in signal character from event-to-event at a fixed station than are the earthquakes; this in large measure reflects changes in propagation path and epicentral distance for the earthquakes but may also represent to some extent mechanism-dependent effects. Bennett *et al.* (1987a,b) showed that such differences could considerably modify the relative amplitudes of the  $P_n$ ,  $P_g$  and  $L_g$  signals as is observed for the earthquakes. However, some differences have also been noted in the different explosions measured at common stations (cf. Bennett *et al.*, 1987a,b) suggesting the possibility that small changes in the explosion source parameters might significantly affect the relative amplitude of  $P_g$  and  $L_g$  and the frequency content of the signals.

In analyzing the more recent LLNL data sample, our studies have focused on the spectral behavior of the regional phases. Time windows encompassing the principal energy in the  $P_g$  and  $L_g$  signals were picked from the records. These were fairly consistent for events with similar source locations; but, in any case, small shifts in the window times produced only minor changes in the computed spectra. Window lengths were taken to be approximately 12.5 seconds for  $P_g$  and approximately 25 seconds for  $L_g$ . The spectra were also computed for noise windows approximately 6.3 seconds in length preceding the P wave. The window lengths were somewhat variable between events because the sampling rate of the LLNL network recording system was not always consistent. For most events the digitizing rate was 40 samples per second, but some events were recorded at a rate of 42 samples per second and several at a rate

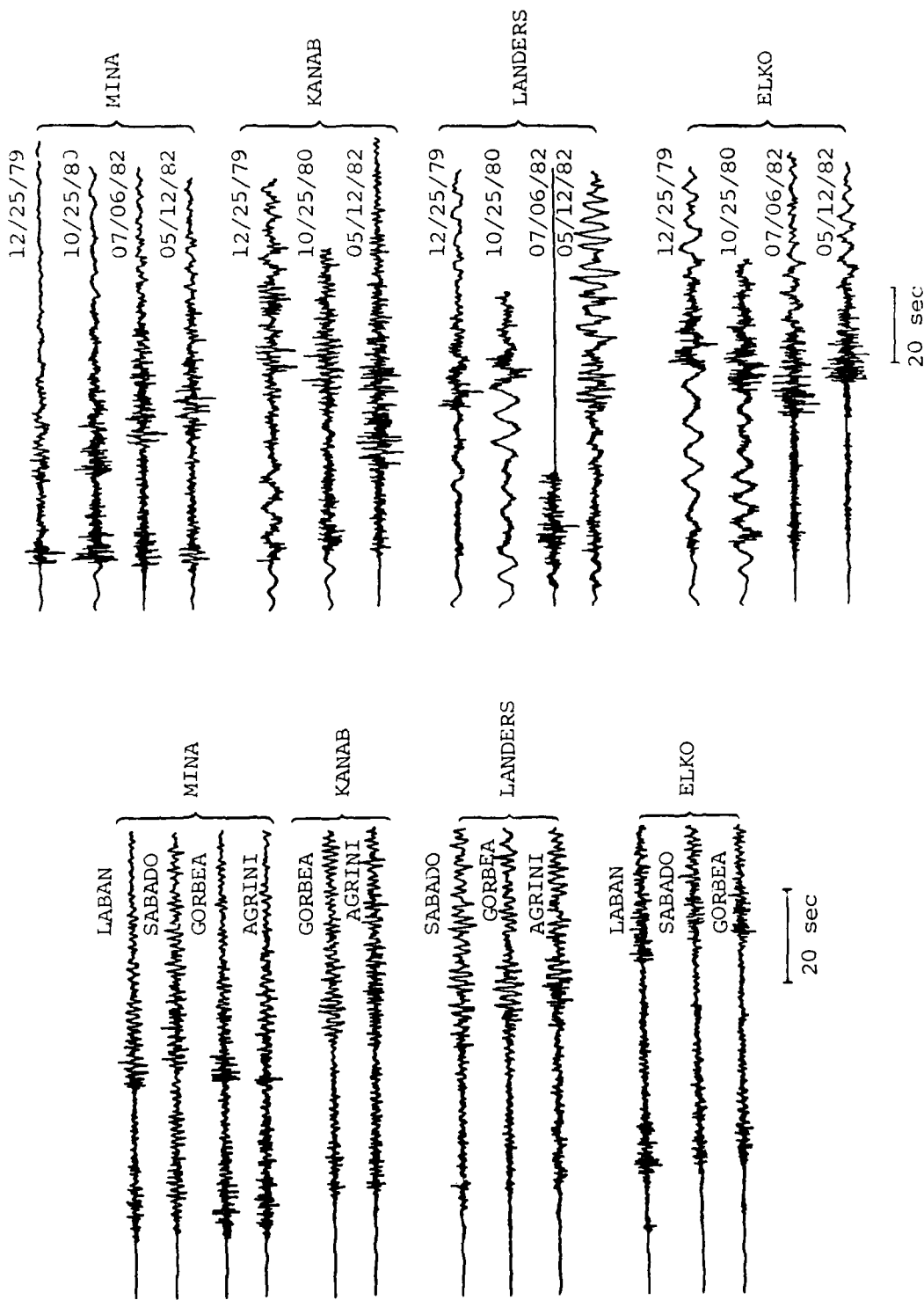


Figure 43. Typical vertical-component records at LLNL stations from NTS explosions (left) and regional earthquakes (right).

of 62.5 samples per second. Such differences are not expected to have a significant effect on the spectral amplitudes in the frequency band of interest because the spectra have been normalized by the window lengths and smoothing was applied to provide roughly comparable frequency resolution.

In a previous report Bennett *et al.* (1987b) showed that the signal-to-noise levels of  $L_g$  and  $P_g$  signals for most events in the LLNL database was good out to frequencies of 10 Hz or so. In some cases the  $L_g$  and  $P_g$  spectra have been found to flatten-out at levels well above the pre-P ground noise at frequencies less than 10 Hz apparently because of limitations on the dynamic range of the recording equipment. It was further noted that the  $L_g$  and  $P_g$  spectra for explosions tended to fall-off more rapidly at higher frequencies than the signals of earthquakes with comparable magnitudes. To check the latter observation with the enhanced LLNL database, the  $L_g$  and  $P_g$  spectra for all events were normalized to common amplitude levels at 1 Hz. Then the explosion and earthquake spectral shapes were averaged separately over the events from each source type out to those frequencies where spectral flattening associated with the dynamic range problem became apparent. Figure 44 shows the average earthquake and explosion spectral shapes for the  $L_g$  signals recorded at each station. In all cases we see that the average earthquake and explosion spectra match fairly closely out to about 2 Hz but the explosion spectrum falls-off at higher frequencies much more rapidly than the average earthquake spectrum. Figure 45 shows the mean plus and minus one standard deviation  $L_g$  spectral shapes. At all stations the  $L_g$  spectral shapes for earthquakes and explosions are observed to be totally separated at the one-sigma level above about 4 Hz. This observation is similar to the behavior of the  $L_g$  spectra previously found by Murphy and Bennett (1982) and Bennett and Murphy (1986) from analyses of the signals recorded at the VELA array stations. In those studies the spectral differences between the explosions and earthquakes could only be observed out to about 4 Hz because of recording instrument limitations. The results here suggest that even greater separation in the  $L_g$  spectra between the NTS explosions and nearby earthquakes is achieved at higher frequencies (viz out to at least 10 Hz). Thus, the  $L_g$  spectral ratio discriminant might be enhanced by observations at higher frequencies. Figure 46 shows similar average spectral shapes for the  $P_g$  phases recorded by the LLNL network stations. Like the  $L_g$  behavior, the explosion and earthquake spectral shapes are observed to match fairly closely at frequencies below about 2 Hz but then separate at higher

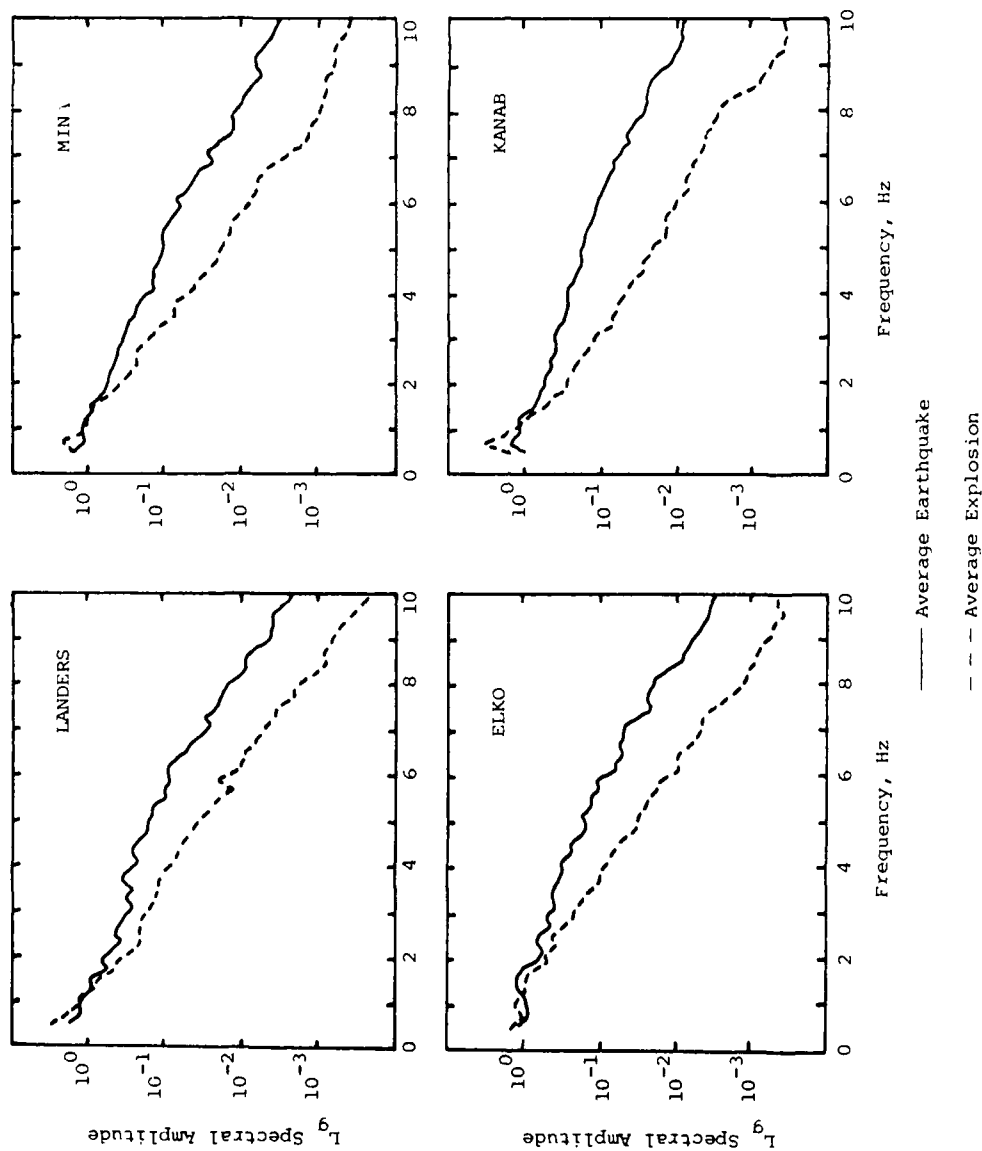


Figure 44. Comparison of average  $L_g$  spectral shapes for NTS explosions and nearby earthquakes recorded by LLNL stations.

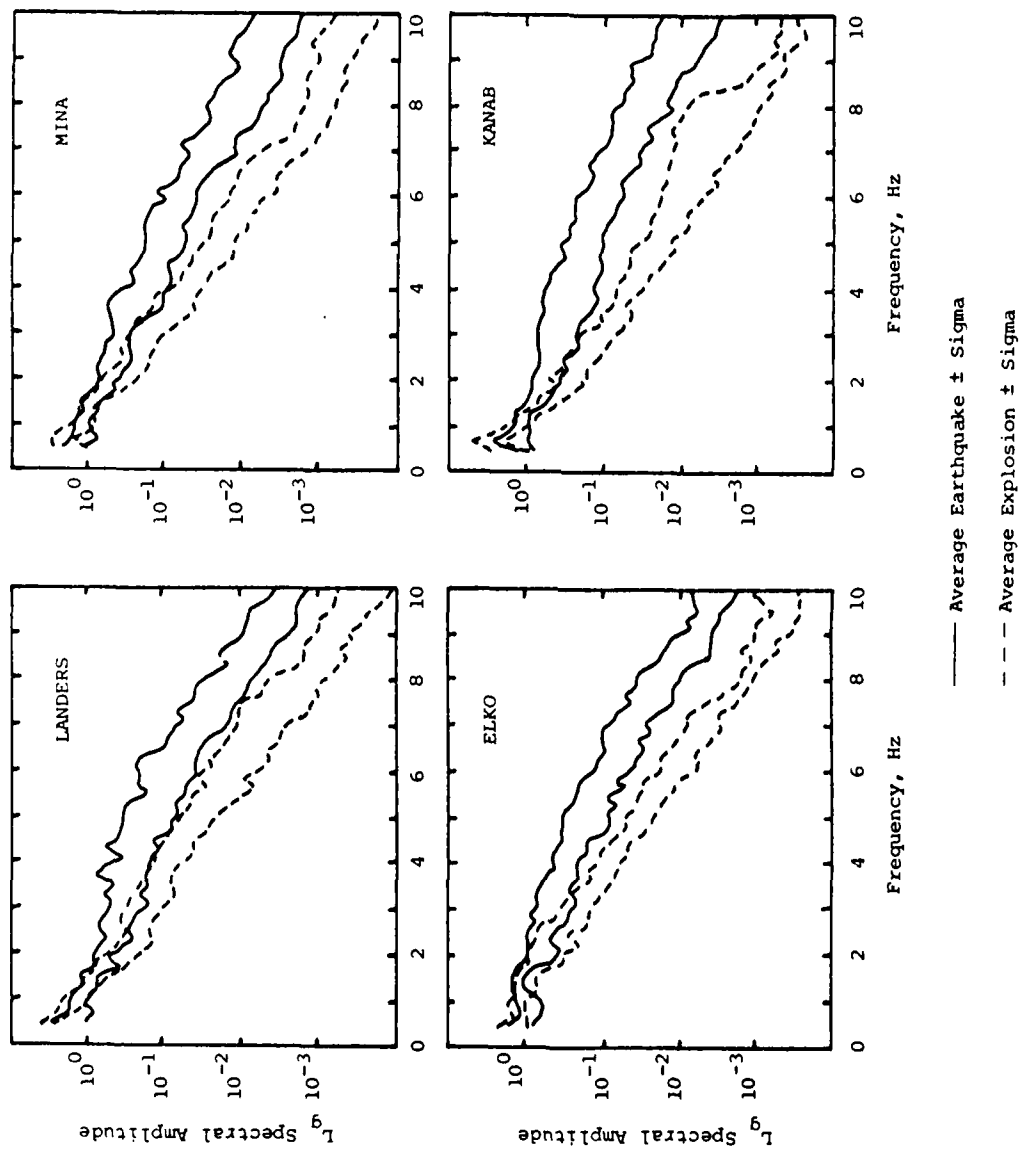


Figure 45. Comparison of one-sigma bounds on average  $L_g$  spectral shapes from Figure 44.



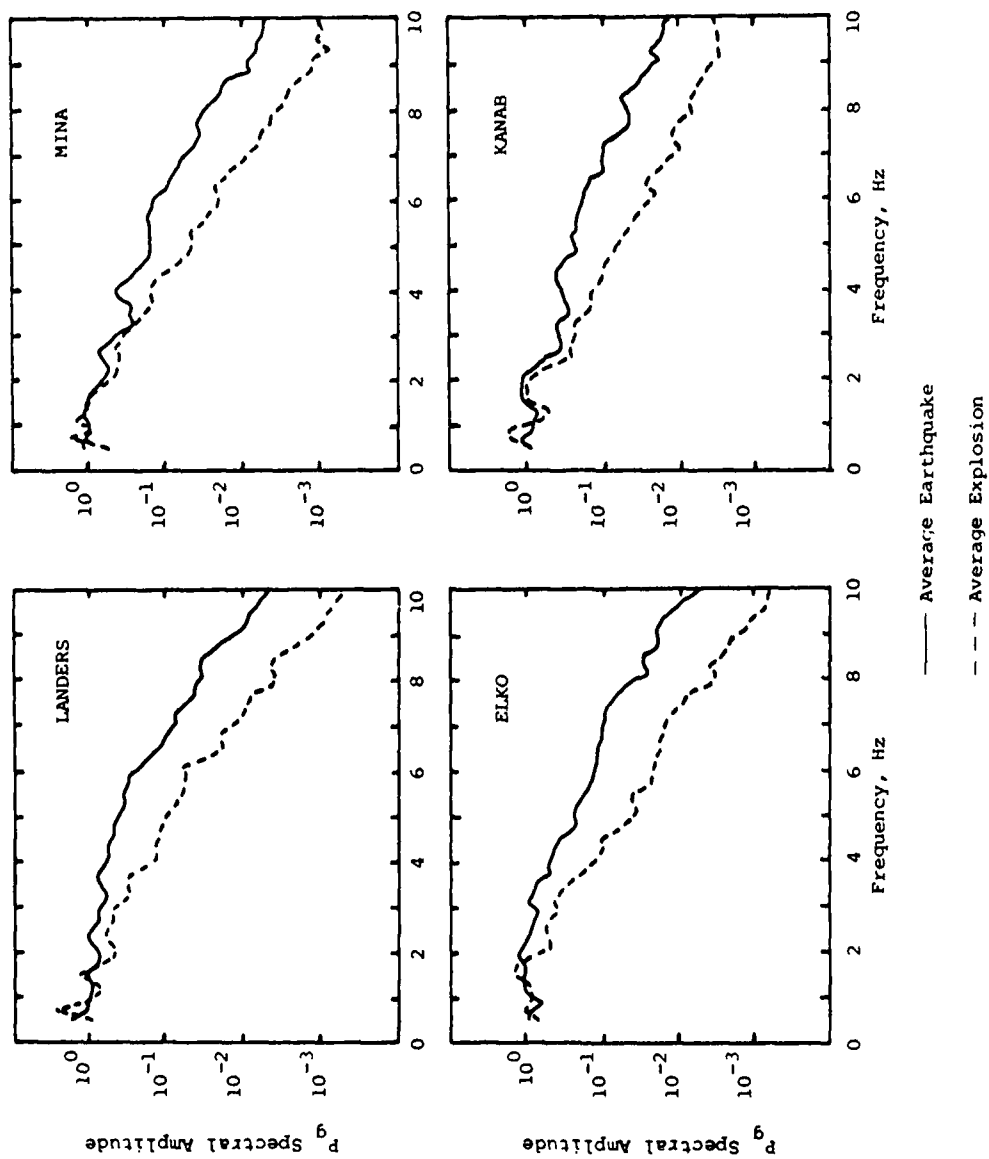


Figure 46. Comparison of average  $P_g$  spectral shapes for NTS explosions and nearby earthquakes recorded by LLNL stations.

frequencies with the earthquake spectra appearing relatively richer in high frequencies. The behavior is again in general agreement with the  $P_g$  spectra previously measured at the VELA array stations (cf. Murphy and Bennett, 1982; Bennett and Murphy, 1986).

One interesting characteristic of the regional signals which isn't obvious from the comparison of the  $L_g$  and  $P_g$  spectra in Figure 44 and 46, is that the relative enrichment of the high frequencies in the earthquake versus the explosion signals is more prominent for the  $L_g$  than for the regional P waves. This can best be seen from bandpass filter analyses of the time histories. Figure 47 shows the results of such an analysis applied to the regional signals from a small explosion (AGRINI) and an earthquake (06/04/83) recorded at the LLNL network station KNB. It can be seen that for the unfiltered trace and for the low-frequency band (0.2-4.0 Hz) the relative amplitudes of the  $L_g$  and  $P_g$  signals are about the same for the explosion and the earthquake. Bennett *et al.* (1987b) showed that  $L_g$ -to- $P_g$  amplitude ratios measured from the unfiltered traces for these explosions and earthquakes were intermingled and had substantial scatter particularly for the earthquakes. However, in the higher frequency bands the  $L_g$  signal for the explosion drops off dramatically relative to the P waves. On the other hand, the  $L_g$  signal for the earthquake in higher frequency bands remains strong relative to the  $P_g$  phase. As a result, the  $L_g$ -to- $P_g$  amplitude ratio at high frequencies is much larger for the earthquake than for the explosion. Figure 48 shows similar results for an additional explosion (BRETON) and earthquake (08/16/79) also recorded at station KNB. The main difference here appears to be that the  $P_n$  phase in explosion BRETON is stronger and the  $L_g$  phase in the 08/16/79 earthquake is stronger. Just as in Figure 47, the  $L_g$ -to-P amplitude ratio in the higher frequency band is much larger for the earthquake than for the explosion. Unfortunately, we have not yet systematically tested the consistency of this observation on a larger event sample; although some additional test cases at other stations for a few frequency bands have produced similar results (cf. Bennett *et al.*, 1987b). A careful comparison of the spectra in Figures 44 and 46 indicates that at high frequencies the  $L_g$ -to- $P_g$  amplitude ratios on the average is larger for earthquakes than explosions measured at two of the stations, KNB and MNV; but this distinction is less obvious at the other two stations. The latter suggests that this observation could be associated with a radiation pattern effect which may be weak at some azimuths.

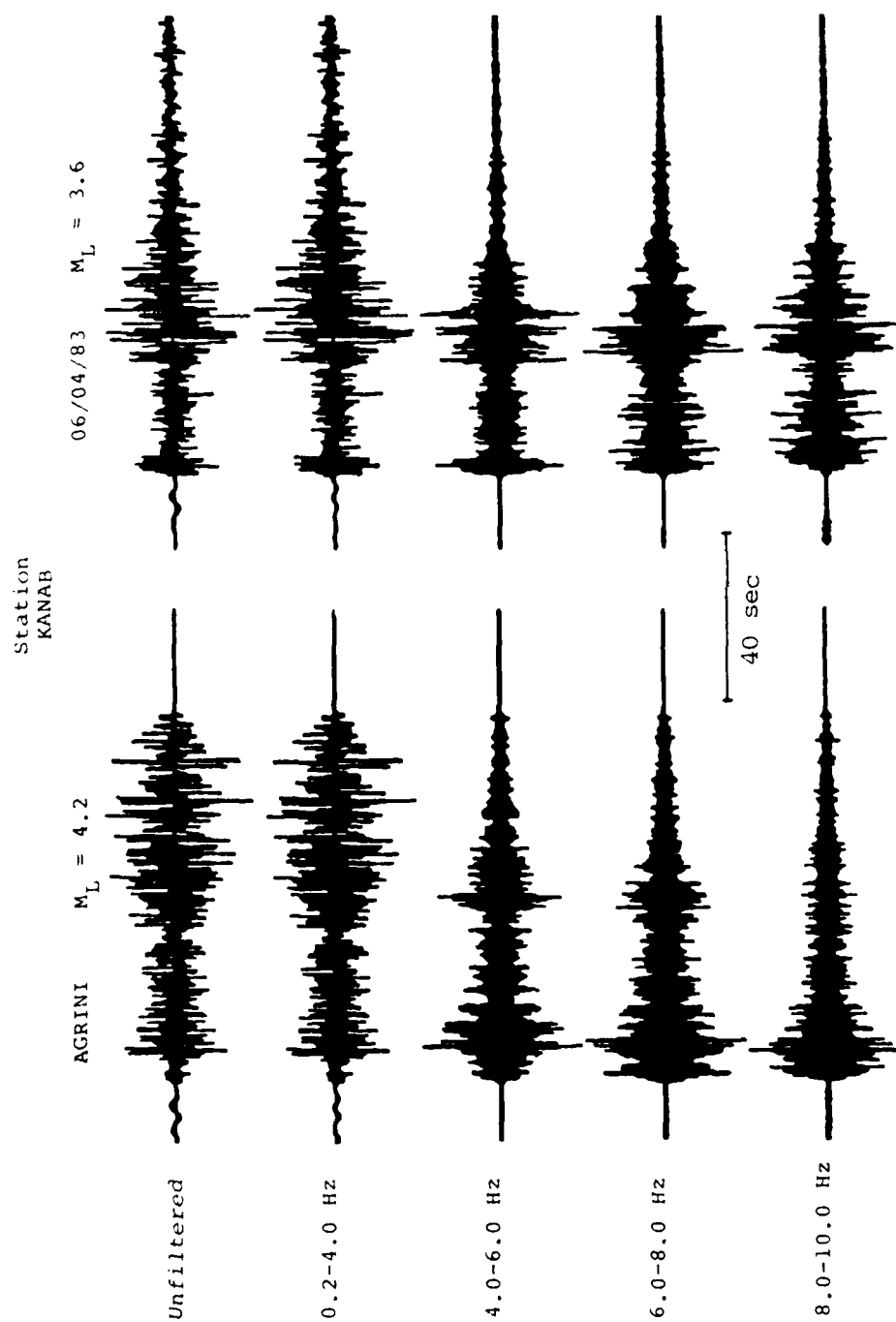


Figure 47. Bandpass filter analysis applied to explosion (left) and nearby earthquake (right) recorded at LLNL station KANAB.

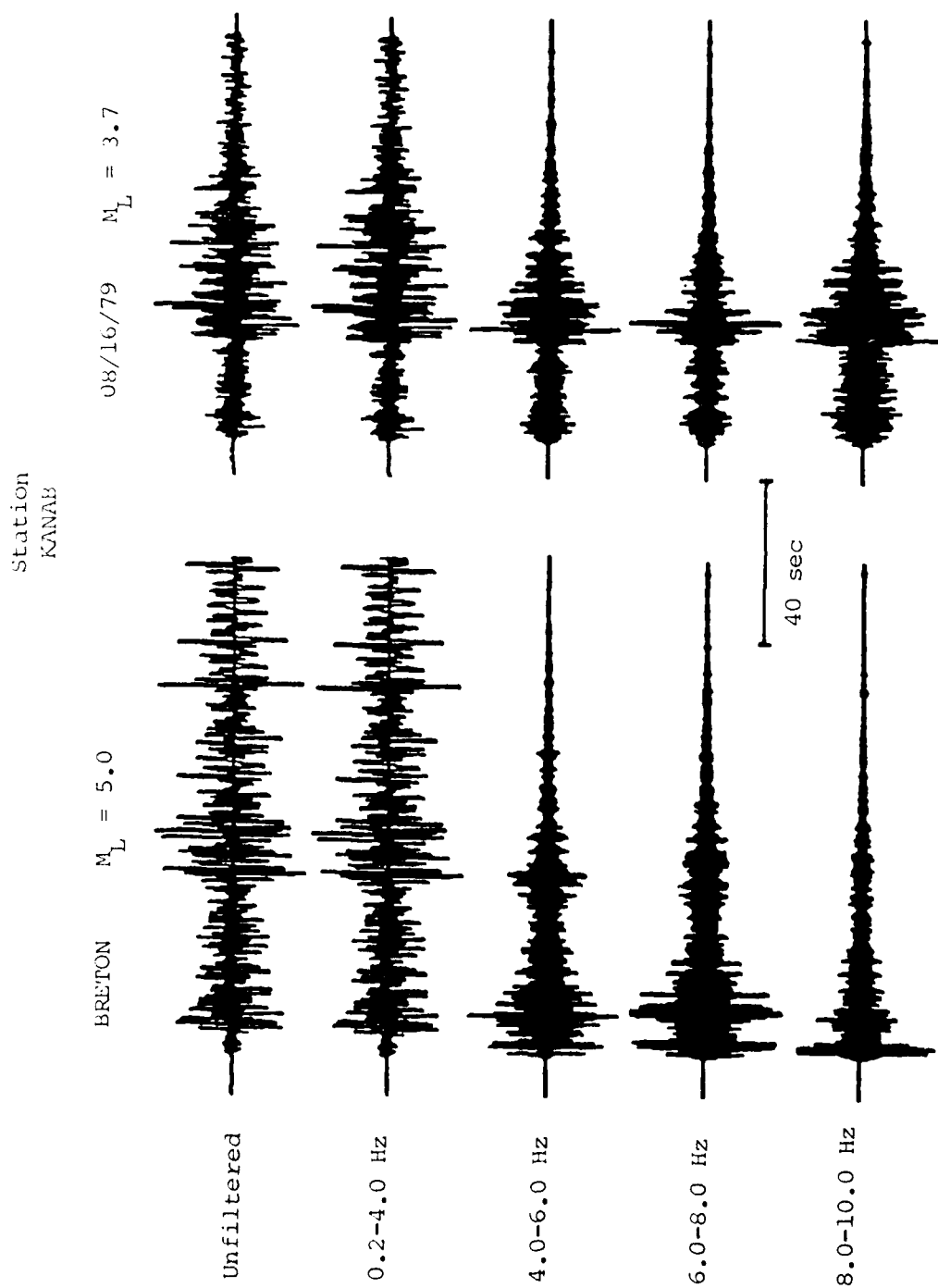


Figure 48. Bandpass filter analysis applied to different explosion (left) and earthquake (right) recorded at LLNL station KANAB.

As pointed out above, one goal in selecting the explosion database, which is a subset of the larger LLNL database, was to include a range of source depths. In particular, we sought a sample with source depths above and below the water table at Yucca Flat, so it could be determined whether this relatively strong contrast in material properties might be affecting the spectral behavior of the regional phase signals from NTS explosions. In a previous report Bennett *et al.* (1987b) found that explosions below the static water table tended to produce only slightly larger  $L_g$ -to- $P_g$  amplitude ratios measured at station ANMO ( $R \approx 900$  km) than those above the water table. It was also found that the  $P_g$  and  $L_g$  spectra at ANMO for a small sample (three above and three below the water table) of Yucca Flat explosions appeared to show little effect of the water table to frequencies of 5 Hz. Taylor *et al.* (1988) found that more deeply buried NTS explosions tended to produce regional phases at LLNL stations which were relatively richer in high frequencies and suggested several mechanisms which might explain this observation. Patton (1988) also saw evidence of  $L_g$  coupling variations within Yucca Flat and, in particular, found that events above the water table showed more scatter in  $L_g$  magnitudes which he attributed to porosity effects. Of the ten Yucca Flat explosions in our LLNL database (cf. Table 7, above) only three had source depths below the static water table (viz the three deepest events). The corresponding average spectral shapes for the  $L_g$  and  $P_g$  signals are shown in Figures 49 and 50, respectively. In both cases there appears to be a slight tendency for explosions below the water table to be richer in high frequencies. This is opposite of the effect that would be expected from the decreased corner frequency associated with the larger magnitudes of these deeper events. The observation is in general agreement with the findings of Taylor *et al.* cited above, but they also suggested that deeply overburied explosions might confound a spectral discriminant of the type described.

Although the effect of burial below the water table seems to be a slight enhancement of the higher frequencies in the regional phase spectra, it isn't clear from the evidence presented here whether this would be adequate to diminish the effectiveness of the regional phase spectral differences between earthquakes and explosions as a discriminant. To obtain additional insight into the problem, we focused on the  $P_g$  and  $L_g$  spectra for only explosions below the water table for our LLNL sample (i.e., three events). Figures 51 and 52 compare the average  $P_g$  and  $L_g$  spectral shapes for these deeper explosions with the average earthquake spectral shapes at the four LLNL stations. The

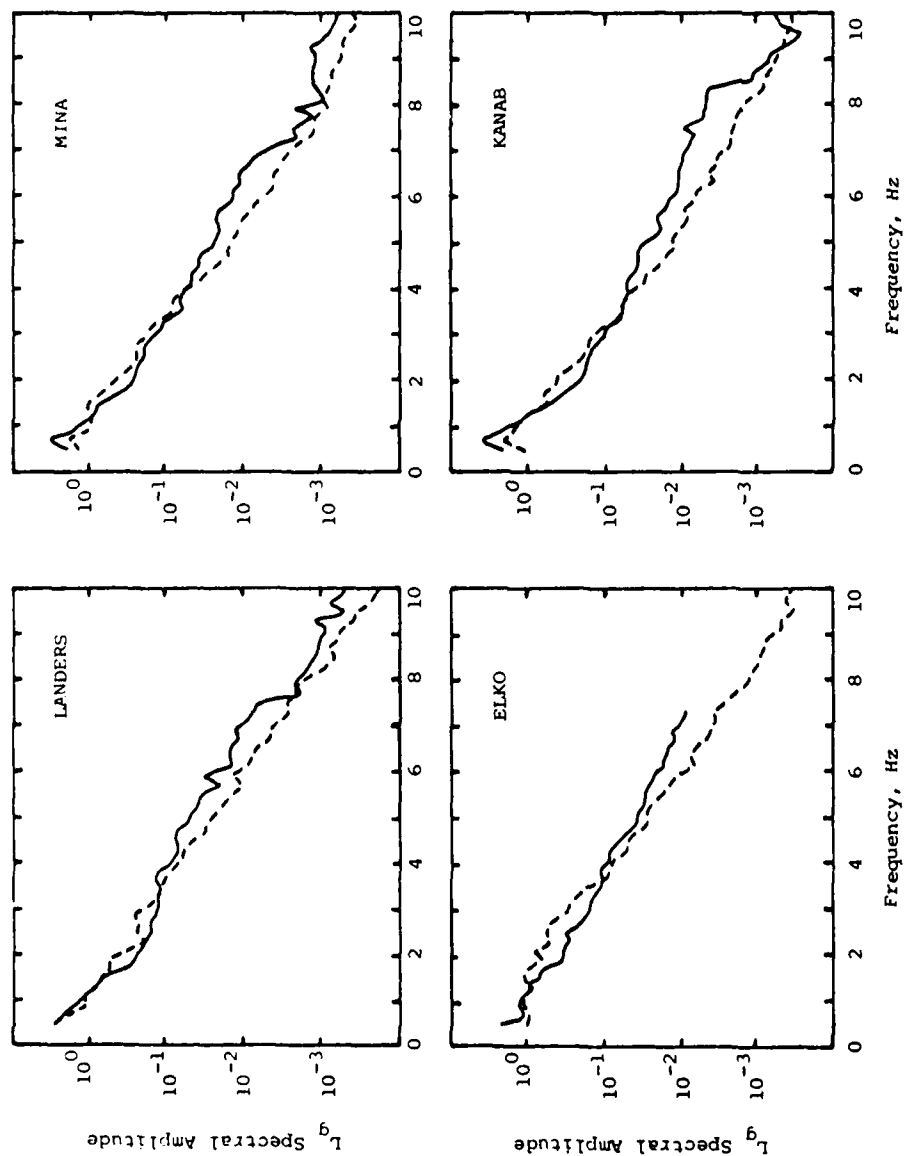


Figure 49. Comparison of  $L_g$  spectral shapes for NTS explosions above and below the water table recorded by LLNL stations.

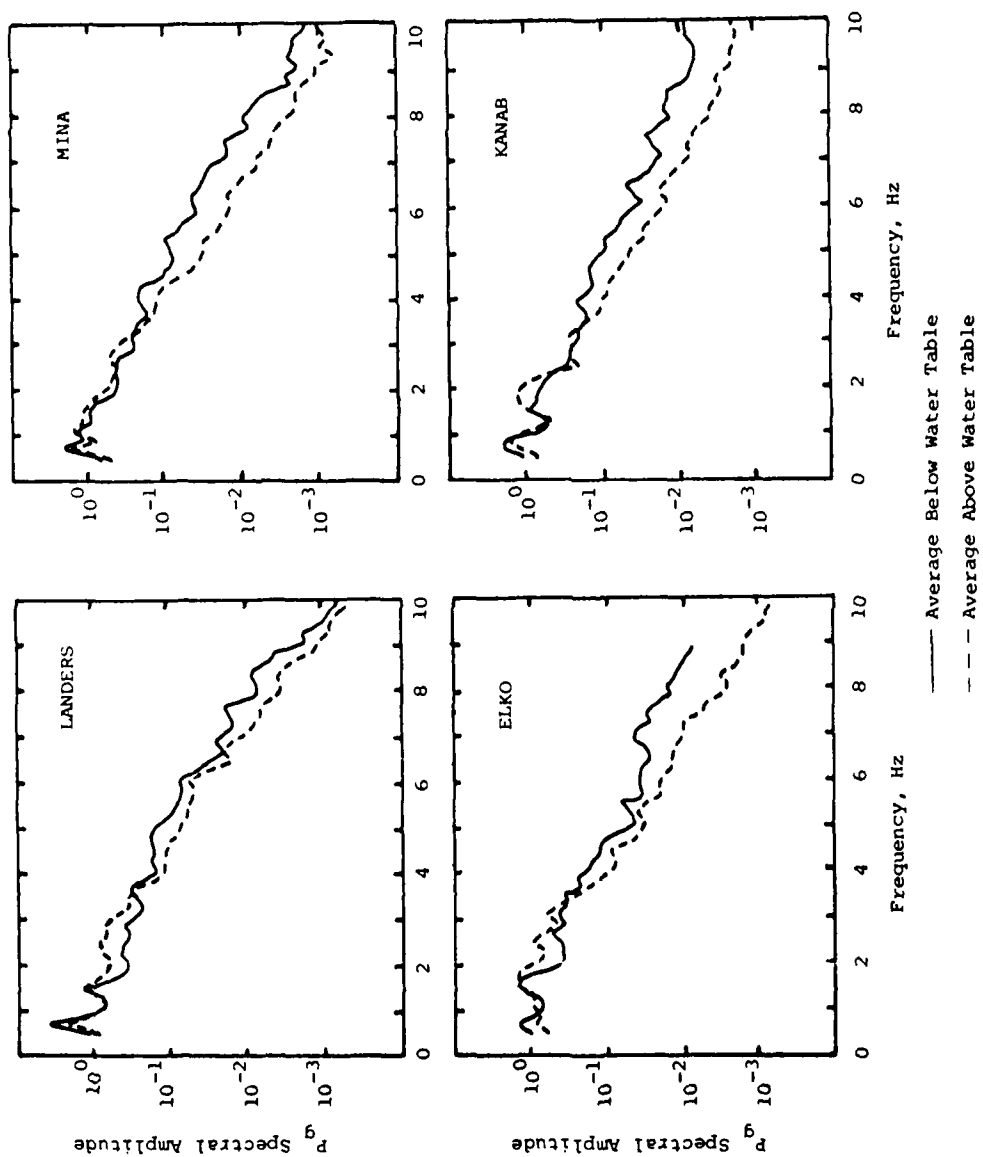


Figure 50. Comparison of  $P_g$  spectral shapes for NTS explosions above and below the water table recorded by LLNL stations.

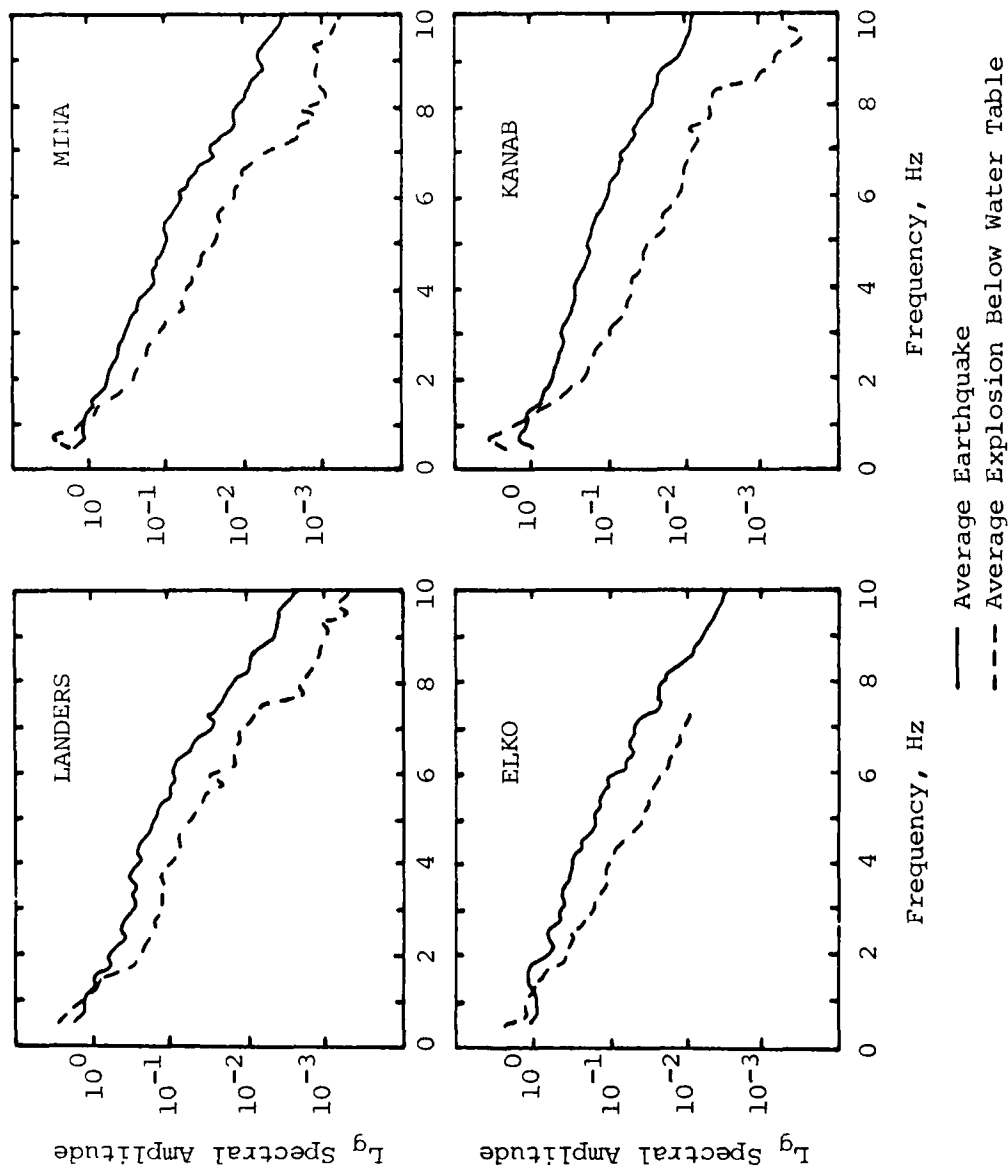


Figure 51. Comparison of Lg spectral shapes for average explosions below the water table and average earthquakes recorded by LLNL stations.



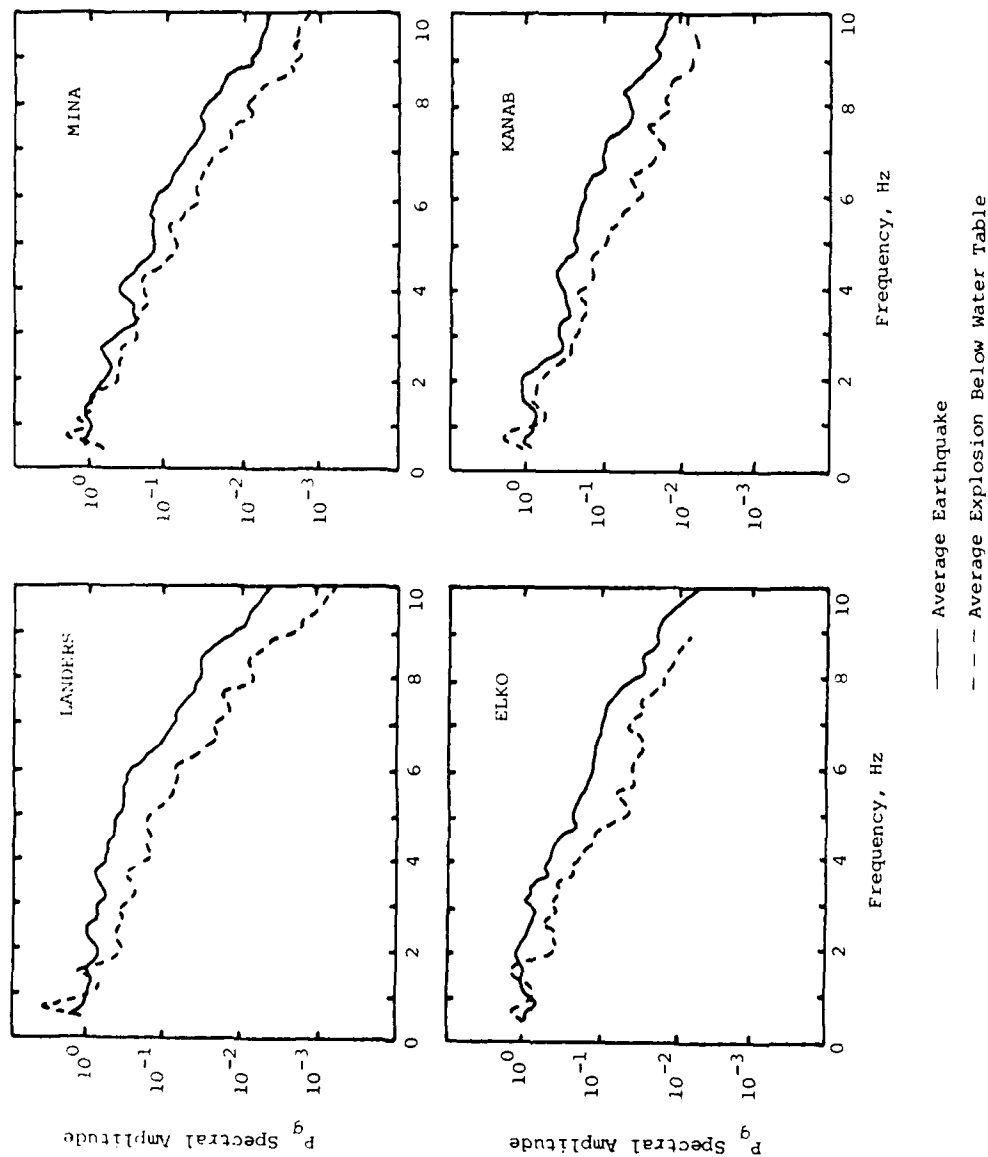


Figure 52. Comparison of  $P_g$  spectral shapes for average explosions below the water table and average earthquakes recorded by LLNL stations.

comparisons show that there is still substantial separation at higher frequencies between the earthquake and explosion spectra. One would intuitively expect from source theory that smaller magnitude explosions, at depths comparable to these three deeper explosions, would further reduce the spectral separation between explosions and earthquakes because of the corner frequency shift. However, there is no way of telling from our limited empirical database how significant these other effects of overburial will be in altering the  $L_g$  and  $P_g$  spectra from small explosions. In this regard it is interesting to note that the two overburied explosions described by Taylor *et al.* (1988) produced  $L_g$  spectral ratios only marginally lower than several other normally contained explosions of comparable magnitude. So, it is not clear to what extent the overburial or other unknown factors might be influencing the observed spectral ratios. The resolution of these questions will ultimately require improved theoretical understanding of  $L_g$  generation by explosion sources and additional observational results to confirm the theory. The LLNL network measurements should continue to provide an excellent data source for such investigations.

#### **4.3 NTS Explosions and Earthquakes at RSSD**

In Section III above we described the characteristics of regional phase signals from Soviet underground nuclear explosions in East Kazakh and comparable earthquakes. It was noted there that available stations for regional monitoring of those events were located at distances considerably larger than those LLNL network stations used in the preceding analysis of discrimination of NTS explosions. To get some idea of regional discrimination capabilities for NTS events using high quality stations at regional distance ranges more comparable to the Soviet experience, we have briefly reviewed the characteristics of regional phases recorded at the RSTN station RSSD from NTS underground nuclear explosions and earthquakes at comparable magnitudes, ranges and azimuths in the western U.S. The RSSD station is located in South Dakota about 1300 km northeast of the explosion source area at NTS. It is noted at the outset that attenuation of regional phases in the crust of the western U.S. is known to be relatively large; so that, even though the distances are comparable to the observations from Soviet events, some adjustments to the regional signals may still be appropriate before results from the two areas can be compared.

Figures 53 and 54 show the vertical-component, short-period records observed at RSSD for a sample of NTS explosions and several earthquakes. Figure 53 shows five Yucca Flat explosions with magnitudes between 4.8 and 5.9  $m_b$ , and Figure 54 shows two Pahute Mesa explosions with magnitudes of 5.5 and 5.7  $m_b$  and three California earthquakes with magnitudes from 5.6 to 6.1. The ranges of the earthquakes from RSSD were from 1430 km to 1670 km compared to explosion ranges between 1280 km and 1290 km. The ranges and paths are somewhat different; but, for the available database from RSSD, these events appear to provide the best comparisons. At these ranges the regional signals at RSSD appear to be dominated by early P phases and  $L_g$ . The early P phases are believed to be associated with upper mantle and deeper crustal propagation paths including  $P_n$  and  $P^*$ ; the  $P_g$  phase following after these early P phases is less distinct at this range appearing as a coda segment of increased amplitude but smaller than the earlier P phases. The P signals from the NTS explosions are remarkably similar in character to those seen above in Figure 21 from Shagan River explosions recorded at station WMQ. In particular, the P signals in both cases include two or three distinct phases with apparent group velocities between about 7.6 and 6.3 km/sec. If the observation of these phases prevails at other far-regional Soviet stations (e.g., the new IRIS stations), detailed comparisons of the signal characteristics between the NTS shots and Soviet explosions may provide important source information. The  $L_g$  signals at RSSD appear on the short-period vertical records as strong signals roughly equivalent in amplitude to the P phases. The  $L_g$ -to-P amplitude ratio is generally near 1.0 or slightly less than 1.0 for the explosions and near 1.0 or slightly greater than 1.0 for the earthquakes.

To get additional insight into the characteristics of these regional signals at RSSD, Fourier spectra were computed for the  $P_n$  (viz initial P),  $P^*$ ,  $P_g$  and  $L_g$  window segments for the explosion CAPROCK ( $m_b = 5.8$ ,  $R = 1280$  km) and the Round Valley earthquake near Mammoth Lakes, California ( $m_b = 5.6$ ,  $R = 1435$  km). These are shown in Figure 55; no instrument correction has been applied. The uncorrected spectra are all rather sharply peaked in the frequency band from 0.5 to 2 Hz and fall off rapidly to noise at higher frequencies. The spectra appear to reach a noise floor near 5 to 7 Hz for the various P phases and near 4 Hz for  $L_g$ . The overall spectral shapes of the individual phases are not greatly different for the explosion and earthquake, even though there appear to be some differences in spectral details. The most notable difference is that

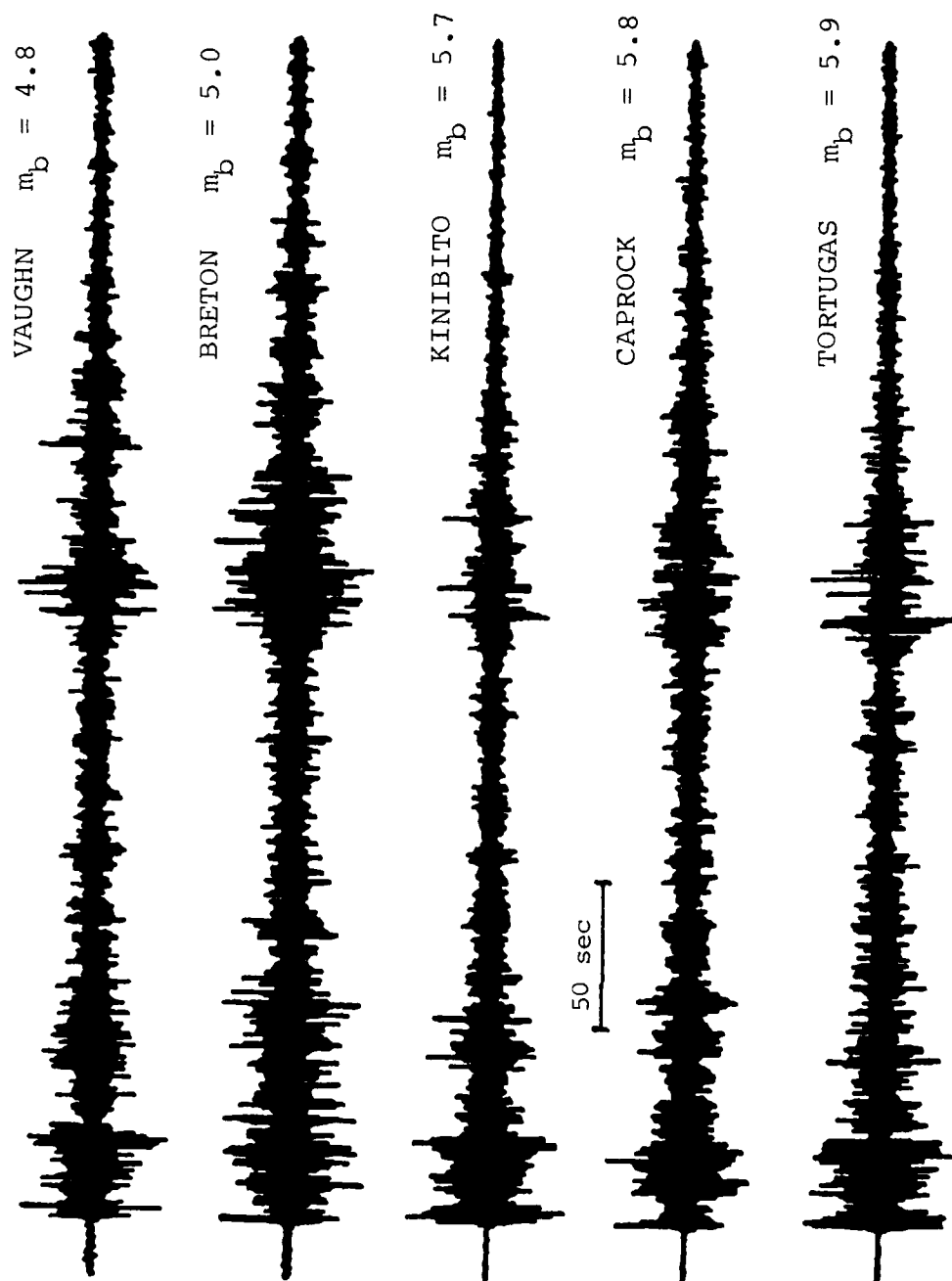
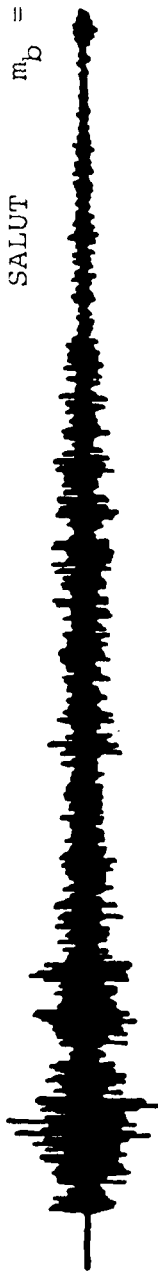


Figure 53. Vertical-component records at station RSSD from five Yucca Flat explosions.

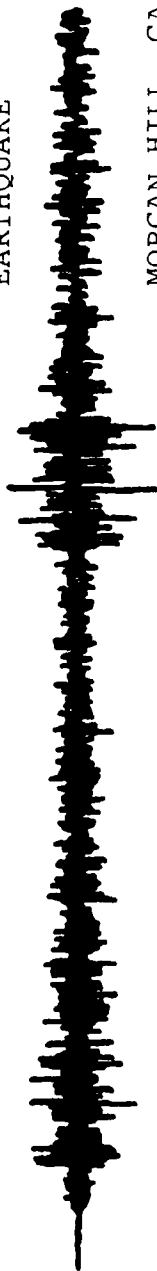
SALUT  $m_b = 5.5$



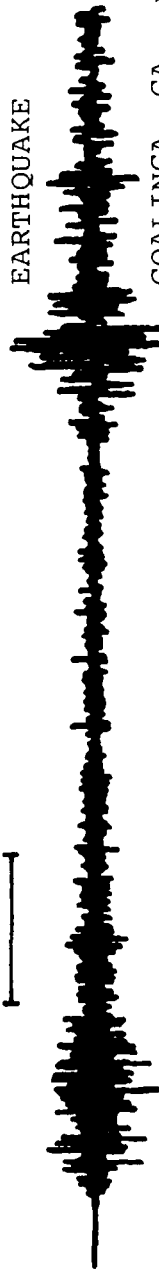
TOWANDA  $m_b = 5.7$



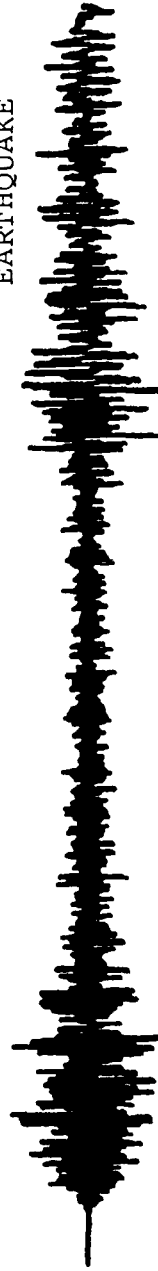
ROUND VALLEY, CA  $m_b = 5.6$   
EARTHQUAKE



MORGAN HILL, CA  $m_b = 5.7$   
EARTHQUAKE



COALINGA, CA  $m_b = 6.2$   
EARTHQUAKE



50 sec

Figure 54. Vertical-component records at station RSSD from two Pahute Mesa explosions and three California earthquakes.

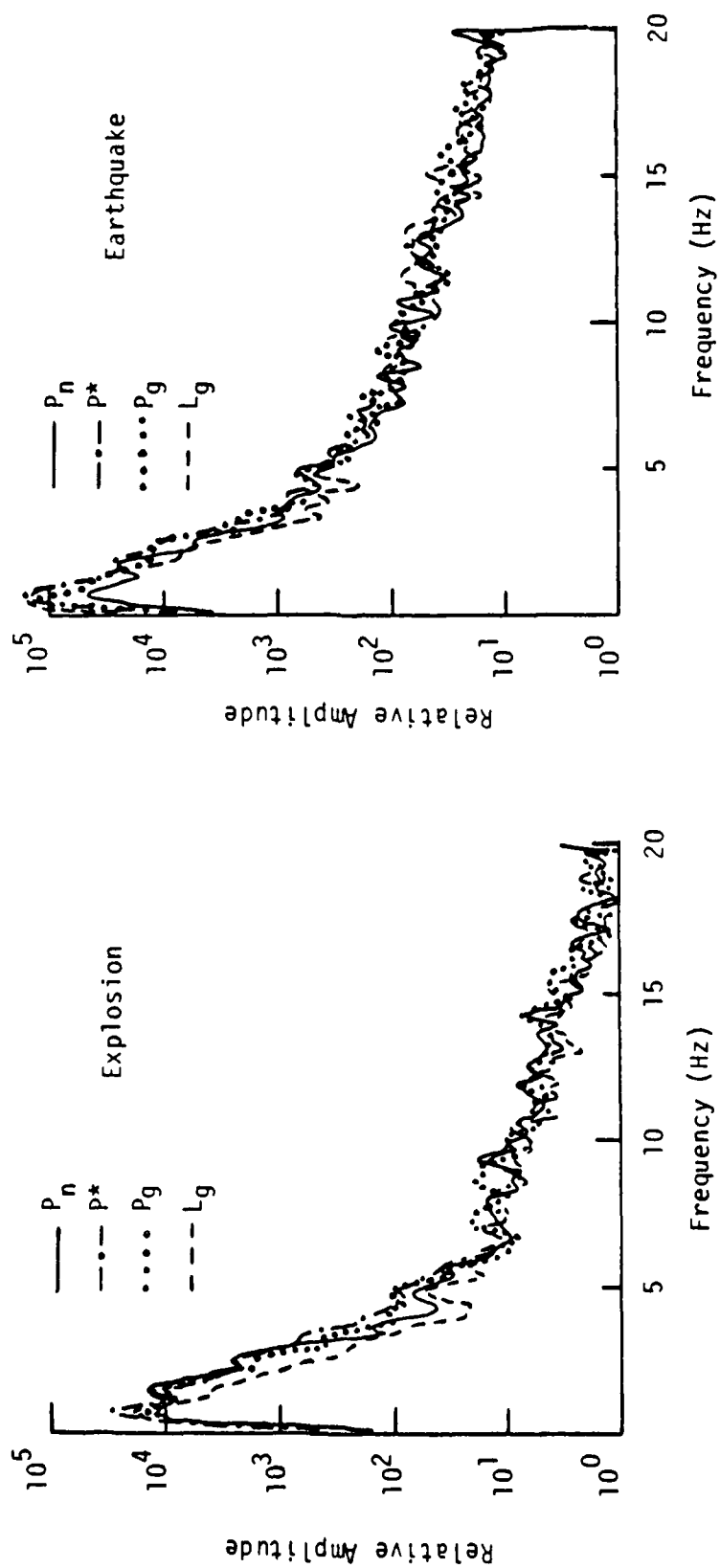


Figure 55. Comparison of regional phase spectra at RSSD for Yucca Flat explosion CAPROCK,  $m_b = 5.8$ , (left) and the Round Valley, California earthquake,  $m_b = 5.6$ , (right).

the explosion spectra seem to be constrained to a somewhat narrower frequency band than the earthquake spectra resulting in sharper spectral peaks. This is particularly apparent in the  $L_g$  signals for the two events. As noted above, the explosion and earthquake have somewhat different magnitudes and ranges which could affect the spectral shapes; but we would expect these two factors to compensate each other to at least some extent for these events. If the observed difference in spectra is real, it is consistent with our findings at smaller ranges that earthquake spectra are relatively richer in high frequencies than explosion spectra.

In Section III above we found from bandpass filter analysis that the  $L_g$ -to-P ratio measured at WMQ for Shagan River explosions was much smaller at high frequencies (greater than about 3 Hz) than similar ratios for the comparable earthquakes in the database. To test the applicability of such a discriminant on the NTS explosions and California earthquakes recorded at RSSD, a similar bandpass filter analysis was performed on several of the events. The results of the analyses for four representative events (two explosions and two earthquakes) are shown in Figures 56 and 57. In general, the results show that the signal-to-noise levels for events of this magnitude are greater than 1.0 for the P and  $L_g$  phases up to about the filter passband of 3 to 6 Hz, and in some cases to even higher frequencies for the P phases.

For the explosion (KINIBITO) and earthquake (Round Valley, California) in Figure 56, it can be seen that the  $L_g$ -to-P ratio at low frequencies (0 to 1.0 Hz) is somewhat less than 1.0 for the explosion and greater than 1.0 for the earthquake. The  $L_g$ -to-P ratio appears to decrease toward higher frequencies for both events, but the decrease is less rapid for the earthquake. As a result, the greatest distinction in the  $L_g$ -to-P ratio between the explosion and the earthquake seems to occur for the 1 to 3 Hz passband. It may also be noteworthy that the initial P is the predominant phase in the filter passbands between 0.5 and 4.0 Hz but not at low frequencies for the explosion in Figure 56. In contrast, the most prominent P phase for the earthquake record is not the initial P but somewhat later crustal phases for all passbands.

The events in Figure 57 (i.e., explosion SALUT and the Morgan Hill, California earthquake) show somewhat different behavior. The most prominent P phase for both the explosion and earthquake, in this case, are not the initial P

# KINIBITO

# Round Valley, CA Earthquake

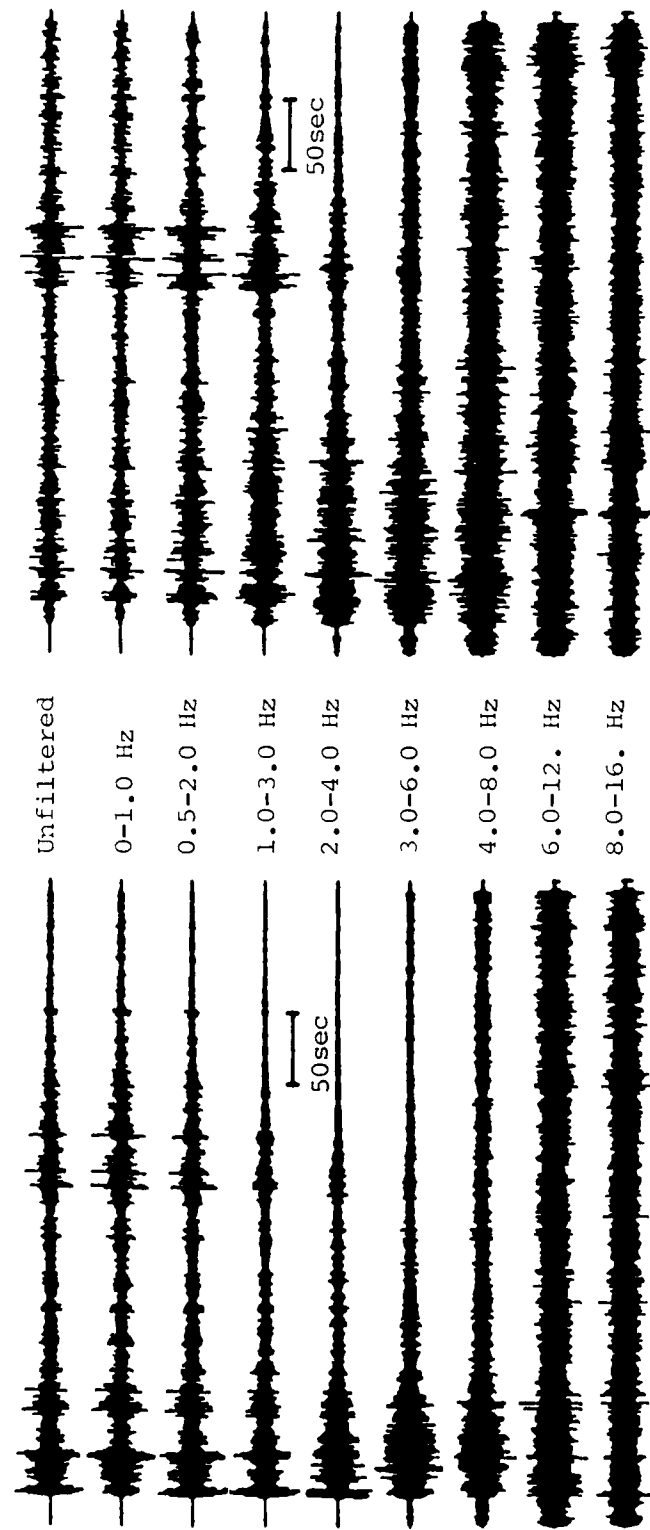


Figure 56. Bandpass filter analyses of vertical component records at station RSSD for explosion KINIBITO,  $m_b = 5.7$ , (left) and Round Valley, California earthquake,  $m_b = 5.6$ , (right).



SALUT

Morgan Hill, CA Earthquake

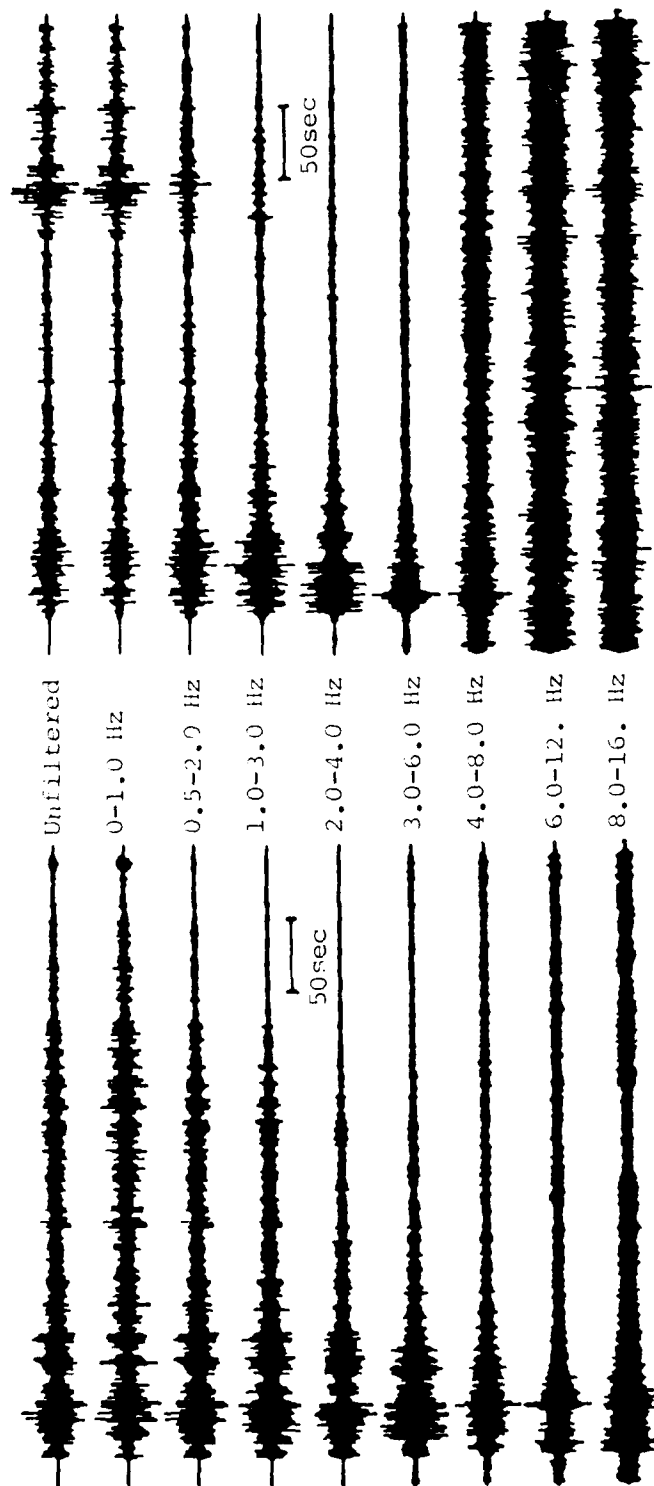


Figure 57. Bandpass filter analyses of vertical component records at station RSSD for explosion SALUT,  $m_b = 5.5$ , (left) and Morgan Hill, California earthquake,  $m_b = 5.7$ , (right).

but later crustal phases. Furthermore, the biggest distinction in the  $L_g$ -to-P ratio seems to be at lower-frequency filter passbands (viz 0 to 1.0 Hz) where the ratio is near 2.0 for the earthquake and only about 0.7 for the explosion. The  $L_g$  signals in the earthquake appear to be severely attenuated above about 2 Hz. It is not clear whether the latter is a propagation or source effect. Complex mechanisms have been attributed to both the Morgan Hill and Round Valley earthquakes (cf. Abrahamson and Darragh, 1985; Corbett, 1985) and the path for the Morgan Hill earthquake includes a segment crossing the Great Valley and Sierra Nevada Batholith which is not present for any of the other events in Figures 56 and 57. A similar analysis of the Coalinga, California earthquake record at RSSD, which also included a Great Valley/Sierra Nevada path segment, was again depleted in  $L_g$  energy at frequencies above 2 Hz.

Thus, while the RSSD observations of larger NTS explosions and comparable California earthquakes offer hope that discrimination capability may persist to some degree at larger regional distances even for some events in the western U.S., they also raise again the caveat that care must be exercised in accounting for propagation and source variations. In areas such as the Soviet Union where the empirical database to test regional discrimination is deficient, the case for regional discrimination will clearly depend on improved knowledge of propagation effects on regional phases at higher frequencies and some understanding of potential earthquake source mechanisms in areas of interest.

## V. CONCLUSIONS AND RECOMMENDATIONS

The objective of this research program has been to investigate the characteristics of regional seismic signals recorded by high-quality, high-frequency stations and to determine how those characteristics might be utilized to distinguish various source types including underground nuclear explosions, earthquakes, and commercial blasts. To accomplish this objective we collected and analyzed the available high-quality digital data from three different tectonic environments: (1) eastern North America, (2) southern Soviet Union, and (3) western U.S. These data included regional signals from each of the source types of interest. The database was drawn from a variety of sources including the RSTN and ECTN for eastern North America, the CDSN and Soviet/NRDC network for the southern Soviet Union, and the LLNL network and RSTN for the western U.S. We found that data from each of these sources provide unique contributions to different aspects of the regional discrimination problem.

For each tectonic environment we performed amplitude and spectral comparisons of the regional signals to delineate differences related to source type. Those comparisons have revealed several differences in the regional phase signals which appear to be source related and which should receive further consideration as potential discrimination measures. In particular, spectral comparisons of the relative excitation of various regional phases continues to show differences which appear to be diagnostic of different source types. Extension of regional signal monitoring to broader bands and higher frequencies appears to offer an opportunity to enhance this capability. It seems likely that many regional events could eventually be categorized by such comparisons. On the other hand, in some cases our analyses have also indicated the sensitivity of the regional signal behavior to propagation path characteristics in addition to source differences. The latter observation emphasizes the need for care in discrimination studies to isolate source differences by properly accounting for propagation effects. This would be particularly important in applying experience from one tectonic environment to another. This capability too should be enhanced as we gain experience from new regional monitoring efforts in the areas of interest. Our studies have also identified potential limitations on techniques for distinguishing small, non-nuclear blasts which could be a particular

problem at lower monitoring thresholds. The results suggest that the regional signals from such events may be sensitive to shooting practice and that bandpass limitations on the signals could reduce the effectiveness of some techniques (viz cepstral analysis) used to distinguish commercial blasts.

For eastern North America we found that small regional events, including earthquakes and presumed mine blasts, generally produced strong regional P and  $L_g$  phases. At station RSCP the mine blast signals were different from the earthquake signals with respect to short-period Rayleigh wave ( $R_g$ ) excitation, relative frequency content of  $L_g$  and P phases, and the  $L_g$ /P amplitude ratio. However, there was considerable variation in the observed characteristics between events. Cepstral analysis of P waves recorded by the ECTN stations revealed similar spectral modulation for both earthquakes and blasts. The most significant observed quefrequencies would correspond to delays considerably longer than those used between individual shots in normal blasting practice. Alternate explanations for the spectral modulation have been identified which do not involve source multiplicity.

For the southern Soviet Union we have seen that the CDSN station WMQ records strong regional signals, including  $L_g$  and several P phases, from East Kazakh explosions and regional earthquakes. Comparisons of these signals indicated that the earthquakes produced larger  $L_g$ /P amplitude ratios than the explosions and that the differences could be enhanced by bandpass filtering at higher frequencies. However, the comparisons involved different propagation paths for the earthquakes and explosions so that attenuation differences were not completely accounted for in the analysis. The Soviet/NRDC network results revealed a large number of small seismic events in the naturally aseismic area around East Kazakh. These events frequently produced strong  $R_g$  phases and are thought to have been mainly mine blasts. The level of this man-made activity could be regarded as indicative of the many events which would need to be considered for a low-threshold monitoring effort in the region.

For the western U.S. the results of processing additional events recorded by the LLNL network were corroborative of our previous findings of spectral differences in the  $L_g$  and  $P_g$  signals for NTS nuclear explosions and nearby earthquakes of comparable magnitude. We saw some influence of the water table depth on the frequency content of the  $L_g$  and  $P_g$  signals from Yucca Flat

explosions, but these effects were small compared to the differences associated with source type. At larger regional distances from NTS, we observed strong  $L_g$  from several larger explosions and California earthquakes of similar magnitude recorded at RSTN station RSSD. Preliminary indications of differences in the  $L_g$  spectra and in the  $L_g/P$  amplitude ratio between the explosions and earthquakes recorded at RSSD cannot be considered definitive until additional knowledge is obtained on the influence of propagation path differences and more events have been analyzed.

In addition to these general conclusions several additional observations are noteworthy:

- Presumed mine blasts in the eastern U.S. frequently produce strong  $R_g$  signals with frequencies near 1 Hz which can be enhanced by bandpass filtering.  $R_g$  may not be present in some cases because of variations in shooting practice or propagation effects.
- The  $L_g$  and  $P_g$  spectra of regional blasts observed at RSCP fall off more rapidly toward higher frequencies than comparable signals from regional earthquakes.
- Although the  $L_g/P_{max}$  amplitude ratios for regional earthquakes at RSCP are on the average larger than similar blast ratios, the data show considerable intermingling.
- Cepstral analysis of P waves from a small sample of commercial blasts and earthquakes in eastern North America recorded by the ECTN stations indicates several significant frequency peaks in the 0.2 to 1.0 second range for both types of events. These delays may correspond to crustal reverberation and not shot effects, which should be shorter, or depth phases, which should be longer.
- Cepstral analysis does not always provide an objective, model-independent analysis of seismic signals and requires careful consideration of bandwidth limitation.
- The digital seismic data recorded by the CDSN station at Urumchi (WMQ) provides an excellent source of high-quality regional signals from Soviet explosions at East Kazakh and regional earthquakes in that area.

The station records strong  $L_g$  signals and several regional P phases at ranges of 1000 km or more from events with magnitudes as low as 4.5  $m_b$ .

- $L_g/P_{max}$  amplitude ratios measured at WMQ average about 4.4 for earthquakes and 3.3 for explosions at low frequency, and the measurements overlap for the different source types. At high frequencies the  $L_g/P_{max}$  ratios are well-separated averaging about 1 for earthquakes and 0.1-0.2 for explosions.
- The  $L_g/P_{max}$  ratios measured at WMQ show no obvious dependence on magnitude but a slight tendency to decrease with epicentral distance. The latter effect does not significantly reduce the difference between event types.
- $L_g$  spectra at WMQ corrected for instrument response appear to have lower corner frequencies for earthquakes than for explosions of comparable magnitudes.
- Interpretation of the relative difference in  $L_g$  spectral decay above 1 Hz for explosions and earthquakes at WMQ depends on assumptions regarding the attenuation differences between the paths for the individual events. These effects are not well known at this time.
- The East Kazakh region of the Soviet Union experiences a large number of commercial blasts comparable to those in the eastern U.S.
- The presumed mine blasts recorded by the Soviet/NRDC network frequently produce strong  $R_g$  which might be useful for investigating variations in geologic structure within the region.
- The NTS explosions and nearby earthquakes recorded by the LLNL network produce  $P_g$  and  $L_g$  signals which are relatively richer in high frequencies for the earthquakes than for the explosions. These differences appear to become progressively greater toward the high frequency limit of the useful frequency band.
- For explosions above and below the water table at Yucca Flat, the  $L_g$  and  $P_g$  spectra for the LLNL stations are slightly enhanced at high frequencies for the deeper events.
- RSSD records strong  $L_g$  and regional P phases from NTS explosions and California earthquakes but the useful frequency band is limited to less than about 5 Hz.

- The P phases for California earthquakes at RSSD show differences in their relative excitation and frequency content which may be related to propagation differences or source complexity.

Finally, these studies have identified several areas where additional research is needed to improve regional discrimination capabilities:

- The eastern North America data from RSTN and ECTN and the Soviet/NRDC data include numerous commercial blasts which could provide a good database for developing systematic procedures to distinguish these events. Comparison of these signals with those from similar events at NORESS could also help define general event characteristics.
- More objective criteria for evaluating the significance of cepstral analysis results are needed to evaluate the reliability of the method for identifying multiple sources. The ECTN and NORESS should provide useful databases for evaluating such methods.
- Additional efforts should be devoted to investigating the usefulness of the  $R_g$  phase for identifying commercial blasts and for determining possible geologic variations within the East Kazakh region.
- The discrimination capability of the  $L_g/P_{\max}$  ratio as a function of frequency for East Kazakh explosions and regional earthquakes should be analyzed more systematically to identify the possible influences of path differences. Additional regional stations and events may be useful in defining these path effects.
- Additional investigation of the spectral characteristics of regional phases recorded by the LLNL stations may be useful in defining their dependence on explosion source conditions. Additional events, particularly smaller explosions in saturated rock, could be particularly valuable in such studies.

## ACKNOWLEDGMENTS

We would like to thank K. Y. Chun at the University of Toronto for providing access to the ECTN data and R. G. North of the Geological Survey of Canada for information on ECTN instrumentation. We would also like to thank S. R. Taylor and his colleagues at Lawrence Livermore National Laboratory for the use of the LLNL network data.



## REFERENCES

- Abrahamson, N. A., and R. B. Darragh (1985). "Observation of a Double Event at Regional Distances: The Morgan Hill Earthquake of 24 April 1984," *Bull. Seism. Soc. Am.*, 75, pp. 1461-1464.
- Alexander, S. H., and A. H. Borkowski (1988). Personal Communication.
- Baumgardt, D. R., and K. A. Ziegler (1988). "Spectral Evidence of Source Multiplicity in Explosions: Application to Regional Discrimination of Earthquakes and Explosions," *Bull. Seism. Soc. Am.*, 78, pp. 1773-1795.
- Bennett, T. J., and J. R. Murphy (1986). "Analysis of Seismic Discrimination Capabilities Using Regional Data from Western United States Events," *Bull. Seism. Soc. Am.*, 76, pp. 1069-1086.
- Bennett, T. J., J. R. Murphy, and H. K. Shah (1987a). "Theoretical Analyses of Regional Phase Behavior," S-Cubed Report, SSS-R-87-8113, Technical Report under Contract No. F08606-85-C-0034.
- Bennett, T. J., J. R. Murphy, H. K. Shah, and B. W. Barker (1987b). "Theoretical and Empirical Investigations of Regional Phase Behavior," S-Cubed Report, SSS-R-87-8510, Final Report under Contract No. F08606-85-C-0034.
- Bennett, T. J., J. R. Murphy, and B. W. Barker (1988a). "Observation and Synthesis of Regional Phase Signals from Quarry Blasts, Earthquakes and Underground Nuclear Explosions," Paper Presented at the 10th Annual AFGL/DARPA Seismic Research Symposium.
- Bennett, T. J., B. W. Barker, and J. R. Murphy (1988b). "Regional Phases from East Kazakh Seismic Events," Abstract, Seismological Research Letters, 59, p. 101.

- Berger, J., J. N. Brune, P. A. Bodin, J. S. Gombert, D. M. Carrel, K. F. Priestley, D. E. Chavez, W. R. Walter, C. B. Archambeau, T. B. Cochran, I. L. Nersesov, M. B. Gokhberg, O. A. Stolyrov, S. K. Daragen, N. D. Tarasov, and Y. A. Sutelow (1987a). "A New U.S.-U.S.S.R. Seismological Program," *EOS*, 68, pp. 105-111.
- Berger, J., H. K. Eissler, F. L. Vernon, I. L. Nersesov, M. B. Gokhberg, O. A. Stolyrov, and N. T. Tarasov (1988). "Studies of High-Frequency Seismic Noise in Eastern Kazakhstan," *Bull. Seism. Soc. Am.*, 78, pp. 1744-1758.
- Blandford, R. R. (1981). "Seismic Discrimination Problems at Regional Distances," in *Identification of Seismic Source - Earthquake or Underground Explosion*, D. Reidel Publishing Co.
- Chun, K.-Y., G. F. West, R. J. Kokoski and C. Samson (1987). "A Novel Technique for Measuring  $L_g$  Attenuation - Results from Eastern Canada Between 1 to 10 Hz," *Bull. Seism. Soc. Am.*, 77, pp. 398-419.
- Chun, K.-Y., R. J. Kokoski, and G. F. West (1988). "Network Calibration for  $L_g$  Magnitude - Method and Test Results from Eastern Canada," *Bull. Seism. Soc. Am.*, 79, pp. 127-140.
- Corbett, E. J., D. M. Martinelli, and K. D. Smith (1985). "Aftershock Locations of the November 23, 1984 Round Valley, California Earthquakes," Abstract, *EOS*, 66, p. 952.
- Dick, R. A., L. R. Fletcher, and D. V. D'Andrea (1983). "Explosives and Blasting Procedures Manual," *Information Circular 8925*, Bureau of Mines, U.S. Department of Interior.
- Dowding, C. H. (1985). *Blast Vibration Monitoring and Control*, Prentice Hall, Englewood Cliffs, N.J., 297 pages.
- Flinn, E. A., T. J. Cohen, and D. W. McGowan (1973). "Detection and Analysis of Multiple Seismic Signals," *Bull. Seism. Soc. Am.*, 63, pp. 1921-1936.

Frantti, G. E. (1963). "Spectral Energy Density for Quarry Explosions," *Bull. Seism. Soc. Am.*, 53, pp. 989-996.

Glaser, R. W., S. R. Taylor, M. D. Denny, and E. S. Vergino (1986). "Regional Discrimination of NTS Explosions and Western U.S. Earthquakes: Multivariate Discriminants," Lawrence Livermore National Laboratory, Report No. UCID-20930 under U.S. DoE Contract No. W-7405-Eng-48.

Goncz, J. H., W. C. Dean, Z. A. Derr, A. C. Lees, K. L. McLaughlin, T. W. McElfresh, and M. E. Marshall (1987). "Propagation and Excitation of  $L_g$ ,  $S_n$ , and  $P-P_n$  Waves from Eastern United States Earthquakes by Regression Analysis of RSTN Data," Teledyne-Geotech Report TGAL-86-7, Final Report on Contract MDA903-85-C-0086.

Gupta, I. N., J. A. Burnetti, R. A. Wagner, and M. E. Marshall (1984). "Discrimination Between Quarry Blasts, Nuclear Explosions and Earthquakes," Teledyne-Geotech Report TGAL-TR-84-1, Technical Report on Contract No. F08606-84-C-0009.

Herrmann, R. B. (1969). "The Structure of the Cincinnati Arch as Determined by Short Period Rayleigh Waves," *Bull. Seism. Soc. Am.*, 59, pp. 399-408.

Kafka, A. L. (1987). " $R_g$  Waves as a Depth Discriminant for Earthquakes and Explosions in New England," Proceedings of the Annual Air Force Geophysics Laboratory Review Meeting, Nantucket, MA.

Kafka, A. L. (1988). "Investigation of  $R_g$  Waves Recorded from Earthquakes and Explosions in New England," Proceedings of the Annual Air Force Geophysics Laboratory Review Meeting, Fallbrook, CA.

Kafka, A. L., and E. C. Reiter (1987). "Dispersion of  $R_g$  Waves in Southeastern Maine: Evidence for Lateral Anisotropy in the Shallow Crust," *Bull. Seism. Soc. Am.*, 77, pp. 925-941.

Leith, W. (1987). "Geology of NRDC Seismic Station Sites in Eastern Kazakhstan," U.S.G.S. Military Geology Project Report.

Leith, W. (1988). Personal Communication.

McEvelly, T. V. (1964). "Central U.S. Crust - Upper Mantle Structure from Love and Rayleigh Wave Phase Velocity Inversion," *Bull. Seism. Soc. Am.*, 54, pp. 1997-2016.

Murphy, J. R. (1981). "Near-Field Rayleigh Waves from Surface Explosions," *Bull. Seism. Soc. Am.*, 71, pp. 223-248.

Murphy, J. R., and T. J. Bennett (1982). "A Discrimination Analysis of Short-Period Regional Seismic Data Recorded at Tonto Forest Observatory," *Bull. Seism. Soc. Am.*, 72, pp. 1351-1366.

Murphy, J. R. and H. K. Shah (1988). "An Analysis of the Effects of Site Geology on the Characteristics of Near-Field Rayleigh Waves," *Bull. Seism. Soc. Am.*, 78, pp. 64-82.

Nuttli, O. W. (1981). "On the Attenuation of  $L_g$  Waves in Western and Central Asia and Their Use as a Discriminant Between Earthquakes and Explosions," *Bull. Seism. Soc. Am.*, 71, pp. 249-261.

Nuttli, O. W. (1986). " $L_g$  Magnitudes of Selected East Kazakhstan Underground Explosions," *Bull. Seism. Soc. Am.*, 76, pp. 1241-1251.

Oppenheim, A. V., and R. W. Schaffer (1975). *Digital Signal Processing*, Prentice Hall, 585 pages.

Patton, H. J. (1988). "Application of Nuttli's Method to Estimate Yield of Nevada Test Site Explosions Recorded on Lawrence Livermore National Laboratory's Digital Seismic System," *Bull. Seism. Soc. Am.*, 78, pp. 1759-1772.

Pomeroy, P. W. (1977). "Aspects of Seismic Wave Propagation in Eastern North America - A Preliminary Report," under Contract No. F49620-78-C-0043, Rondout Associates, Inc., Stone Ridge, New York.

- Pomeroy, P. W. (1979). "Regional Seismic Wave Propagation," Semi-Annual Technical Report No. 3, under Contract No. F49620-78-C-0043, Rondout Associates, Inc., Stone Ridge, New York.
- Pomeroy, P. W., W. J. Best and T. V. McEvilly (1982). "Test Ban Treaty Verification with Regional Data - A Review," *Bull. Seism. Soc. Am.*, 72, pp. S89-S129.
- Priestley, K. F. and W. R. Walter (1988). "Analysis of Teleseismic Data Recorded in Eastern Kazakh," Proceedings of the Annual Air Force Geophysics Laboratory Review Meeting, Fallbrook, CA.
- Ringdal, F. (1988). "Magnitudes of Large Semipalatinsk Explosions Using P Coda and  $L_g$  Measurements at NORSAR," Proceedings of the Annual Air Force Geophysics Laboratory Review Meeting, Fallbrook, CA.
- Ruzaikin, A., I. Nersesov, U. Khalturin and P. Molnar (1977). "Propagation of  $L_g$  and Lateral Variations in the Crustal Structure of Asia," *J. Geophys. Res.*, 82, pp. 307-316.
- Shumway, R. H. (1988). *Applied Statistical Time Series Analysis*, Prentice Hall, 379 pages.
- Smith, A. T. (1988a). "High-Frequency P-Wave Attenuation Near the East Kazakh Test Site Using a New Method with Spectral Ratio," Abstract, *Seismological Research Letters*, 59, p. 45.
- Smith, A. T. (1988b). "High-Frequency Seismic Observations and Models of Chemical Explosions: Implications for the Discrimination of Ripple-Fired Mining Blasts," UCRL-99353, Lawrence Livermore National Laboratory preprint submitted to *Bull. Seism. Soc. Am.*
- Smith, A. T. and Grose, R. D. (1987). "High-Frequency Observations of Signals and Noise Near RSON: Implications for Discrimination of Ripple-Fired Mining Blasts," Lawrence Livermore National Laboratory, Report No. UCID-20945 under U.S. DoE Contract No. W-7405-Eng-48.

Taylor, S. R., M. D. Denny, and E. S. Vergino (1986). "Regional  $m_b$ - $M_s$  Discrimination of NTS Explosions and Western United States Earthquakes: A Progress Report," Lawrence Livermore National Laboratory, Report No. UCID-20642 under U.S. DoE Contract No. W-7405-Eng-48.

Taylor, S. R., N. W. Sherman, and M. D. Denny (1988). "Spectral Discrimination Between NTS Explosions and Western United States Earthquakes at Regional Distances," *Bull. Seism. Soc. Am.*, 78, pp. 1563-1579.

Willis, D. E. (1963). "A Note on the Effect of Ripple Firing on the Spectra of Quarry Shots," *Bull. Seism. Soc. Am.*, 53, pp. 79-85.

CONTRACTORS (United States)

Professor Keiiti Aki  
Center for Earth Sciences  
University of Southern California  
University Park  
Los Angeles, CA 90089-0741

Professor Thomas Ahrens  
Seismological Lab, 252-21  
Div. of Geological and Planetary  
Sciences  
California Institute of Technology  
Pasadena, CA 91125

Professor Charles B. Archambeau  
Cooperative Institute for Resch  
in Environmental Sciences  
University of Colorado  
Boulder, CO 80309

Dr. Thomas C. Bache Jr.  
Science Applications Int'l Corp.  
10210 Campus Point Drive  
San Diego, CA 92121 (2 copies)

Dr. Muawia Barazangi  
Institute for the Study of  
of the Continent  
Cornell University  
Ithaca, NY 14853

Dr. Douglas R. Baumgardt  
Signal Analysis & Systems Div.  
ENSCO, Inc.  
5400 Port Royal Road  
Springfield, VA 22151-2388

Dr. Jonathan Berger  
Institute of Geophysics and  
Planetary Physics  
Scripps Institution of Oceanography  
A-025  
University of California, San Diego  
La Jolla, CA 92093

Dr. S. Bratt  
Science Applications Int'l Corp.  
10210 Campus Point Drive  
San Diego, CA 92121

Dr. Lawrence J. Burdick  
Woodward-Clyde Consultants  
P.O. Box 93245  
Pasadena, CA 91109-3245 (2 copies)

Professor Robert W. Clayton  
Seismological Laboratory/Div. of  
Geological & Planetary Sciences  
California Institute of Technology  
Pasadena, CA 91125

Dr Karl Coyner  
New England Research, Inc.  
76 Olcott Drive  
White River Junction, VT 05001

Dr. Vernon F. Cormier  
Department of Geology & Geophysics  
U-45, Room 207  
The University of Connecticut  
Storrs, Connecticut 06268

Dr. Steven Day  
Dept. of Geological Sciences  
San Diego State U.  
San Diego, CA 92182

Dr. Zoltan A. Der  
ENSCO, Inc.  
5400 Port Royal Road  
Springfield, VA 22151-2388

Professor John Ferguson  
Center for Lithospheric Studies  
The University of Texas at Dallas  
P.O. Box 830688  
Richardson, TX 75083-0688

Professor Stanley Flatter  
Applied Sciences Building  
University of California,  
Santa Cruz, CA 95064

Dr. Alexander Florence  
SRI International  
333 Ravenswood Avenue  
Menlo Park, CA 94025-3493

Professor Steven Grand  
University of Texas at Austin  
Dept of Geological Sciences  
Austin, TX 78713-7909

Dr. Henry L. Gray  
Associate Dean of Dedman College  
Department of Statistical Sciences  
Southern Methodist University  
Dallas, TX 75275

Professor Roy Greenfield  
Geosciences Department  
403 Deike Building  
The Pennsylvania State University  
University Park, PA 16802

Professor David G. Harkrider  
Seismological Laboratory  
Div of Geological & Planetary Sciences  
California Institute of Technology  
Pasadena, CA 91125

Professor Donald V. Helmberger  
Seismological Laboratory  
Div of Geological & Planetary Sciences  
California Institute of Technology  
Pasadena, CA 91125

Professor Eugene Herrin  
Institute for the Study of Earth  
and Man/Geophysical Laboratory  
Southern Methodist University  
Dallas, TX 75275

Professor Robert B. Herrmann  
Department of Earth & Atmospheric  
Sciences  
Saint Louis University  
Saint Louis, MO 63156

Professor Bryan Isacks  
Cornell University  
Dept of Geological Sciences  
SNEE Hall  
Ithaca, NY 14850

Professor Lane R. Johnson  
Seismographic Station  
University of California  
Berkeley, CA 94720

Professor Thomas H. Jordan  
Department of Earth, Atmospheric  
and Planetary Sciences  
Mass Institute of Technology  
Cambridge, MA 02139

Dr. Alan Kafka  
Department of Geology &  
Geophysics  
Boston College  
Chestnut Hill, MA 02167

Professor Leon Knopoff  
University of California  
Institute of Geophysics  
& Planetary Physics  
Los Angeles, CA 90024

Professor Charles A. Langston  
Geosciences Department  
403 Deike Building  
The Pennsylvania State University  
University Park, PA 16802

Professor Thorne Lay  
Department of Geological Sciences  
1006 C.C. Little Building  
University of Michigan  
Ann Arbor, MI 48109-1063

Dr. Randolph Martin III  
New England Research, Inc.  
76 Olcott Drive  
White River Junction, VT 05001

Dr. Gary McCartor  
Mission Research Corp.  
735 State Street  
P.O. Drawer 719  
Santa Barbara, CA 93102 (2 copies)

Professor Thomas V. McEvilly  
Seismographic Station  
University of California  
Berkeley, CA 94720

Dr. Keith L. McLaughlin  
S-CUBED,  
A Division of Maxwell Laboratory  
P.O. Box 1620  
La Jolla, CA 92038-1620

Professor William Menke  
Lamont-Doherty Geological Observatory  
of Columbia University  
Palisades, NY 10964

Professor Brian J. Mitchell  
Department of Earth & Atmospheric  
Sciences  
Saint Louis University  
Saint Louis, MO 63156

Mr. Jack Murphy  
S-CUBED  
A Division of Maxwell Laboratory  
11800 Sunrise Valley Drive  
Suite 1212  
Reston, VA 22091 (2 copies)

Professor J. A. Orcutt  
IGPP, A-205  
Scripps Institute of Oceanography  
Univ. of California, San Diego  
La Jolla, CA 92093



Professor Keith Priestley  
University of Nevada  
Mackay School of Mines  
Reno, NV 89557

Professor Paul G. Richards  
Lamont-Doherty Geological  
Observatory of Columbia Univ.  
Palisades, NY 10964

Wilmer Rivers  
Teledyne Geotech  
314 Montgomery Street  
Alexandria, VA 22314

Dr. Alan S. Ryall, Jr.  
Center of Seismic Studies  
1300 North 17th Street  
Suite 1450  
Arlington, VA 22209-2308 (4 copies)

Professor Charles G. Sammis  
Center for Earth Sciences  
University of Southern California  
University Park  
Los Angeles, CA 90089-0741

Professor Christopher H. Scholz  
Geological Sciences  
Lamont-Doherty Geological Observatory  
Palisades, NY 10964

Dr. Jeffrey L. Stevens  
S-CUBED,  
A Division of Maxwell Laboratory  
P.O. Box 1620  
La Jolla, CA 92038-1620

Professor Brian Stump  
Institute for the Study of Earth & Man  
Geophysical Laboratory  
Southern Methodist University  
Dallas, TX 75275

Professor Ta-liang Teng  
Center for Earth Sciences  
University of Southern California  
University Park  
Los Angeles, CA 90089-0741

Dr. Clifford Thurber  
State University of New York at  
Stony Brooks  
Dept of Earth and Space Sciences  
Stony Brook, NY 11794-2100

Professor M. Nafi Toksoz  
Earth Resources Lab  
Dept of Earth, Atmospheric and  
Planetary Sciences  
Massachusetts Institute of Technology  
42 Carleton Street  
Cambridge, MA 02142

Professor Terry C. Wallace  
Department of Geosciences  
Building #77  
University of Arizona  
Tucson, AZ 85721

Weidlinger Associates  
ATTN: Dr. Gregory Wojcik  
4410 El Camino Real, Suite 110  
Los Altos, CA 94022

Professor Francis T. Wu  
Department of Geological Sciences  
State University of New York  
at Binghamton  
Vestal, NY 13901

OTHERS (United States)

Dr. Monem Abdel-Gawad  
Rockwell Internat'l Science Center  
1049 Camino Dos Rios  
Thousand Oaks, CA 91360

Professor Shelton S. Alexander  
Geosciences Department  
403 Deike Building  
The Pennsylvania State University  
University Park, PA 16802

Dr. Ralph Archuleta  
Department of Geological  
Sciences  
Univ. of California at  
Santa Barbara  
Santa Barbara, CA

J. Barker  
Department of Geological Sciences  
State University of New York  
at Binghamton  
Vestal, NY 13901

Mr. William J. Best  
907 Westwood Drive  
Vienna, VA 22180

Dr. N. Biswas  
Geophysical Institute  
University of Alaska  
Fairbanks, AK 99701

Dr. G. A. Bollinger  
Department of Geological Sciences  
Virginia Polytechnical Institute  
21044 Derring Hall  
Blacksburg, VA 24061

Mr. Roy Burger  
1221 Serry Rd.  
Schenectady, NY 12309

Dr. Robert Burrige  
Schlumberger-Doll Resch Ctr.  
Old Quarry Road  
Ridgefield, CT 06877

Dr. Terry Barker  
S-CUBED, A Division of Maxwell Lab  
P.O. Box 1620  
La Jolla, CA 92038-1620

Dr. B.W. Barker  
S-CUBED, A Division of Maxwell Lab  
11800 Sunrise Valley Dr, Suite 1212  
Reston, VA 22091

Science Horizons, Inc.  
ATTN: Dr. Theodore Cherry  
710 Encinitas Blvd., Suite 101  
Encinitas, CA 92024 (2 copies)

Professor Jon F. Claerbout  
Professor Amos Nur  
Dept. of Geophysics  
Stanford University  
Stanford, CA 94305 (2 copies)

Dr. Anton W. Dainty  
AFGL/LWH  
Hanscom AFB, MA 01731

Professor Adam Dziewonski  
Hoffman Laboratory  
Harvard University  
20 Oxford St.  
Cambridge, MA 02138

Professor John Ebel  
Dept of Geology and Geophysics  
Boston College  
Chestnut Hill, MA 02167

Dr. Donald Forsyth  
Dept of Geological Sciences  
Brown University  
Providence, RI 02912

Dr. Anthony Gangi  
Texas A&M University  
Department of Geophysics  
College Station, TX 77843

Dr. Freeman Gilbert  
Institute of Geophysics &  
Planetary Physics  
University of California, San Diego  
P.O. Box 109  
La Jolla, CA 92037

Mr. Edward Giller  
Pacific Seirra Research Corp.  
1401 Wilson Boulevard  
Arlington, VA 22209

Dr. Jeffrey W. Given  
Sierra Geophysics  
11255 Kirkland Way  
Kirkland, WA 98033

Rong Song Jih  
Teledyne Geotech  
314 Montgomery Street  
Alexandria, Virginia 22314

Professor F.K. Lamb  
University of Illinois at  
Urbana-Champaign  
Department of Physics  
1110 West Green Street  
Urbana, IL 61801

Dr. Arthur Lerner-Lam  
Lamont-Doherty Geological Observatory  
of Columbia University  
Palisades, NY 10964

Dr. L. Timothy Long  
School of Geophysical Sciences  
Georgia Institute of Technology  
Atlanta, GA 30332

Dr. Peter Malin  
University of California at  
Santa Barbara  
Institute for Central Studies  
Santa Barbara, CA 93106

Dr. George R. Mellman  
Sierra Geophysics  
11255 Kirkland Way  
Kirkland, WA 98033

Dr. Bernard Minster  
IGPP, A-205  
Scripps Institute of Oceanography  
Univ. of California, San Diego  
La Jolla, CA 92093

Professor John Nabelek  
College of Oceanography  
Oregon State University  
Corvallis, OR 97331

Dr. Geza Nagy  
U. California, San Diego  
Dept of Ames, M.S. B-010  
La Jolla, CA 92093

Dr. Jack Oliver  
Department of Geology  
Cornell University  
Ithaca, NY 14850

Dr. Robert Phinney/Dr. F. A. Dahlen  
Dept of Geological  
Geological Science University  
Princeton University  
Princeton, NJ 08540

RADIX System, Inc.  
Attn: Dr. Jay Pulli  
2 Taft Court, Suite 203  
Rockville, Maryland 20850

Dr. Norton Rimer  
S-CUBED  
A Division of Maxwell Laboratory  
P.O. 1620  
La Jolla, CA 92038-1620

Professor Larry J. Ruff  
Department of Geological Sciences  
1006 C.C. Little Building  
University of Michigan  
Ann Arbor, MI 48109-1063

Dr. Richard Sailor  
TASC Inc.  
55 Walkers Brook Drive  
Reading, MA 01867

Thomas J. Sereno, Jr.  
Service Application Int'l Corp.  
10210 Campus Point Drive  
San Diego, CA 92121

Dr. David G. Simpson  
Lamont-Doherty Geological Observ.  
of Columbia University  
Palisades, NY 10964

Dr. Bob Smith  
Department of Geophysics  
University of Utah  
1400 East 2nd South  
Salt Lake City, UT 84112

Dr. S. W. Smith  
Geophysics Program  
University of Washington  
Seattle, WA 98195

Dr. Stewart Smith  
IRIS Inc.  
1616 N. Fort Myer Drive  
Suite 1440  
Arlington, VA 22209

Rondout Associates  
ATTN: Dr. George Sutton,  
Dr. Jerry Carter, Dr. Paul Pomeroy  
P.O. Box 224  
Stone Ridge, NY 12484 (4 copies)

Dr. L. Sykes  
Lamont Doherty Geological Observ.  
Columbia University  
Palisades, NY 10964

Dr. Pradeep Talwani  
Department of Geological Sciences  
University of South Carolina  
Columbia, SC 29208

Dr. R. B. Tittmann  
Rockwell International Science Center  
1049 Camino Dos Rios  
P.O. Box 1085  
Thousand Oaks, CA 91360

Professor John H. Woodhouse  
Hoffman Laboratory  
Harvard University  
20 Oxford St.  
Cambridge, MA 02138

Dr. Gregory B. Young  
ENSCO, Inc.  
5400 Port Royal Road  
Springfield, VA 22151-2388

FOREIGN (OTHERS)

Dr. Peter Basham  
Earth Physics Branch  
Geological Survey of Canada  
1 Observatory Crescent  
Ottawa, Ontario  
CANADA K1A 0Y3

Professor Ari Ben-Menahem  
Dept of Applied Mathematics  
Weizman Institute of Science  
Rehovot  
ISRAEL 951729

Dr. Eduard Berg  
Institute of Geophysics  
University of Hawaii  
Honolulu, HI 96822

Dr. Michel Bouchon - Universite  
Scientifique et Medicale de Grenoble  
Lab de Geophysique - Interne et  
Tectonophysique - I.R.I.G.M.-B.P.  
38402 St. Martin D'Herès  
Cedex FRANCE

Dr. Hilmar Bungum/NTNF/NORSAR  
P.O. Box 51  
Norwegian Council of Science,  
Industry and Research, NORSAR  
N-2007 Kjeller, NORWAY

Dr. Michel Campillo  
I.R.I.G.M.-B.P. 68  
38402 St. Martin D'Herès  
Cedex, FRANCE

Dr. Kin-Yip Chun  
Geophysics Division  
Physics Department  
University of Toronto  
Ontario, CANADA M5S 1A7

Dr. Alan Douglas  
Ministry of Defense  
Blacknest, Brimpton,  
Reading RG7-4RS  
UNITED KINGDOM

Dr. Manfred Henger  
Fed. Inst. For Geosciences & Nat'l Res.  
Postfach 510153  
D-3000 Hannover 51  
FEDERAL REPUBLIC OF GERMANY

Ms. Eva Johannisson  
Senior Research Officer  
National Defense Research Inst.  
P.O. Box 27322  
S-102 54 Stockholm  
SWEDEN

Tormod Kvaerna  
NTNF/NORSAR  
P.O. Box 51  
N-2007 Kjeller, NORWAY

Mr. Peter Marshall, Procurement  
Executive, Ministry of Defense  
Blacknest, Brimpton,  
Reading FG7-4RS  
UNITED KINGDOM (3 copies)

Dr. Robert North  
Geophysics Division  
Geological Survey of Canada  
1 Observatory crescent  
Ottawa, Ontario  
CANADA, K1A 0Y3

Dr. Frode Ringdal  
NTNF/NORSAR  
P.O. Box 51  
N-2007 Kjeller, NORWAY

Dr. Jorg Schlittenhardt  
Federal Inst. for Geosciences & Nat'l Res.  
Postfach 510153  
D-3000 Hannover 51  
FEDERAL REPUBLIC OF GERMANY

University of Hawaii  
Institute of Geophysics  
ATTN: Dr. Daniel Walker  
Honolulu, HI 96822

FOREIGN CONTRACTORS

Dr. Ramon Cabre, S.J.  
Observatorio San Calixto  
Casilla 5939  
La Paz Bolivia

Professor Peter Harjes  
Institute for Geophysik  
Rhur University/Bochum  
P.O. Box 102148, 4630 Bochum 1  
FEDERAL REPUBLIC OF GERMANY

Dr. E. Husebye  
NTNF/NORSAR  
P.O. Box 51  
N-2007 Kjeller, NORWAY

Professor Brian L.N. Kennett  
Research School of Earth Sciences  
Institute of Advanced Studies  
G.P.O. Box 4  
Canberra 2601  
AUSTRALIA

Dr. B. Massinon  
Societe Radiomana  
27, Rue Claude Bernard  
7,005, Paris, FRANCE (2 copies)

Dr. Pierre Mechler  
Societe Radiomana  
27, Rue Claude Bernard  
75005, Paris, FRANCE

Dr. Svein Mykkeltveit  
NTNF/NORSAR  
P.O. Box 51  
N-2007 Kjeller, NORWAY (3 copies)

GOVERNMENT

Dr. Ralph Alewine III  
DARPA/NMRO  
1400 Wilson Boulevard  
Arlington, VA 22209-2308

Dr. Robert Blandford  
DARPA/NMRO  
1400 Wilson Boulevard  
Arlington, VA 22209-2308

Sandia National Laboratory  
ATTN: Dr. H. B. Durham  
Albuquerque, NM 87185

Dr. Jack Evernden  
USGS-Earthquake Studies  
345 Middlefield Road  
Menlo Park, CA 94025

U.S. Geological Survey  
ATTN: Dr. T. Hanks  
Nat'l Earthquake Resch Center  
345 Middlefield Road  
Menlo Park, CA 94025

Dr. James Hannon  
Lawrence Livermore Nat'l Lab.  
P.O. Box 808  
Livermore, CA 94550

Paul Johnson  
ESS-4, Mail Stop J979  
Los Alamos National Laboratory  
Los Alamos, NM 87545

Ms. Ann Kerr  
DARPA/NMRO  
1400 Wilson Boulevard  
Arlington, VA 22209-2308

Dr. Max Koontz  
US Dept of Energy/DP 5  
Forrestal Building  
1000 Independence Ave.  
Washington, D.C. 20585

Dr. W. H. K. Lee  
USGS  
Office of Earthquakes, Volcanoes,  
& Engineering  
Branch of Seismology  
345 Middlefield Rd  
Menlo Park, CA 94025

Dr. William Leith  
U.S. Geological Survey  
Mail Stop 928  
Reston, VA 22092

Dr. Richard Lewis  
Dir. Earthquake Engineering and  
Geophysics  
U.S. Army Corps of Engineers  
Box 631  
Vicksburg, MS 39180

Dr. Robert Masse'  
Box 25046, Mail Stop 967  
Denver Federal Center  
Denver, Colorado 80225

Richard Morrow  
ACDA/VI  
Room 5741  
320 21st Street N.W.  
Washington, D.C. 20451

Dr. Keith K. Nakanishi  
Lawrence Livermore National Laboratory  
P.O. Box 808, L-205  
Livermore, CA 94550 (2 copies)

Dr. Carl Newton  
Los Alamos National Lab.  
P.O. Box 1663  
Mail Stop C335, Group ESS-3  
Los Alamos, NM 87545

Dr. Kenneth H. Olsen  
Los Alamos Scientific Lab.  
P.O. Box 1663  
Mail Stop C335, Group ESS-3  
Los Alamos, NM 87545

Howard J. Patton  
Lawrence Livermore National  
Laboratory  
P.O. Box 808, L-205  
Livermore, CA 94550

Mr. Chris Paine  
Office of Senator Kennedy  
SR 315  
United States Senate  
Washington, D.C. 20510

AFOSR/NP  
ATTN: Colonel Jerry J. Perrizo  
Bldg 410  
Bolling AFB, Wash D.C. 20332-6448

HQ AFTAC/TT  
Attn: Dr. Frank F. Pilotte  
Patrick AFB, Florida 32925-6001

Mr. Jack Rachlin  
USGS - Geology, Rm 3 C136  
Mail Stop 928 National Center  
Reston, VA 22092

Robert Reinke  
AFWL/NTESG  
Kirtland AFB, NM 87117-6008

Dr. Byron Ristvet  
HQ DNA, Nevada Operations Office  
Attn: NVCG  
P.O. Box 98539  
Las Vegas, NV 89193

HQ AFTAC/TGR  
Attn: Dr. George H. Rothe  
Patrick AFB, Florida 32925-6001

Donald L. Springer  
Lawrence Livermore National Laboratory  
P.O. Box 808, L-205  
Livermore, CA 94550

Dr. Lawrence Turnbull  
OSWR/NED  
Central Intelligence Agency  
CIA, Room 5G48  
Washington, D.C. 20505

Dr. Thomas Weaver  
Los Alamos National Laboratory  
P.O. Box 1663  
MS C 335  
Los Alamos, NM 87545

GL/SULL  
Research Library  
Hanscom AFB, MA 01731-5000 (2 copies)

Secretary of the Air Force (SAFRD)  
Washington, DC 20330  
Office of the Secretary Defense  
DDR & E  
Washington, DC 20330

HQ DNA  
ATTN: Technical Library  
Washington, DC 20305

DARPA/RMO/RETRIEVAL  
1400 Wilson Blvd.  
Arlington, VA 22209

DARPA/RMO/Security Office  
1400 Wilson Blvd.  
Arlington, VA 22209

GL/XO  
Hanscom AFB, MA 01731-5000

GL/LW  
Hanscom AFB, MA 01731-5000

DARPA/PM  
1400 Wilson Boulevard  
Arlington, VA 22209

Defense Technical  
Information Center  
Cameron Station  
Alexandria, VA 22314  
(5 copies)

Defense Intelligence Agency  
Directorate for Scientific &  
Technical Intelligence  
Washington, D.C. 20301

Defense Nuclear Agency/SPSS  
ATTN: Dr. Michael Shore  
6801 Telegraph Road  
Alexandria, VA 22310

AFTAC/CA (STINFO)  
Patrick AFB, FL 32925-6001

Dr. Gregory van der Vink  
Congress of the United States  
Office of Technology Assessment  
Washington, D.C. 20510

Mr. Alfred Lieberman  
ACDA/VI-OA'State Department Building  
Room 5726  
320 - 21st Street, NW  
Washington, D.C. 20451



TACTEC  
Battelle Memorial Institute  
505 King Avenue  
Columbus, OH 43201 (Final report only)